THE DEVELOPMENT OF A HIGH STABILITY SUM-COINCIDENCE SPECTROMETER and STUDIES ON Ge^{69} DECAY

by

Dale Gedcke

Submitted in partial fulfillment
of the requirements for the degree of
Master of Science.

Department of Physics,
Faculty of Pure and Applied Science,
The University of Ottawa,
Ottawa, Canada.

1964

ABSTRACT

A high stability sum-coincidence spectrometer with improved versatility is described. Complete circuit descriptions of the transistorized equipment are presented. Since gain stability is an important factor, a thorough analysis of the characteristics of high stability operational amplifiers is included.

The Hoogenboom theory for the resolution and detection efficiency of the sum-coincidence spectrometer is reviewed, and a new, more accurate, and more versatile expression for the detection efficiency is derived.

Theory for the limits of time resolution in scintillation detectors is reviewed, and measurements made on the equipment are presented for comparison. Several proposals arising out of this work are made for improved fast coincidence circuits.

Studies on the decay scheme of Ge^{69} are described. The sum-coincidence spectrometer was used to measure γ-γ cascades from several levels in Ga^{69} following Ge^{69} decay. The "1.92 MeV level" in Ga^{69} was found to be composed of two levels: a 1.87 MeV level and a 1.92 MeV level.

An oscillating tritium target, developed for long irradiation times at high neutron fluxes is described for use with the Texas Nuclear neutron generator.

ACKNOWLEDGEMENTS

I wish to thank my supervisor, Dr. I. L. Fairweather, for suggesting this project, and for his direction throughout the work.

The frequent discussions and criticism offered by Mr. W. J. McDonald and Mr. T. H. Hsu helped greatly in the development of this project. Their willingness to discuss ideas involved in this work was highly appreciated.

Mr. C. L. Cornish's assistance in running and servicing the neutron generator was invaluable. Along with Mr. R. Hart, he contributed a great deal to the construction of the oscillating tritium target.

I also thank my wife, who assisted in the preparation of the final thesis manuscript.

I am grateful to the Ontario Provincial Government, and to the National Research Council for the granting of their scholarships.

Thanks is also due to two summer students, Miss C. Knowles, and Mr. Orazio Berolo, for assistance in the analysis of parts of the project.

Valuable experience in transistor electronics was gained during the summer of 1962 under Mr. A. R. Jones at Atomic Energy of Canada Limited, Chalk River, Ontario. I wish to express my gratitude for the valuable training Mr. Jones provided in nuclear pulse electronics.

The typewritten manuscript was prepared by Miss R. M. Ralph.

TABLE OF CONTENTS

LIST OF ILLUSTRATIONS

LIST OF TABLES

CHAPTER 1

INTRODUCTION

1.1 General.

Gamma-ray spectroscopy, the study of γ-rays emitted by radioactive nuclei, is a well established and useful field in low energy nuclear physics. Studies of decay schemes and γ-ray energies yield information about the energy levels of the daughter nucleus. Angular correlation determinations on γ-ray cascades permit evaluation of the spins and parities of the excited states. By measuring the relative intensities of the various gamma-ray energies emitted, the transition probabilities between levels can be calculated. It is hoped, of course, that when all the data is collected for a given nucleus, the levels can be fitted to a prediction based on an appropriate theory.

The facilities most required in a gamma-ray spectrometer are:

(1) The ability to measure energy with a high resolving power.

(2) A provision for determining the intensities of γ-rays.

(3) An ability to measure easily angular correlations.

A recently developed spectrometer which meets these conditions

quite well is the Hoogenboom Sum-coincidence γ-γ Spectrometer.

The original aim of the project for this thesis was to assemble a sum-coincidence spectrometer, and apply it to a radioactive nucleus produced with a 14 MeV neutron generator.

1.2 Early Attempts.

A spectrometer, such as is shown in Figure 2.2, was assembled from readily available equipment. Using standard sources such as Co^{60} and Ba^{133}, the system was put through a series of tests. Over a short period of time the spectrometer operated reasonably well. However, when the system was to be run for periods of more than 5 hours, serious gain drift was encountered. This drift was as large as ± 5% in some cases, and proved to be unacceptable for practical measurements. The available amplifiers were tube amplifiers and had a great deal of noise on the outputs. In addition, the scintillator-photomultiplier combinations available did not provide a matched pair of detectors.

At this point it became obvious that a completely new system would have to be designed to overcome the gain drift and noise problems, and to improve the flexibility of the spectrometer. With these criteria in mind, a

transistorised sum-coincidence spectrometer was designed and built. Two matched, high stability detectors were purchased, and a fast coincidence circuit was added to improve the spectrometer versatility. The results achieved with this system showed a substantial improvement.

Since a major portion of this project involved the development of the high stability spectrometer, a large section of this thesis deals with the electronic design and operating characteristics.

1.3 Selection of the Radioactive Isotope.

After surveying compiled data on various nuclei, it was decided to study the gamma-rays following the decay of Ge^{69} into Ga^{69}. At the time the source was selected, the only previous work on this decay had been done with single channel analysers. Much of the decay scheme was very uncertain, particularly the transitions from the higher energy levels. None of the spins or parities of the excited levels in Ga^{69} had been determined.

The source was made using an (n,2n) reaction on the Ge^{70} contained in pure germanium. 14 MeV neutrons from the University of Ottawa neutron generator were used. Since the half-life of Ge^{69} is about 40 hours, and the reaction cross-section is not large (600 mb), a special, long-life, oscillating tritium target had to be designed

for the neutron generator. The transition intensities from the top levels in Ga^{69} are very weak. Consequently the spectrometer had to be stable enough to run for periods as long as 5 days without gain shifts. Since the source decayed rapidly, gain shift with counting rate also had to be prevented.

From early trials, it was realised that a complete analysis of Ga^{69} was far beyond the scope of this project. For this reason, only the top two levels were studied in what might be considered preliminary measurements. Further, refined, and more extensive measurements should follow as part of another project.

1.4 Digressive Topics.

During the course of the work, several important concepts came under consideration; notably, the fast coincidence resolving time. Since several worthwhile ideas grew out of these considerations, some discussion on these topics has been included. It is expected that these digressions will provide valuable information for an improvement of the system.

1.5 Background.

To facilitate the analysis of results for those who continue this work, much of the theoretical background for the sum-coincidence spectrometer has been compiled. Some of this theory has not been developed in published papers.

CHAPTER 2

THE HOOGENBOOM SUM-COINCIDENCE TECHNIQUE

2.1 The NaI(Tl) Scintillation Detector.

The detector which has found widest use in γ-ray spectroscopy is a crystal of thallium activated sodium iodide mounted on the cathode of a photomultiplier[1,2,3]. A typical spectrum obtained from such a detector with the 662 KeV gamma-ray from the Cs^{137} decay is shown in Fig. 2.1. The bell-shaped "photo peak" or "full energy peak" arises from events in which the full energy of the gamma-ray is deposited in the crystal. The broad Compton peak is formed when the γ-ray undergoes Compton collisions and leaves only part of its energy in the crystal. It is this peak which gives rise to much of the difficulty in analysing complicated decay schemes. The peak at 32 KeV is an X-ray given off in the decay.

In most cases there are several gamma-rays emitted by a radioactive source. Frequently, the lower energy "full energy peaks" are superimposed on the broad Compton peaks of high energy gamma-rays. This makes the low energy peaks difficult to resolve, particularly if their relative intensities are very low.

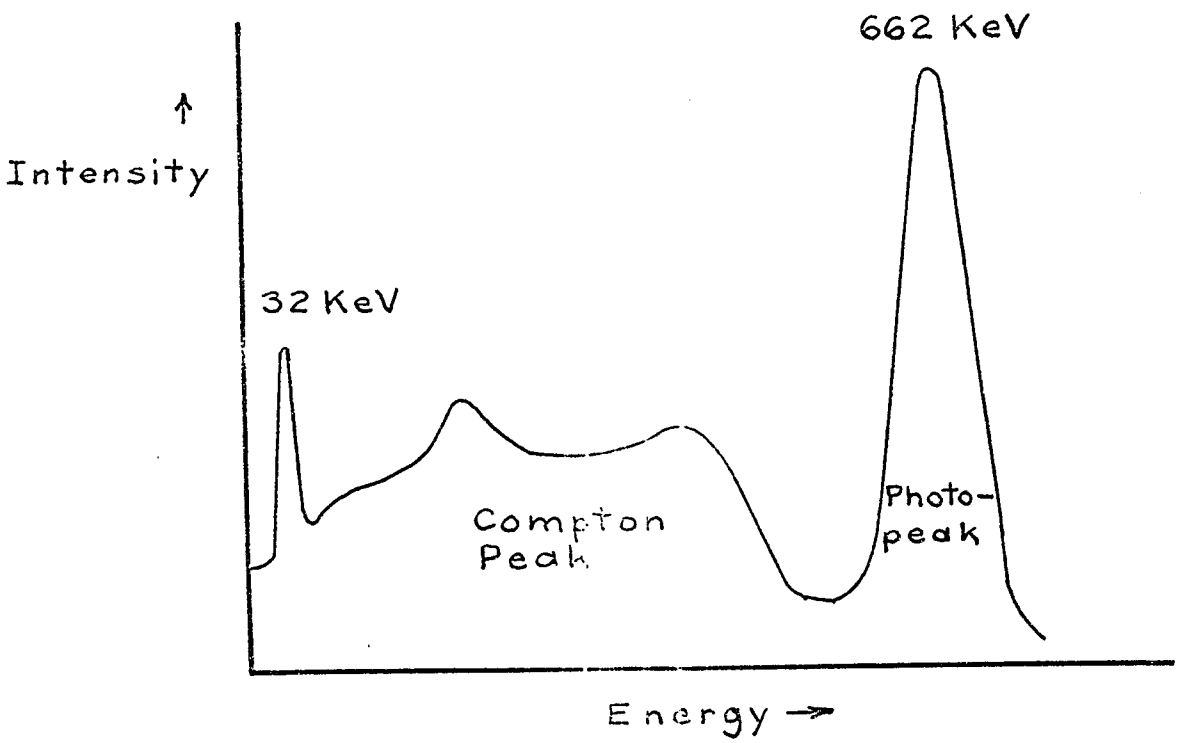

Fig. 2.1. A Cs^{137} spectrum obtained with an NaI(Tl) scintillation detector.

Many attempts have been made to eliminate the interfering Compton peak[5]. In one system[4], the central detecting crystal has been surrounded by a large volume scintillator, to detect the events which left only a part of the total energy in the analysing crystal. By operating the outside scintillator in anticoincidence with the analyser, the Compton peak was reduced by a factor of about 10. One drawback of this system is that a large volume is required if an efficient reduction in the Compton peak is to be achieved. For measuring very weak intensities, a factor of 10 is not a sufficient reduction.

In general, the attempts to reduce the Compton peak have been characterised by a resultant low detection efficiency of the system, and an awkward complexity associated with the radiation detectors.

2.2 The Hoogenboom Sum-Coincidence Spectrometer.

In 1958 A. M. Hoogenboom published a paper on a new gamma-ray spectrometer[6] which very effectively overcame the problems mentioned above. Since that time the system has found very widespread use, and has proved to be a very powerful instrument.

The advantages of this technique are many. The resolving power of the system is greatly improved, in that the spectrometer selects only "full energy peaks" and rejects all Compton peaks. In addition, it is possible to improve upon the intrinsic resolution (full width at half maximum height*) of the photo-peaks, where necessary. These two improvements are achieved with a reasonable detection efficiency. Usually, the relative intensities of competing cascades de-exciting a common level are desired. The Hoogenboom system will measure this data for a given level with one setting of the analyser. Concurrently, the relative intensity of the cross-over to ground gamma-ray for the same level can be determined.

In the case where angular correlation determinations are of interest, the correlations for all pairs of gamma-rays de-exciting the same level are measured simultaneously. A substantial advantage in this determination is found in the fact that no correction for a rapidly decaying activity is necessary as the measurements are taken at different angles in sequence.

*Abbreviated, F.W.H.M.

Figure 2.2 shows a block diagram of the Hoogenboom Sum-coincidence Gamma-Ray Spectrometer. Two scintillator-photomultiplier combinations view the radioactive source. The high voltages on the photomultipliers are adjusted so that both detectors have the same energy calibration. From the preamplifier outputs the pulses are fed into a linear adding circuit. The output signal voltage from this circuit represents the sum of the energies deposited in the two crystals. A linear amplifier and a differential discriminator allow the multi-channel analyser to be gated by a selected narrow energy range. Simultaneously, the signal from preamplifier A is fed via a linear amplifier to the kicksorter to be analysed.

With the aid of Figure 2.3, the logic of the system may be understood. An energy level E_s is de-excited by a prompt cascade of gamma-rays of energy E_1 and E_2. Each gamma-ray will produce a spectrum from the detectors similar in shape to that shown in Fig. 2.1. It will be noticed, however, that the sum of the energies given by their respective "full energy peaks" will be equal to E_s, the energy of the initial level. If the window of the differential discriminator is set across the energy E_s, as shown in Fig. 2.3, then the kicksorter will be gated to

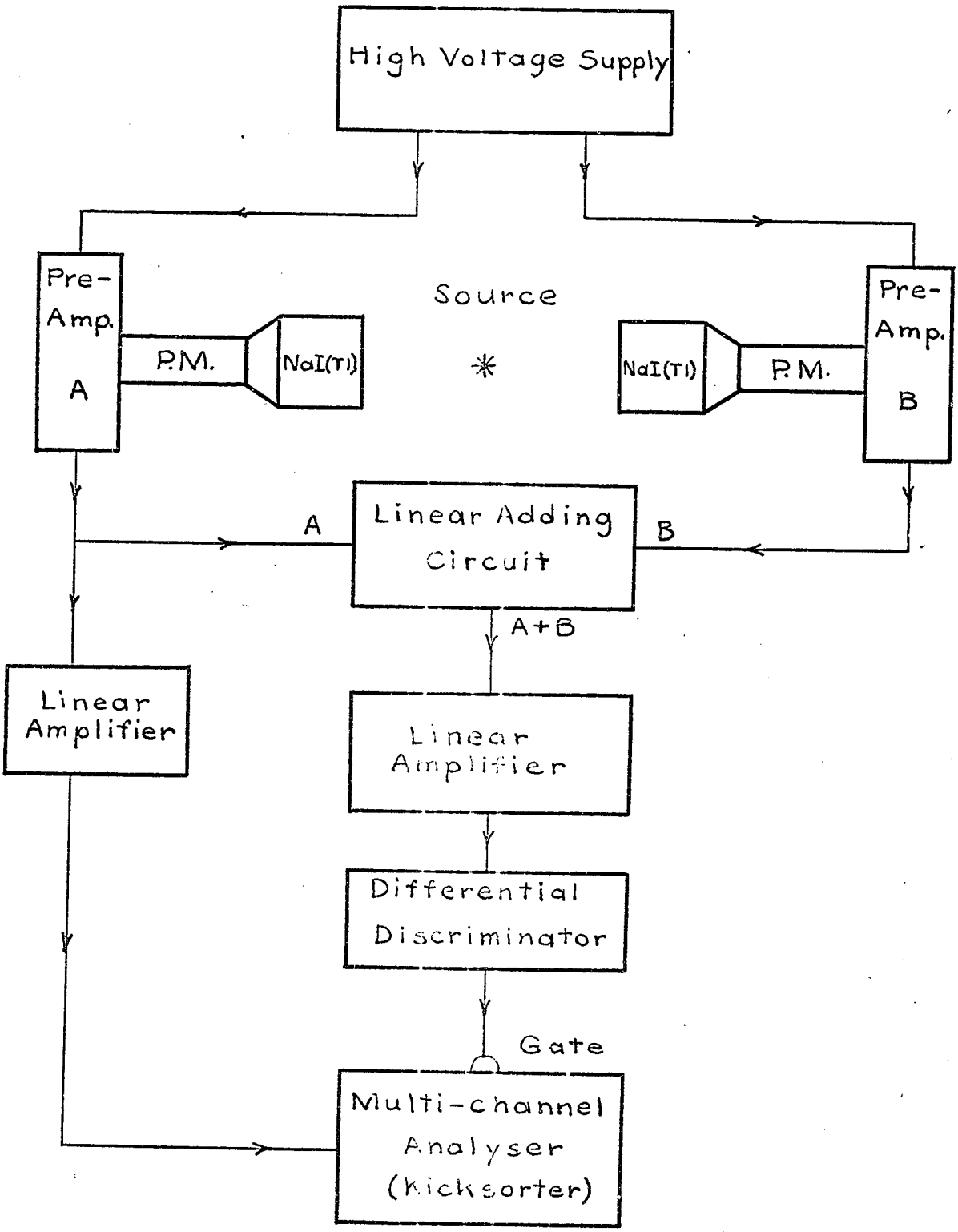

Fig 2.2. The Hoogenboom Sum-coincidence γ-ray Spectrometer.

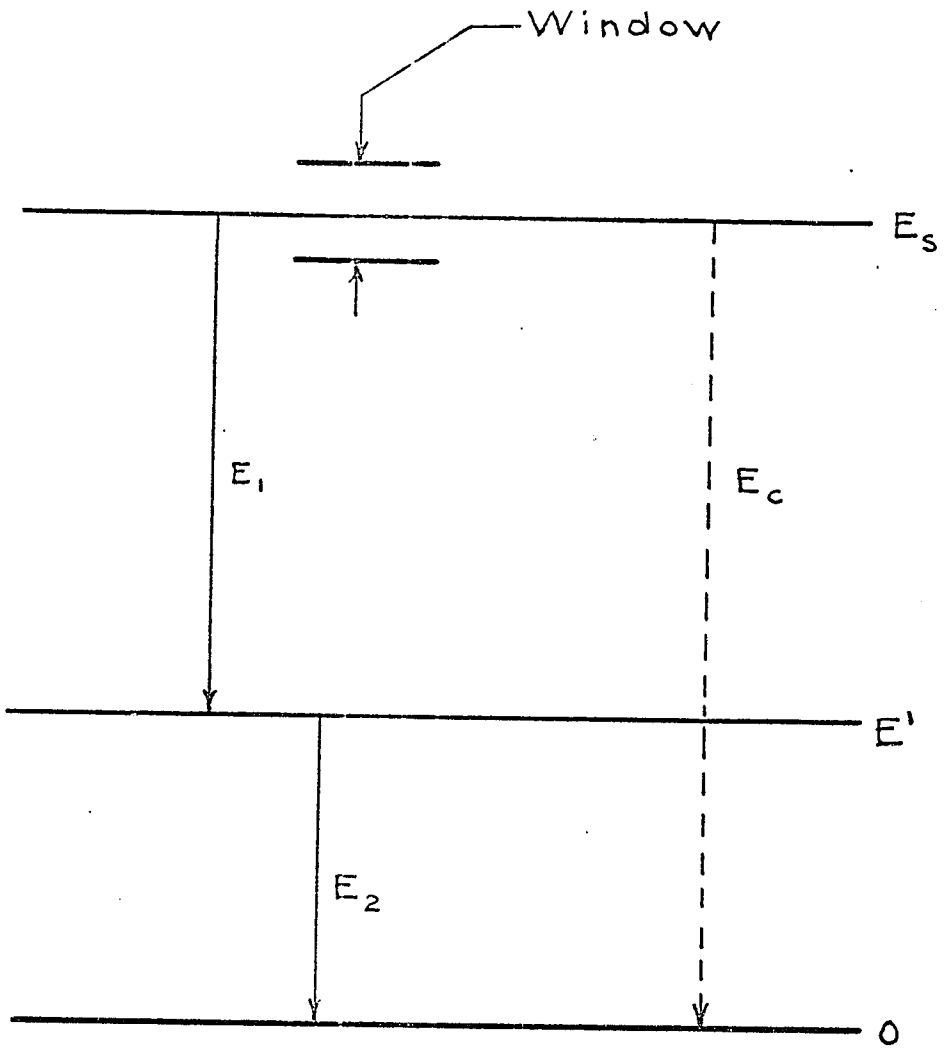

Fig. 2.3. A prompt cascade of two γ-rays, de-exciting an energy level E_s.

analyse the detector A output only when a pulse corresponding to the energy E_s is observed at the adding network output. This event can occur only when the total energy of the gamma-rays E_1 and E_2 is deposited in the detectors. Thus, the spectrum analysed by the kicksorter will consist of the "full energy peaks" only. Several cases can occur:

(1) Gamma-ray E_1 enters detector A, while gamma-ray E_2 enters detector B.

(2) Gamma-ray E_2 enters detector A, while gamma-ray E_1 enters detector B.

(3) Both gamma-rays enter detector A.

All other events, and all cases where the full energies are not deposited in the detectors will be rejected by the multi-channel analyser. Typical spectra are shown in Figures 2.4 and 2.5 for Co^{60}.

Since each of the 3 events given have an equal probability of occurring when the angle defined by detector A, the source, and detector B is 180°, the area or number of counts under each of the peaks in the sum-coincidence spectrum should be identical. Fig. 2.5 illustrates this fact very well. The very small peaks in Fig. 2.5 occur when one of the gamma-rays loses part of its energy in one crystal and the remainder in the other crystal. This 180° backscatter is usually eliminated by lead shielding between the two detectors.

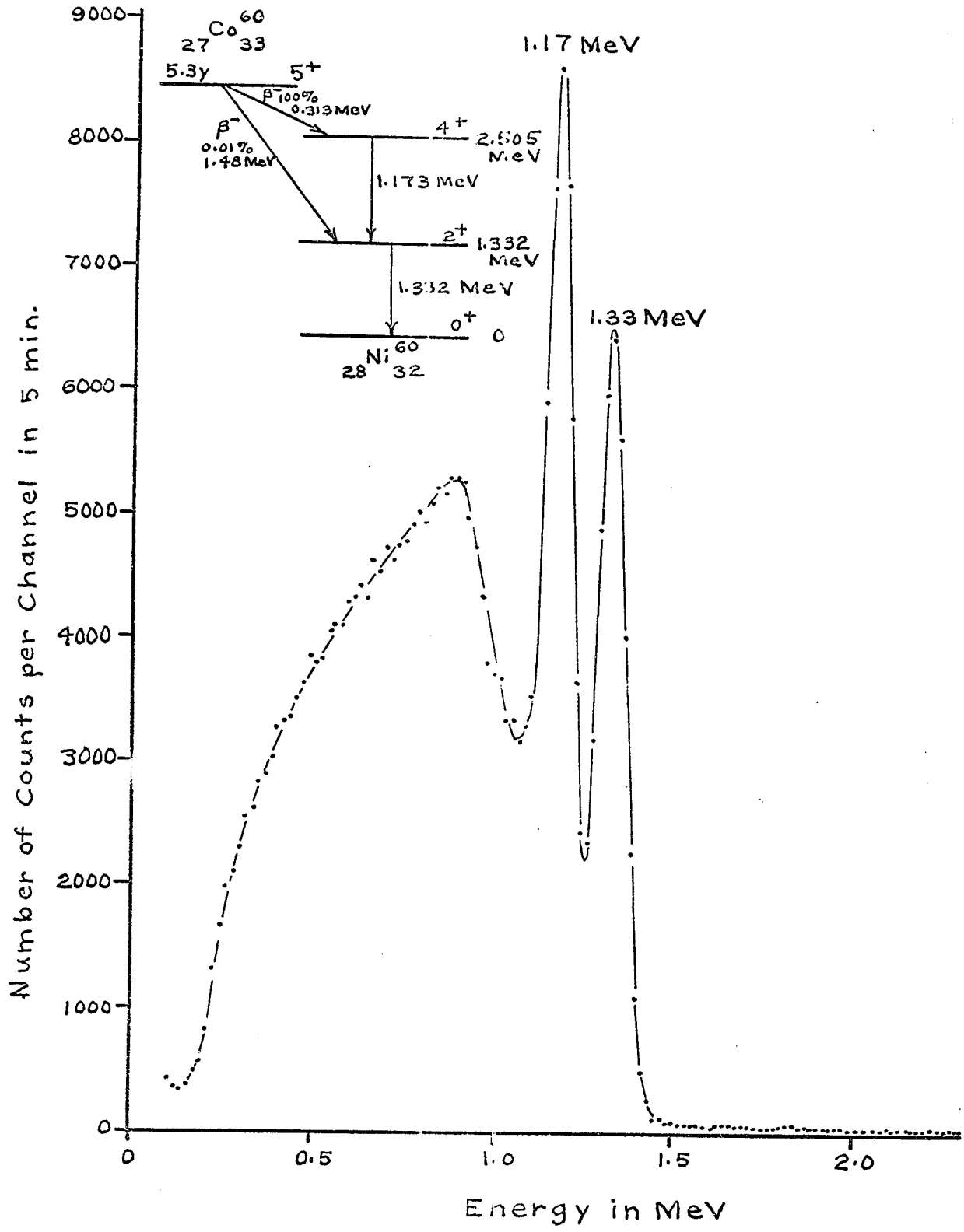

Fig. 2.4. A single-crystal, γ-ray spectrum on a Co^{60} source.

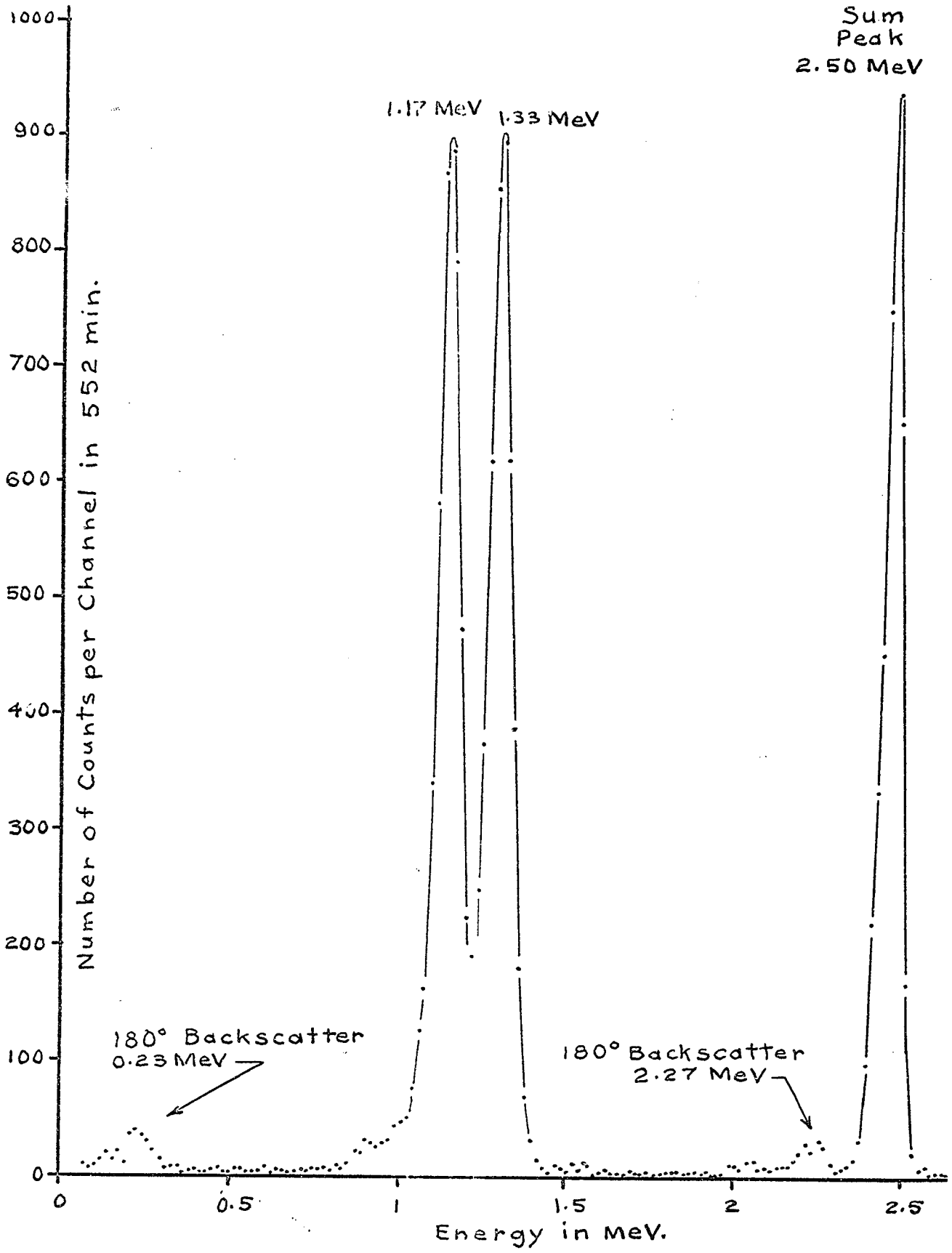

Fig. 2.5. A sum-coincidence spectrum on the Co^{60} source with a 2.1 percent window at 2.50 MeV.

This simple illustration can easily be extended to a situation where several energy levels exist below the initial level, and there are competing cascades. Clearly, the relative frequencies of the various two-gamma-ray cascades can be obtained from the areas under the respective peaks.

If there exists a cross-over gamma-ray, designated E_c in Fig. 2.3, then the area under the sum peak will be augmented by an amount corresponding to the transition probability of the cross-over. Hence, a subtraction of one half the total area of peaks outside the sum peak from the area under the sum peak yields the number of cross-over events.

2.3 Resolution and Efficiency[6,7].

Predicted resolutions and efficiencies for the spectrometer are of vital importance when analysing a radioactive source. If one assumes a Gaussian shape for the full energy peaks and the gated sum-peak, the resolutions and efficiencies can be easily calculated. This Gaussian approximation turns out to be sufficiently accurate to agree well with experimental results. The calculations are performed in Appendix I.

The F.W.H.M. of the peak corresponding to the gamma-ray E_1 in the sum-coincidence spectrum is given by

$$\Gamma_{1s} = \frac{\Gamma_1\sqrt{\Gamma_2^2 + \Gamma_s^2}}{\sqrt{\Gamma_1^2 + \Gamma_2^2 + \Gamma_s^2}} \qquad (2.1)$$

The F.W.H.M. of the gamma-ray E_2 peak is

$$\Gamma_{2s} = \frac{\Gamma_2\sqrt{\Gamma_1^2 + \Gamma_s^2}}{\sqrt{\Gamma_1^2 + \Gamma_2^2 + \Gamma_s^2}} \qquad (2.2)$$

where Γ_1 and Γ_2 are the full widths at half maximum for the gamma rays E_1 and E_2 in the single crystal spectrum. Γ_s is the F.W.H.M. for the gated sum peak. This width is determined by the differential discriminator window setting.

If $\Gamma_s \ll \Gamma_1$ or Γ_2 the equations simplify to

$$\Gamma_{1s} = \Gamma_{2s} = \frac{\Gamma_1\ \Gamma_2}{\sqrt{\Gamma_1^2 + \Gamma_2^2}} \qquad (2.3)$$

Equation (2.3) represents the limit of improvement of resolution. Usually, any gross deviation from these predicted values can be interpreted due to background from higher energy gamma-rays. This criterion can be very useful in the analysis of a complicated decay scheme.

Máthé, Hórenaji and Scharbert[6] have discussed the sources of these deviations in great detail. Their treatment of the problem is rigourous and straight forward, and will not be presented here. It suffices to point out that a very careful setting of the discriminator window is necessary. One must also be aware of the presence of higher energy cascades, whose Compton peaks can give rise to broad peaks in the sum-coincidence spectrum. In cases where these interfering cascades are of high intensity, they must be investigated first. Then a simple graphical analysis is sufficient to subtract their effect from the lower cascades. Schriber and Hogg[11] have recently investigated the problem of "false peaks", and have developed a simple method of dealing with them.

The efficiency for the detection of gamma-rays E_1 and E_2 in the sum-coincidence spectrum is

$$\epsilon'_{1s} = \epsilon'_{2s} = 2\sqrt{\frac{4\pi}{\pi}} \frac{\epsilon_1 \epsilon_2 \Gamma_s}{\sqrt{\Gamma_1^2 + \Gamma_2^2 + \Gamma_s^2}} \qquad (2.4)$$

where ϵ_1 and ϵ_2 are the efficiencies for detecting gamma-ray full energies E_1 and E_2 respectively in a single crystal. It is assumed in these calculations that the two detectors have identical characteristics. Note that the efficiencies are symmetric. This means that the areas under the two peaks are equal.

To be completely accurate, one must include the effect of angular anisotropy or angular correlation in the calculation of the efficiencies. This gives

$$\epsilon_{1s} = \epsilon_{2s} = W(\theta)\epsilon'_{1s} = W(\theta)\epsilon'_{2s} \qquad (2.5)$$

where $W(\theta)$ is the angular correlation function[9,10] for two gamma-rays in cascade given off at an angle θ to each other.

It is interesting to note that equation (2.5) also gives the efficiency for the detection of both gamma-rays in the analysed crystal. $W(0^\circ) = W(180^\circ)$, so that for the two detectors at 180°, the area under the sum peak is equal to the area under either of the two single peaks. This is of course will not be true if there is a cross-over transition. In this case the area under the peak will be added to by an amount ϵ_g, which is the efficiency for detecting the cross-over full energy in a single crystal. Hence the presence of a cross-over may be detected by a simple subtraction process with data taken at 180°.

In the case of no cross-over, and several competing cascades, the area under the sum peak will be 1/2 the total area under the rest of the peaks. At angles other than $\theta = 180^\circ$, $W(\theta)$ will, of course, have to be taken into account.

At this point it is easy to see the power of the Hoogenboom sum-coincidence technique for angular correlation determinations. The counts in the sum peak represent the data for $W(0^{\circ})$, while data for $W(\theta)$ is obtained from the single peaks. Since both sets of data are equally affected by a change of counting rate, the ratio of $W(\theta)/W(0^{\circ})$ is independent of counting rate. Thus the window may be set for a desired level and angular correlations for all the cascades may be measured with no concern over changing counting rates. In practice this turns out to be an appreciable advantage.

2.4 Stability.

By far, the most difficult problem encountered in a sum-coincidence spectrometer is gain drift. Usually the window on the sum channel is set to a width between 2% and 5% of the pulse height setting. If the spectrometer is to function properly, the fluctuations in gain calibration of both singles channels must not be appreciable with respect to the window width. Changes in the energy calibration can result in a distortion of the sum-coincidence spectrum.

These gain drifts can arise from three sources.

(1) Random drift with time.

(2) Change in gain due to temperature fluctuations.

(3) Change of gain with counting rate.

All three effects can take place in both the electronic apparatus and the photomultipliers themselves. Gain stability is relatively easy to achieve in amplifiers. Multiplier phototubes, with good gain stability, on the other hand, are difficult to obtain[12,13,14,15].

Several designs have been published for feedback servo-systems to correct for these gain drifts. One device is presently available on the commercial market. These methods will be discussed in chapter 10.

CHAPTER 3

A GENERAL DESCRIPTION OF THE SPECTROMETER EQUIPMENT.

3.1 Block Diagram.

Figure 3.1 shows a block diagram of the equipment actually used for this project. It will be noticed that the system differs somewhat from Figure 2.2. One major difference is that the slow pulses from the preamplifiers are amplified before passing into the linear adding circuit. This change was made to better accommodate a gain stabilizer. (See chapter 10). A fast and slow coincidence circuit has been added to improve the flexibility of the system. The dotted elements show possible feedback loops for gain stabilization.

A conventional, high voltage, regulated power supply was used†. Its output was fed to the High Voltage Attenuator. The purpose in using one high voltage supply is to ensure that any change in the high voltage will cause the gain calibrations of both photomultipliers to track together.

†HJE Corporation Model S-325, 500 - 2500 VDC, 0 - 10 ma, High Voltage Supply.

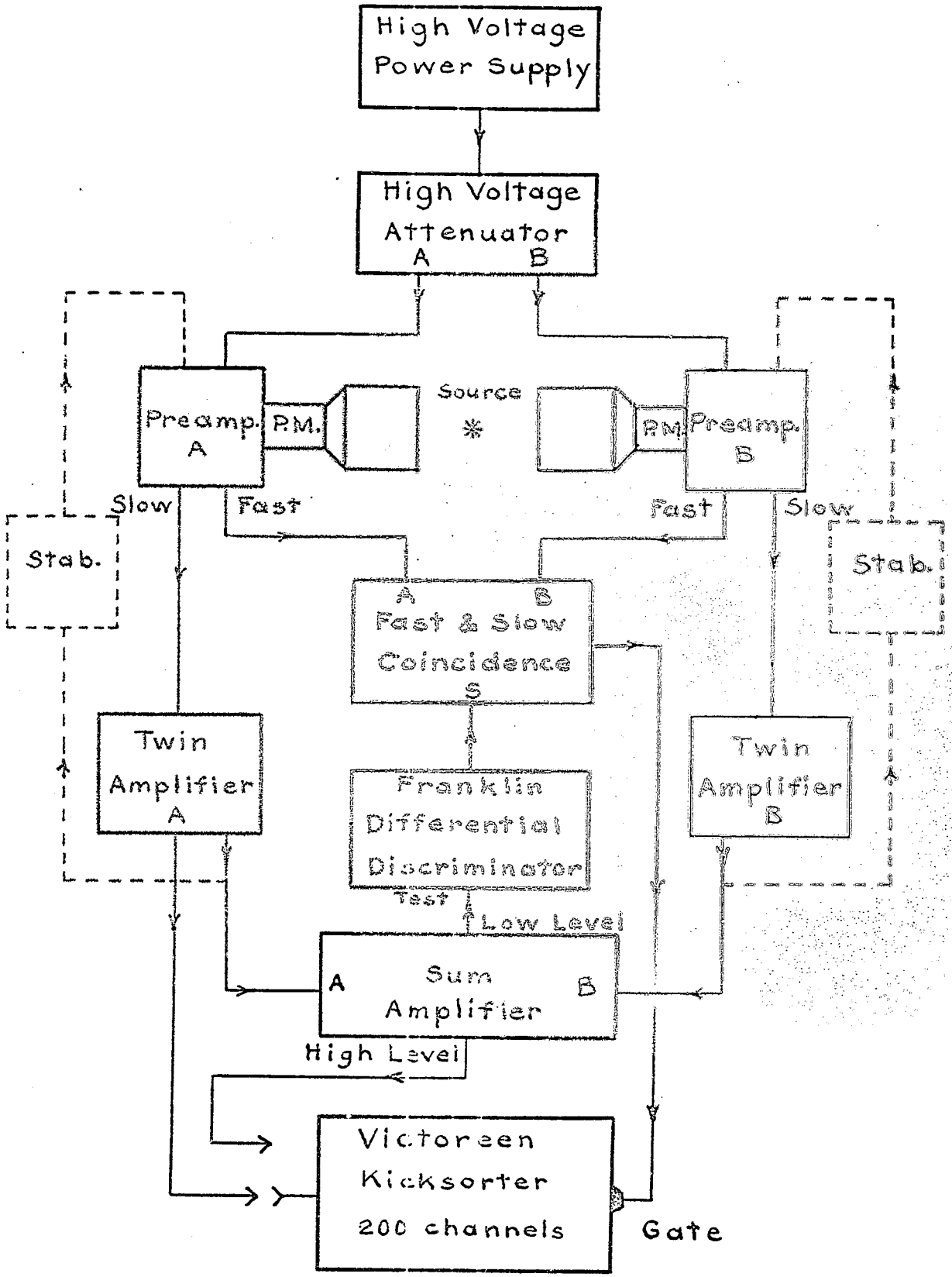

Fig. 3.1. The sum-coincidence spectrometer used in this work.

The detectors used were 3" x 3" Harshaw NaI(Tl) crystals, mounted on RCA type 8054 multiplier phototubes. The detector is offered as a sealed unit by the Harshaw Chemical Company[1]. They guarantee an energy resolution of less than 7.6% on the Cs^{137} 662 KeV peak, as well as a gain shift of less than 1% per day at 10^3 counts/second, and a gain shift of less than 1% for a change in counting rate from 10^3 to 10^4 counts/second. In addition to having a good stability, the 8054 phototube is a low noise tube. The Harshaw "Integral Line" assembly was chosen mainly for its high gain stability.

To obtain a differential discriminator, the low level output from the Sum Amplifier was fed into the test input of a Franklin Linear Amplifier (Model 358). This applies a gain of 30 before the Franklin differential discriminator. The negative discriminator output was fed to a slow coincidence circuit, followed by a flip-flop to operate the kicksorter gate.

It is suggested that an improvement could be made by constructing a differential discriminator which is accessible without passing through any gain. A desirable design would include a zero cross-over output time reference, or a strobe pulse which comes at a fixed time after the input pulse. It is important that the discriminator

settings be very stable. If two identical discriminators were constructed, the flexibility of the system would be improved, since it is sometimes advantageous to select restricted energy ranges on the Twin Amplifier outputs.

Provisions were made to feed either of the Twin Amplifier outputs or the Sum Amplifier output to the 200 channel Victoreen Kicksorter.

3.2 Operational Amplifiers.

In the design of the electronics, great care was taken to ensure a high gain stability. For this reason, operational amplifiers were used wherever possible. These units are characterised by a high degree of gain stability and extremely linear operation over a large signal range[16,17]. Figure 3.2 shows three types of operational amplifiers.

Generally, the operational amplifiers used in the equipment consisted of a transistor amplifier with open loop current gain = A, bypassed by a feedback impedance Z_f. Complete calculations for the characteristics of the generalized operational amplifier are carried out in Appendix II.

Equation (II.12) gives the voltage gain as

$$\frac{V_o}{V_i} = -\frac{Z_f}{Z_i}$$

where V_o is the output signal voltage, V_i is the input voltage, Z_i is the input load impedance, and Z_f is the feedback impedance. Z_L is the parallel combination of any load impedance in the amplifier, with any external load to be driven by the output.

The current gain is given by equation (II.16) as

$$\frac{i_L}{i_i} = -\frac{Z_f}{Z_L}$$

where i_i is the input signal current and i_L is the output current into the load Z_L.

In figure 3.2(b) $Z_i = R_i$ and $Z_f = R_f$, so both Z_i and Z_f are resistive. In this instance, the operational amplifier multiplies the input voltage by a constant to give the inverted output voltage.

$$V_o = -\frac{R_f}{R_i} V_i \qquad (3.1)$$

In figure 3.2(c) the input loads and feedback impedance are again resistive.

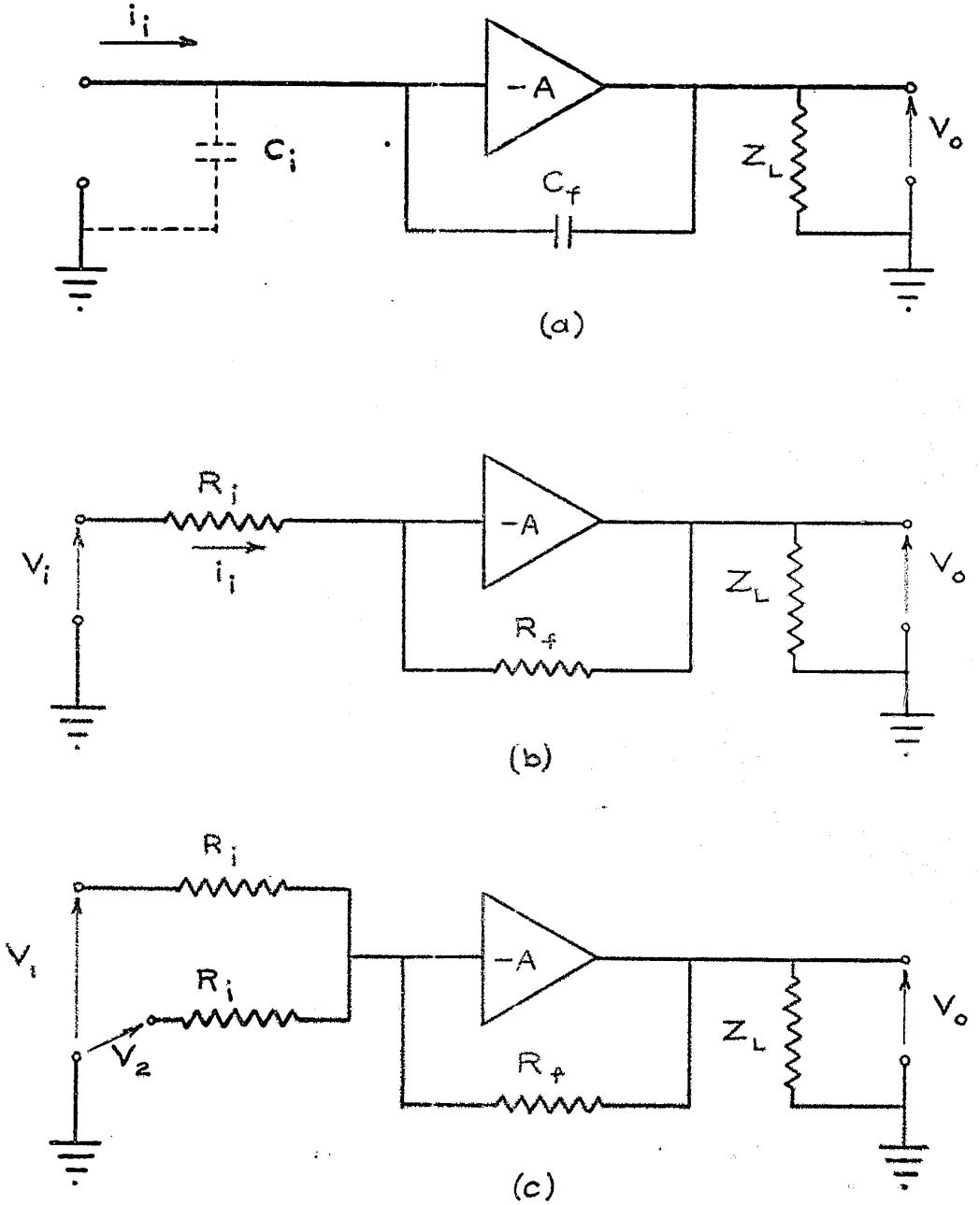

Fig. 3.2. (a) The operational integrator. (b) The operational amplifier. (c) The operational adder.

In this case, however, the output voltage is a superposition of the two input signals. The output voltage is

$$V_o = -\frac{R_f}{R_1} V_1 - \frac{R_f}{R_1} V_2$$

$$= -\frac{R_f}{R_1} (V_1 + V_2) \qquad (3.2)$$

Since the junction of the two input loads and the feedback resistor is a virtual ground (vis. Appendix II), there is a negligible interaction between the two inputs (~ 0.02%). Hence, this configuration becomes an operational linear adder, or sum amplifier.

In figure 3.2(a), the feedback impedance is a capacitor, and the relation between the input current, i_1, and the output voltage, V_o, is considered. Equation (II.12) gives

$$V_o = -Z_f \frac{V_1}{Z_1} = -Z_f i_1 \qquad (3.3)$$

Now, if we consider the definition of impedance as

$$V = Zi \qquad (3.4)$$

and compare this to the equation for a capacitor

$$V = \frac{Q}{C} = \frac{1}{C}\int_t i\,dt \qquad (3.5)$$

where Q is the total charge on the capacitor, then Z may be defined for a capacitor as the operator

$$Z = \frac{1}{C}\int_t dt \qquad (3.6)$$

Substitution of this form in equation (3.3) gives the output voltage as

$$V_o = -\frac{1}{C_f}\int_t i_1\,dt \qquad (3.7)$$

The circuit of figure 3.2(a) provides an output voltage proportional to the integrated input current. It is thus an operational integrator.

The operational integrator is very useful as a preamplifier for photomultipliers, where an integration of the output current is required. If C_f is about 50 pf, then the virtual ground on the input, given by equation (II.19), is equivalent to an input capacitance of 1.3 μf to ground. Typical values used in equation (II.19) were

$$R_b = 200\ \Omega$$

$$Z_f = \frac{1}{j\omega C_f} = \frac{1}{50 \times 10^{-12}\, j\omega}$$

$$Z_L = R_L = 10^3\ \Omega$$

$$A = 5 \times 10^3$$

It is obvious that any stray capacitance at the photomultiplier dynode (~ 10 pf), or any fluctuations in stray capacitance will be negligible, and will not affect the output signal.

3.3 Stability of Operational Amplifiers.

The stability and linearity of an operational amplifier can be appreciated if one calculates the change in gain due to changes in the amplifier components. Equation (II.12) gives the voltage gain as

$$G_v = \frac{V_o}{V_i} = -\frac{A}{A+F} \cdot \frac{Z_f}{Z_i} \qquad (3.8)$$

where $F = 1 + \frac{Z_f + R_b}{Z_L} \sim 6$ (3.9)

The effect of a change of value in each of the components is obtained by partial differentiation.

$$\frac{dG_v}{G_v} = \frac{F}{A+F} \cdot \frac{dA}{A} - \frac{1}{A+F}\left[\frac{Z_f}{Z_L} \cdot \frac{dZ_f}{Z_f} + \frac{R_b}{Z_L} \cdot \frac{dR_b}{R_b} - \frac{(Z_f + R_b)}{Z_L} \cdot \frac{dZ_L}{Z_L}\right] + \frac{dZ_f}{Z_f} - \frac{dZ_i}{Z_i} \qquad (3.10)$$

Equation (3.10) shows that, even if the amplifier gain A ($\sim 10^4$) changes by 20%, the change in G_v is only 0.002%. The operational amplifier is obviously insensitive to changes in transistor gain and supply voltage. The second term can be shown to be as insensitive to changes in impedances as the first term is to gain changes.

If Z_i and Z_f have the same temperature coefficient of impedance, then the last two terms will cancel for temperature changes. Using 1% high stability resistors, the contribution of the last two terms can be made sufficiently small.

An analysis of the current gain will give similar results. The operational integrator, on the other hand, gives somewhat different results in that the output is more strongly dependent on the passive feedback element C_f. However, very stable capacitors are available, and can be used if necessary.

Since most non-linearity arises from transistor gain, equation (3.10) shows that the operational amplifier is extremely linear. It is this good linearity and high gain stability, along with the flexibility for mathematical operations, that makes the operational amplifier highly suitable for the Sum-coincidence Spectrometer.

CHAPTER 4

THE HIGH VOLTAGE ATTENUATOR.

Figure 4.1 shows the circuit for the High Voltage Attenuator designed for use with the spectrometer. A conventional regulated high voltage power supply was used to supply the regulated DC voltage at the input. The attenuator was built to accept up to 2,500 VDC.

Basically the attenuator consists of two cathode followers, each providing an adjustable voltage drop with a low output impedance. Resistors R1 through to R12 provide two variable voltage attenuators. These dividers set a reference voltage for the grids of tubes V_1 and V_2. The cathode of each tube follows the voltage set by its grid.

Since the input voltage is highly regulated, and the output impedance of a cathode follower is low, the reference voltage generated on the variable divider guarantees that the output voltage is well regulated. Capacitors C1 and C2 are included to filter out any AC voltage resulting from the tube heaters. The voltage on either output is read by means of the D.P.D.T. switch S_2 and the 100 μ amp. meter.

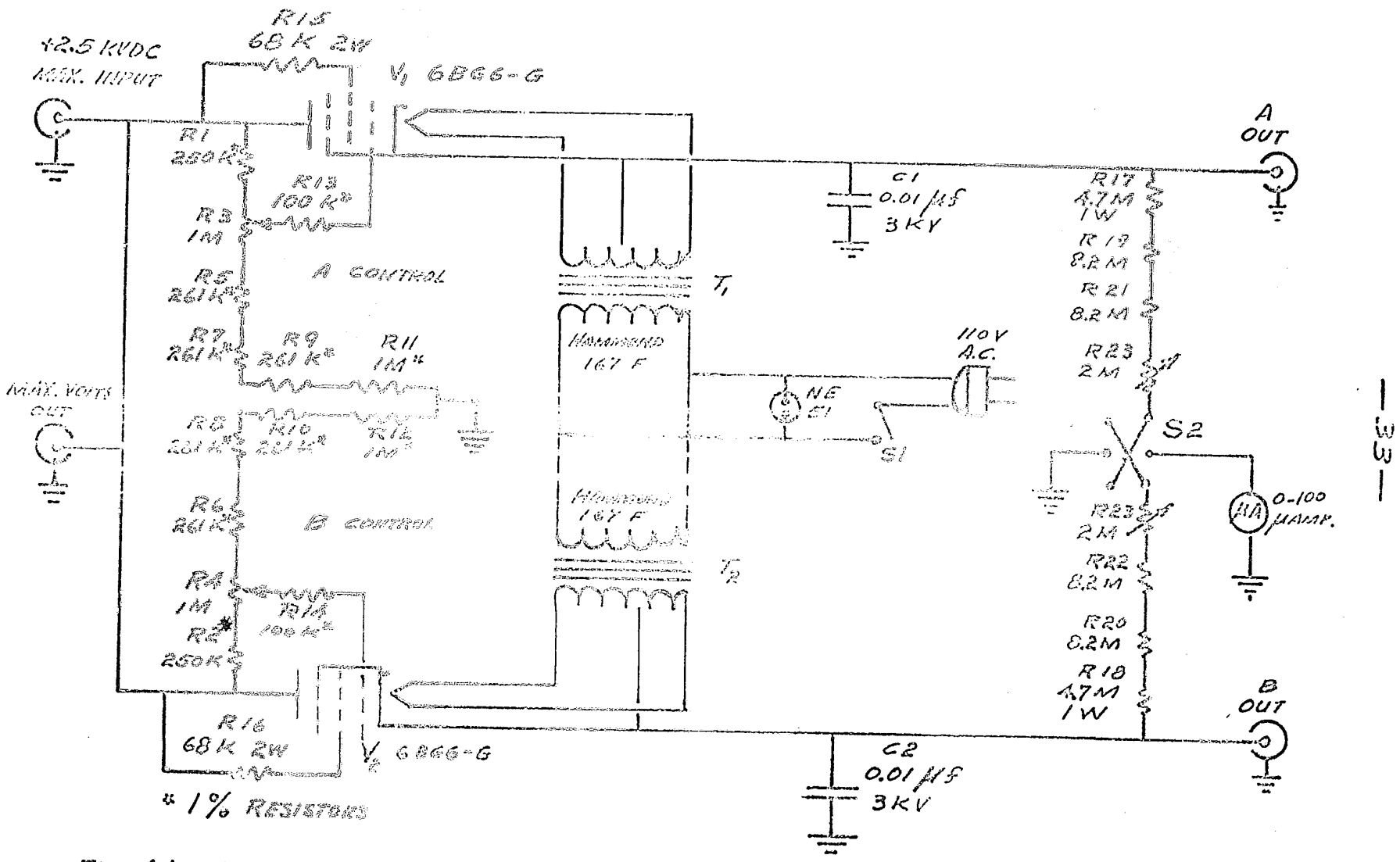

Fig. 4.1 THE HIGH VOLTAGE ATTENUATOR

The 6BQ6-G tubes cannot stand more than about 500 volts across them so they are mounted on a plexiglass chassis. The heaters are run at the cathode voltage. This was achieved by employing transformers capable of standing a high voltage between the primary and secondary windings. Precision resistors were used in the voltage divider to ensure a maximum stability. The transformers, the potentiometers R_3 and R_4, and their shafts were well insulated from the chassis with plexiglass.

Each channel output is individually controllable by about 25% of the input voltage. The output impedance is less than 5,000 ohms. In comparison with the photomultiplier load of about 1.5 megohms, this is a negligible impedance.

CHAPTER 5

THE PHOTOMULTIPLIER PREAMPLIFIERS.

5.1 Introduction.

Transistorized preamplifiers were designed and built to provide the necessary pulse height and time information derivable from the scintillation detectors. The preamplifiers include a high voltage bias chain for the photomultiplier, a slow channel for pulse height analysis, and a fast limiter for fast coincidence work, all within a 4" x 6" x 2" chassis. Both fast and slow outputs are capable of driving long, 100 ohm cables.

5.2 The Photomultiplier Voltage Supply.

The schematic drawing in Figure 5.1 shows the photomultiplier and its high voltage bias chain. The multiplier phototube used was an RCA 8054 tube. The dynode resistors were chosen to be 100K to ensure that the divider chain current would be large compared to the photomultiplier current. R13 and R15 are variable resistors which allow adjustment of the first dynode and focussing grid voltages for maximum gain. The ANODE H.V. INPUT is fitted to take a positive, regulated high voltage up to 2000 volts. A connector is also provided for supplying

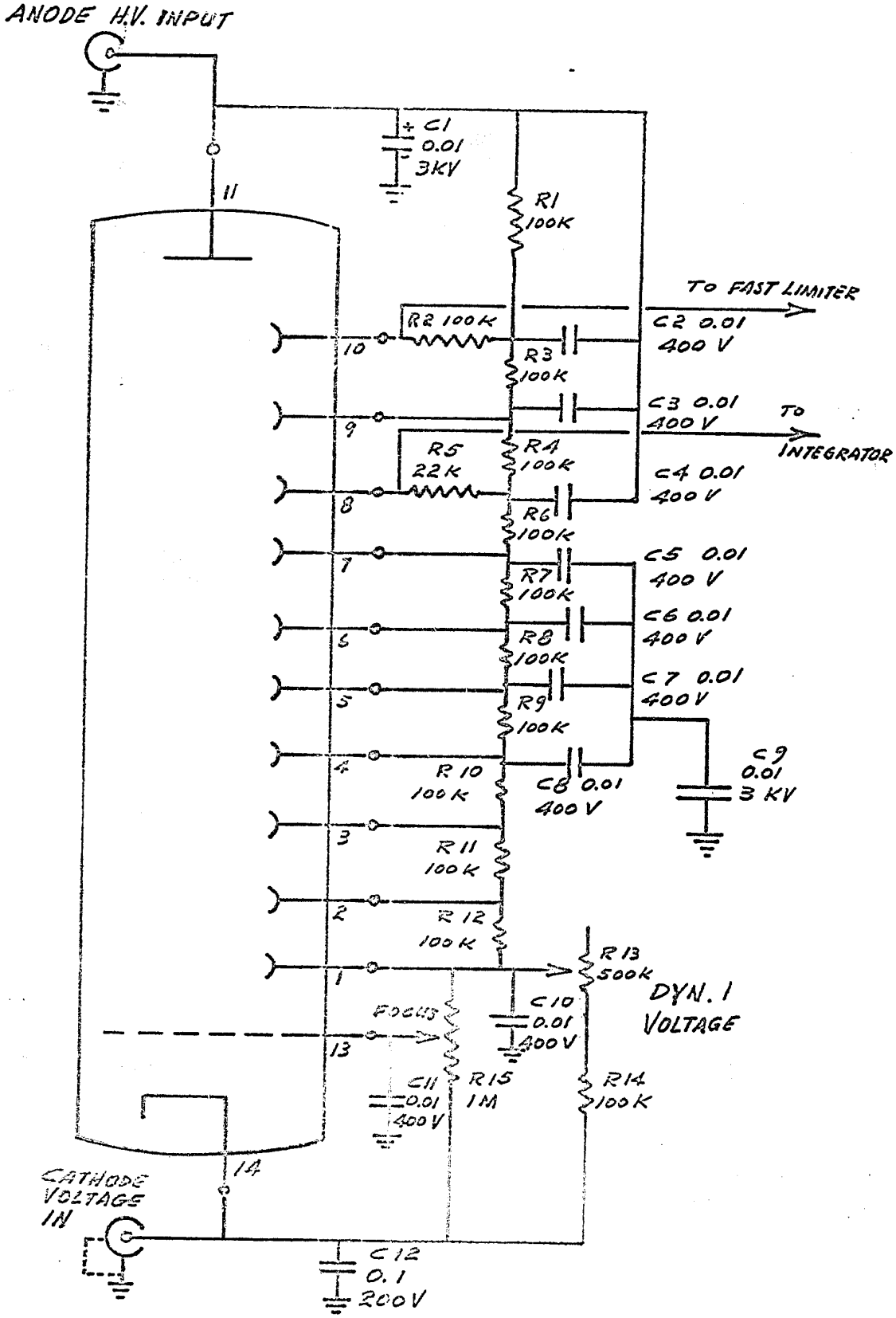

Fig. 5.1 MULTIPLIER PHOTOTUBE AND DIVIDER CHAIN

from zero to plus 200 volts to the cathode. This input was included to make the system adaptable to a gain stabilizer. Normally, the cathode is shorted to ground with a shorted B.N.C. plug.

In order to reduce stray noise pick-up, the outer aluminum shield on the integrally packaged detector was strapped to the preamplifier ground. Output pulses are fed to the fast limiter and the integrator from the tenth and eighth dynodes respectively.

Harshaw guarantees the resolution and gain stability of the scintillation detector at an anode voltage of about 1100 volts. For studying gamma-ray energies up to 2.7 MeV, it was possible to operate at 1400 volts. Above this value non-linearity of the phototube restricted the energy range to about 1.4 MeV.

5.3 The Slow Channel Preamplifier.

Figure 5.2 shows the preamplifier used to process the photomultiplier pulses for subsequent pulse height analysis. It is essentially an operational integrator as described in Chapter 2, and is similar to an original design by Goulding[18]. Transistors Q1 and Q2 comprise an amplifier with an open-loop current gain of about 5000. The capacitor C5 is the feedback capacitor, C_f, of the operational amplifier.

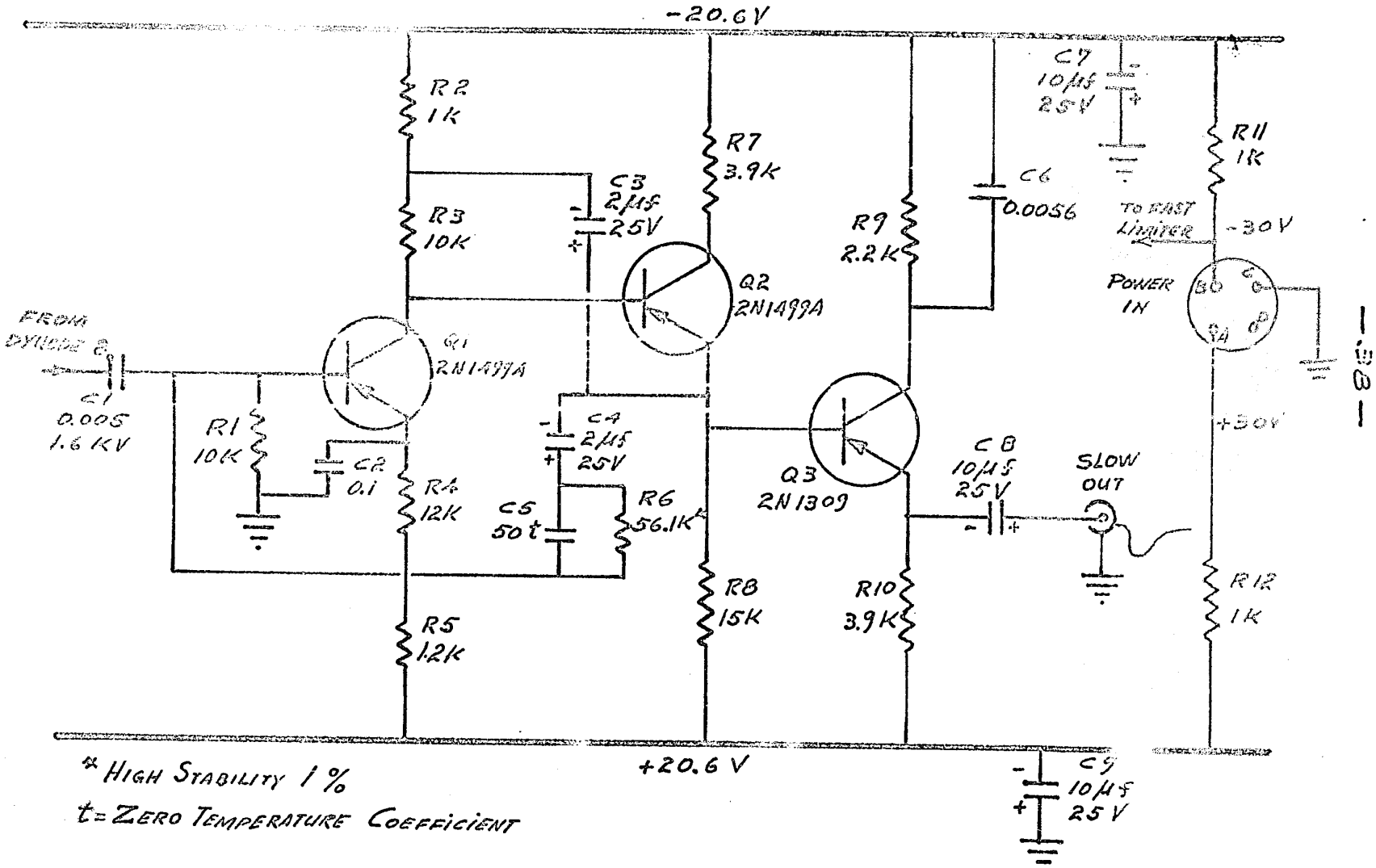

Fig. 52 SLOW CHANNEL INTEGRATOR PRE-AMPLIFIER

The emitter of transistor Q1 is biased to about +0.4 volts by the resistor R1. This sets the quiescent point of the collector of Q1 at about -5 volts. The emitter of Q2 "follows" this voltage.

When a current pulse arrives from dynode 6, it tends to turn Q1 off. This generates a negative voltage pulse at the collector of Q1. By virtue of the bootstrap through capacitor C3, the current which previously was drawn by the collector of Q1 is switched to the base of transistor Q2. Thus a current gain of β^2 exists between the base of Q1 and the emitter of Q2. For the 2N1499A the β is about 70.

As shown in Chapter 2, the 50 pf feedback capacitor C5 converts the amplifier into an operational integrator. The output voltage at the emitter of Q2 is

$$V_o = -\frac{1}{C_5}\int i_1 \, dt \qquad (5.1)$$

The resistor R6 in conjunction with C5 gives an exponential decay time of 2.8 μsec to the output pulse. C4 is included merely to decouple the DC voltages.

Q3 serves as an emitter follower to allow the integrator to drive a long 100 ohm cable. This prevents the capacitance of the cable from causing a phase shift in the feedback loop, thus avoiding ringing.

Good gain stability is achieved by using a zero temperature coefficient capacitor for C5, and a 1% high stability resistor for R6. As previously shown, the output voltage is independent of the transistor gain and the supply voltage. In addition non-linearity is negligible.

A calculation of the input impedance seen at the base of Q1 shows that the impedance is equivalent to about a 1.3 μf capacitor to ground. Clearly, stray capacitance can be neglected at the input.

The output pulse is negative, rises exponentially with a 0.25 μ sec time constant, and falls with a 2.8 μ sec decay time. The output noise has been measured to be less than 0.5 millivolts.

5.4 The Fast Limiter.

Figure 5.3 shows the fast limiter. Its design was based on a unit designed by Fraser and Tomlinson[19] at Chalk River for use with fast scintillators in neutron time of flight studies. Several modifications have been made to their original circuit (e.g. the addition of Q1).

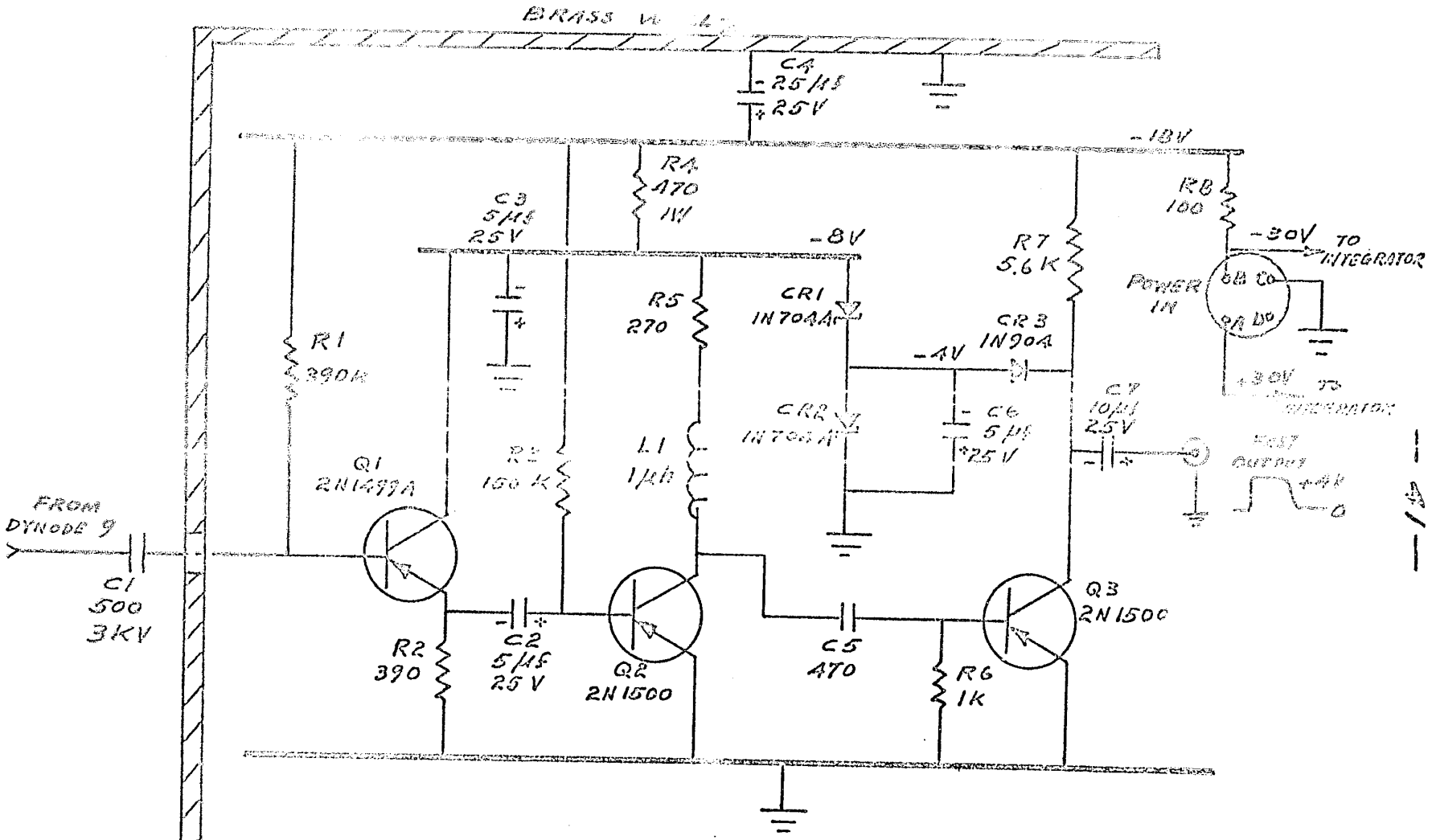

Fig. 5.3 FAST LIMITER PRE-AMPLIFIER

Transistor Q1 is an emitter follower. In the quiescent state, its emitter sits at about -2 volts. A positive pulse from dynode 10 tends to turn Q1 off and its emitter follows the input signal with a current gain of approximately 70. Q2 is held partially on by the 120 μamp current flowing in resistor R3. The positive pulse from Q1 turns Q2 off. Since Q2 is not in saturation, a high gain and fast rise time are achieved. Transistor Q3 is normally biased off. However, its collector voltage is held to -4 volts by the diode CR3. The negative pulse from the collector of Q2 turns Q3 on hard, giving a fast rising, 4 volt, positive pulse at the output on the collector of Q3. A terminated 100 ohm cable at the output is relied on to provide a low impedance load for Q3. This ensures a fast rise time. CR1 and CR2 are 4 volt Zener diodes included to set the proper voltages.

An input current to the base of Q1 of 2.3 μamp at 47 mV is sufficient to completely trigger transistor Q2. Using a mercury pulser, the minimum rise time of the output was found to be less than 3 nanoseconds, in good agreement with the value measured by Fraser and Tomlinson. Due to the rise time of the photomultiplier, the minimum

output rise time achieved in actual operation was about 6 nano-seconds. The pulse duration is about 700 nano-seconds.

Operating at an anode voltage of 1400 volts, the limiter triggered at a gamma-ray energy of from 10 to 20 KeV, depending on the individual photomultiplier. When the high voltage was increased to 1600 volts, a triggering level of less than 2 KeV was obtained. In this case, the equivalent noise level was about 0.5 KeV.

In order to prevent cross-talk to the slow channel, the fast limiter was carefully grounded and surrounded with a brass wall.

The output pulse from the limiter can be fed directly to a fast coincidence circuit, or to a time-to-amplitude convertor. A great advantage is gained in that no fast, distributed amplifiers are necessary to bring the limiter pulse to a workable level. The limiter preamplifier is very versatile. It can be used in conventional fast coincidence circuits or in a variety of timing experiments. The preamplifier has already been employed to observe gamma-rays from inelastic 14 MeV

neutron scattering on calcium†. There, the fast limiter was used in a time of flight technique with a time-to-amplitude convertor to separate the unwanted, delayed neutron pulses from the prompt gamma-ray pulses.

The possibility also exists of using the fast limiters in conjunction with Fraser and Tomlinson's time-to-amplitude convertor to operate as a fast coincidence unit. This suggestion is discussed in Chapter 9.

†Work done by W. J. McDonald at the University of Ottawa.

CHAPTER 6

TWIN AMPLIFIERS.

6.1 Design Aims.

In order to have a completely symmetrical and flexible system, two matched, or twin amplifiers were built. Adjustable components were included so that the pulse shapes in both channels of the system could be made identical. Both amplifiers were built into a single chassis along with a delay. Operational amplifiers, and 1% high stability resistors were used throughout to ensure a high degree of gain stability.

The amplifier included an RC differentiation, so that with the preamplifier pulse the whole system would provide double RC clipping. Inherent in the design was a non-overloading characteristic. The circuit was designed with a gain of about 140, variable down to 40; the useable positive output range being from zero to slightly over 10 volts. With the preamplifier attached, the output noise at maximum gain was ± 0.03 volts. In 10 volts, this gives a signal to noise ratio of 333:1. The noise due to the Twin Amplifiers themselves was ± 1 mV at minimum gain and ± 2 mV at maximum gain. This allows a signal to noise

ratio between 5,000:1 and 10,000:1 for the amplifiers alone.

As for the preamplifiers, an external, regulated power supply was used for the +30 and -30 volt lines.

6.2 Circuit Description.

Figure 6.1 shows the circuit used for both of the Twin Amplifiers. It consists of two operational amplifier units and an output stage. The operational amplifier units are a modification of the basic circuit first presented by Goulding[18,20].

Neglecting resistors R1 and R2, transistors Q1 and Q2 form an operational amplifier with a current gain variable between 5 and 10.2.

Transistors Q_1 and Q_2 provide an open loop current gain of about 20,000. Resistor R4 is the feedback resistor. The load resistance is a parallel combination of resistor R5 plus resistor R6 with resistor R9. The effective load is variable from 453 ohms to 921 ohms by means of the ten turn potentiometer R6. The operation of this stage is analogous to that of Q1 and Q2 in the preamplifier integrator, except that the negative feedback is applied through the resistance R4.

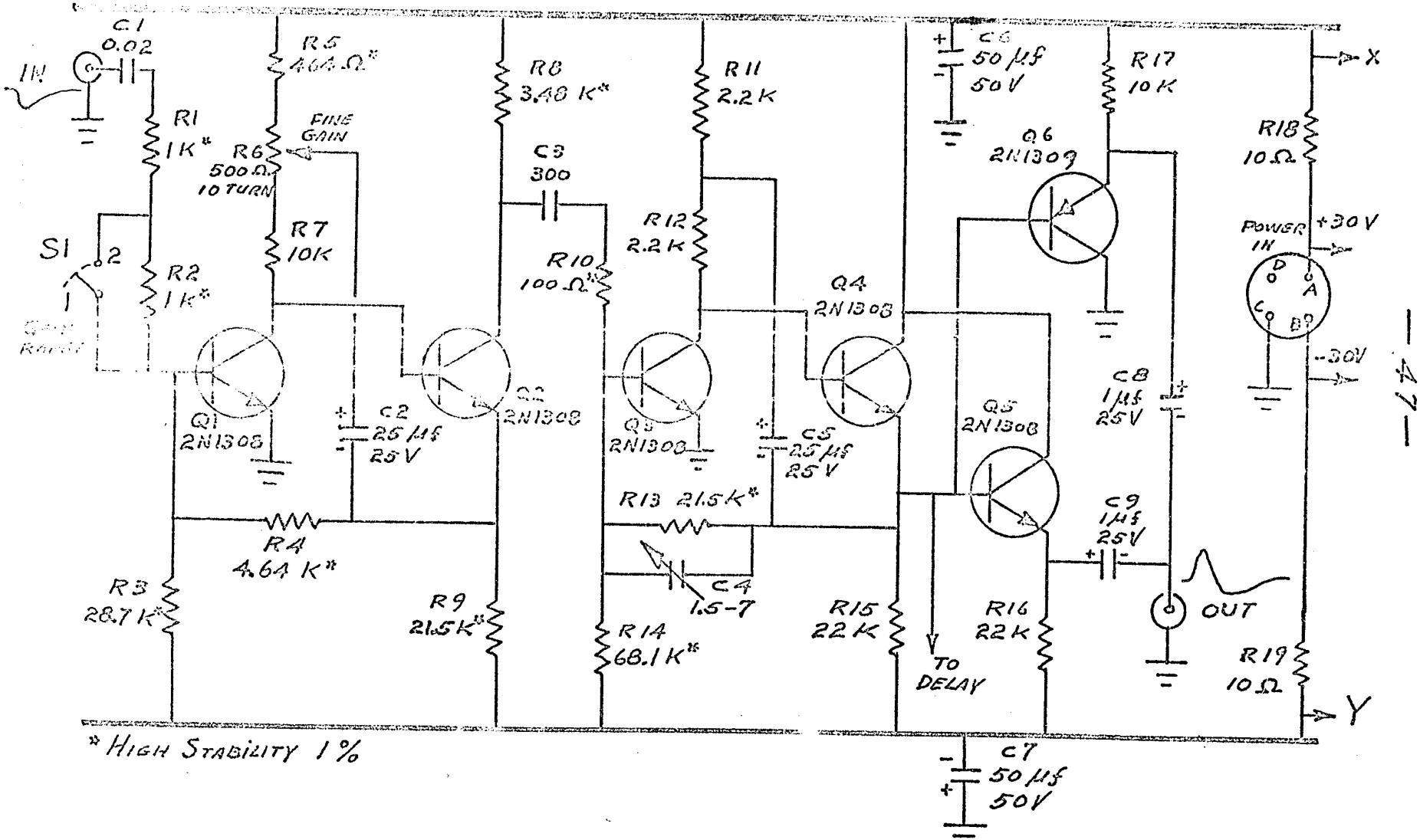

Fig. 6.1 THE CIRCUIT FOR EACH OF THE TWIN AMPLIFIERS

The output current of this stage is derived from the collector of Q2. The collector current is α times the emitter current. For the 2N1308, α is about 0.994. From equation (II.16) the collector current is calculated as

$$i_c = 0.994\, i_e = 0.994\left(\frac{R_4}{R_L}\right) i_i \qquad (6.1)$$

where i_e is the emitter current of Q2, i_i is the input current to the base of Q1, and R_L is variable from 453 ohms to 921 ohms. The current gain of this stage is therefore variable between 5 and 10.2.

The resistors R8 and R10 together with C3 give a differentiating time constant of 1.07 μsec. From this point on, the pulse is bipolar. The choice of a short time constant is made to minimize "pile-up" at high counting rates, while the double differentiation prevents base line shift.

Q3 and Q4 form another operational amplifier similar to the first stage. The difference here is that the output voltage and not the current is selected. Also, the gain is not variable.

From either equation (II.12) or equation (II.16) one can write

$$V_o = - i_i Z_f \qquad (6.2)$$

where V_o is the output voltage, i_i is the input current, and Z_f is the feedback impedance. For the second stage, this equation becomes

$$V_o = - i_i R_{13} \qquad (6.3)$$

Now, if the two stages are combined, and resistors R1 and R2 are taken into the calculation, the gain of the amplifier is

$$\frac{V_o}{V_i} = -0.994\left(\frac{R_4}{R_L}\right)\left(\frac{R_{13}}{R_i}\right)K \qquad (6.4)$$

where R_L is the load in stage one, variable between 453 ohms and 921 ohms, R_i is the input resistance to the amplifier, either $R_1 + R_2$ or R_1, and K is the attenuation factor due to the differentiation between stages. An approximate value may be obtained for K if we consider that the leading edge of the pulse is part of a sine wave whose period is 2 μ sec. This is a crude estimate, in that the factor K will depend very strongly on the input pulse shape. The magnitude of the impedance of C3 to the sign wave is 1.06 KΩ. Combining this with the values of R8 and R10 gives the value for K as 0.75. Putting this value in equation (6.4) gives, for the two extreme cases, a gain variable from 40 to 164. The measured values were 39 and 135.

Transistors Q5 and Q6 are complementary emitter followers for the output stage. Their voltage gain is nearly unity, and they have a 10 ohm output impedance. Using an N-P-N and a P-N-P transistor in parallel allows this stage to drive both positive and negative pulses with a low impedance. This is especially useful if the output must drive a long 100 ohm cable without pulse shape distortion. It is possible to drive the output directly from the emitter of Q4. However, if long cables are driven from this point, their capacity can introduce a phase shift in the feedback network and cause ringing.

The GAIN RANGE switch, S1, and the FINE GAIN control allow the gain to be varied from 25% to 100% of its maximum value. A single turn potentiometer was originally used for R6, but it was found to be too coarse to permit an accurate balance of the energy calibrations of the two channels.

The capacitor C4 permits a fine adjustment of the differentiating time constant between stages. Using this trimmer, it is possible to match the pulse shapes in the two channels. For the sum-coincidence technique, it is very important that the pulse shapes in both channels are identical.

The Twin Amplifiers accept negative pulses at the input and give initially positive, bipolar pulses at the output. With the pulse provided by the preamplifier, the cross-over on the output occurs 2 μ sec after the start of the pulse. The rise time of the output pulse is about 0.15 μ sec. The delay line is fed from the emitter of Q4, to prevent any change in the output pulse height due to the removal or addition of the delay line load.

6.3 The Delay Unit.

In order that the amplifier pulses would arrive at the kicksorter just after the gate pulses from the discriminator, the amplifier pulses had to be delayed by 3 μ sec. Figure 6.2 shows the delay circuit.

A 4,000 ohm, 1 μ sec/ft delay line was used. The switch S1 allowed the delay to be connected to whichever Twin Amplifier output was to be fed to the kicksorter. An operational inverter with a gain of unity and good gain stability provides the negative pulse required by the kicksorter. The HH4000 delay cable was placed outside the chassis, and was not wound over itself, in order to prevent cross-talk and stray pick-up. The delay was terminated in the 4.22 KΩ precision resistor, R1, which is the input resistor for the operational amplifier. The operational amplifier, composed of Q1 and Q2, is similar to those in

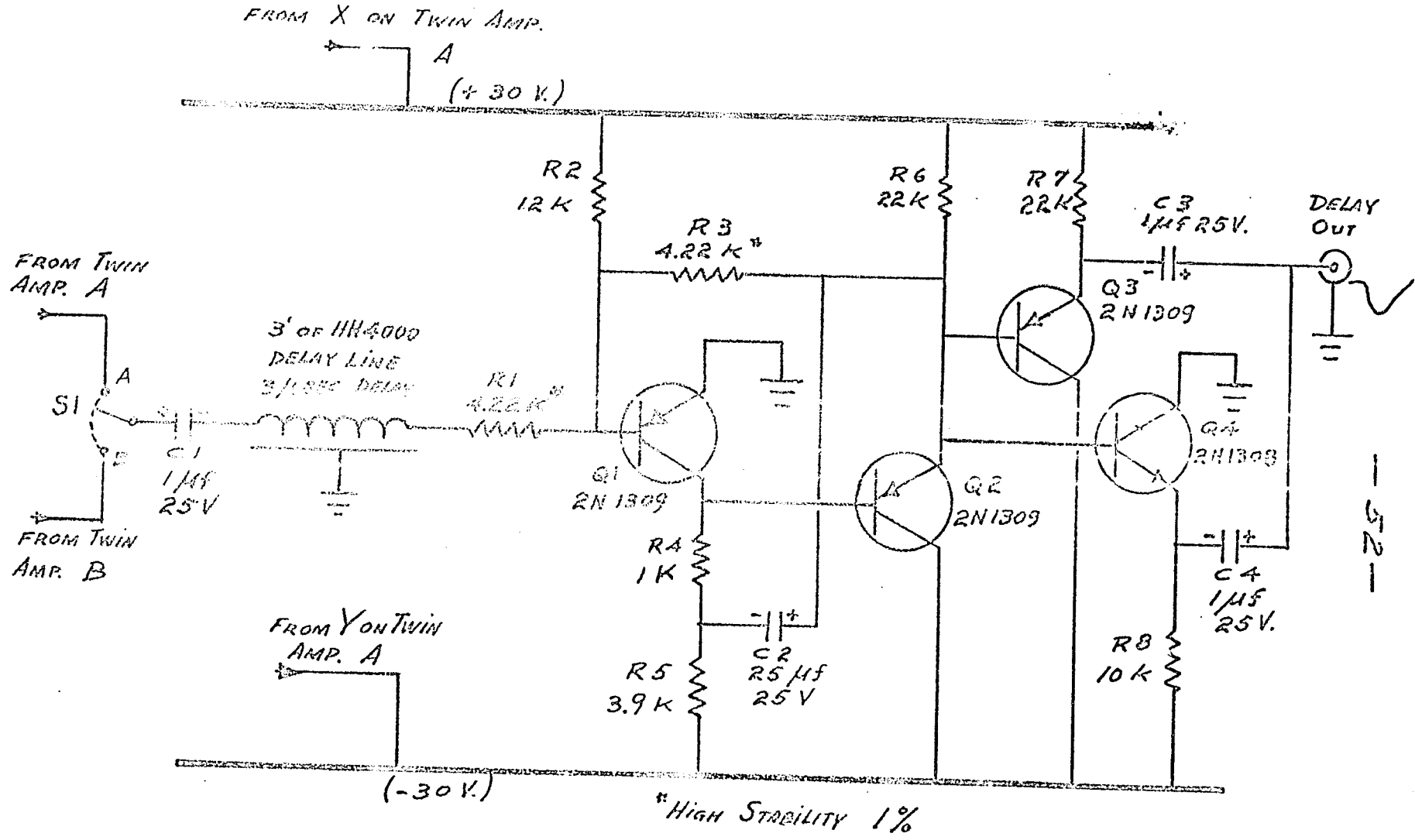

Fig. 6.2 TWIN AMPLIFIER DELAY UNIT

the Twin Amplifiers with a voltage gain of

$$\frac{V_o}{V_i} = -\frac{R_3}{R_1} = -1 \qquad (6.5)$$

Again, complementary emitter followers, Q3 and Q4 permit the invertor to drive a long 100 ohm cable.

CHAPTER 7

THE SUM AMPLIFIER

7.1 General Design.

The Sum Amplifier is an operational adding amplifier as described in chapter 3. It was designed to add the positive outputs from the Twin Amplifiers. A 3 μ sec delay was included so that, in conjunction with a fast coincidence, the kicksorter could record the channel A plus channel B spectrum. This mode of operation greatly improves the versatility of the sum-coincidence spectrometer, in that sum peaks corresponding to the total energies of the cascades may be observed, and the sum-coincidence window then set on each of these sum peak energies. This technique eliminates the necessity to blindly sweep the spectrum with the sum-coincidence window. The delayed output also allows one to check the gain calibration of the two channels through the Sum Amplifier on the kicksorter.

In order to drive the Franklin TEST INPUT, an attenuator and invertor stage was included. High stability, 1% resistors were used where necessary to guarantee a high gain stability. Since operational amplifiers were used, the addition was extremely linear and there was no cross-talk between channels.

7.2 The Operational Adder.

In Figure 7.1 the left side of the diagram, including transistors Q1 and Q2, performs the adding operation. Transistors Q1 and Q2, with their associated circuitry, form an operational amplifier similar to those described in chapter 5. The two inputs through resistors R3 and R5 give a gain

$$\frac{V_o}{V_i} = -\frac{R_7}{R_3 + \frac{R_4}{2}} = -0.99 \qquad (7.1)$$

where V_i is the input voltage and V_o is the output voltage at the emitter of Q2. As previously demonstrated, the output voltage at the emitter of Q2 will be

$$V_{o_{HL}} = -R_7 \left[\frac{V_A}{R_3 + \frac{R_4}{2}} + \frac{V_B}{R_5 + \frac{R_4}{2}} \right]$$

$$= -0.99 \ (V_A + V_B) \qquad (7.2)$$

where V_A and V_B are the respective input voltages. The resistor R_4 is included to balance the input resistor values.

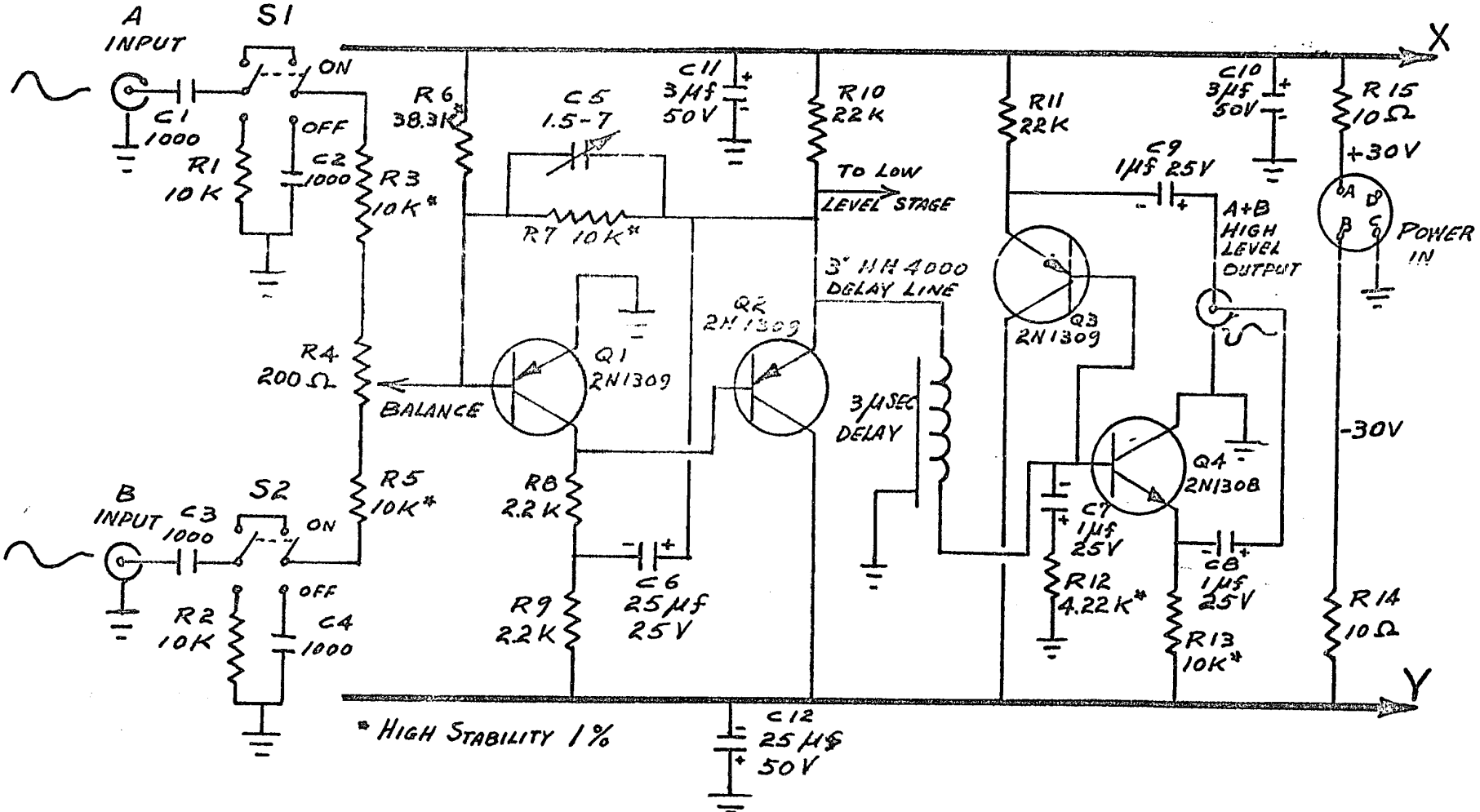

Fig. 7.1 THE HIGH LEVEL SECTION OF THE SUM AMPLIFIER

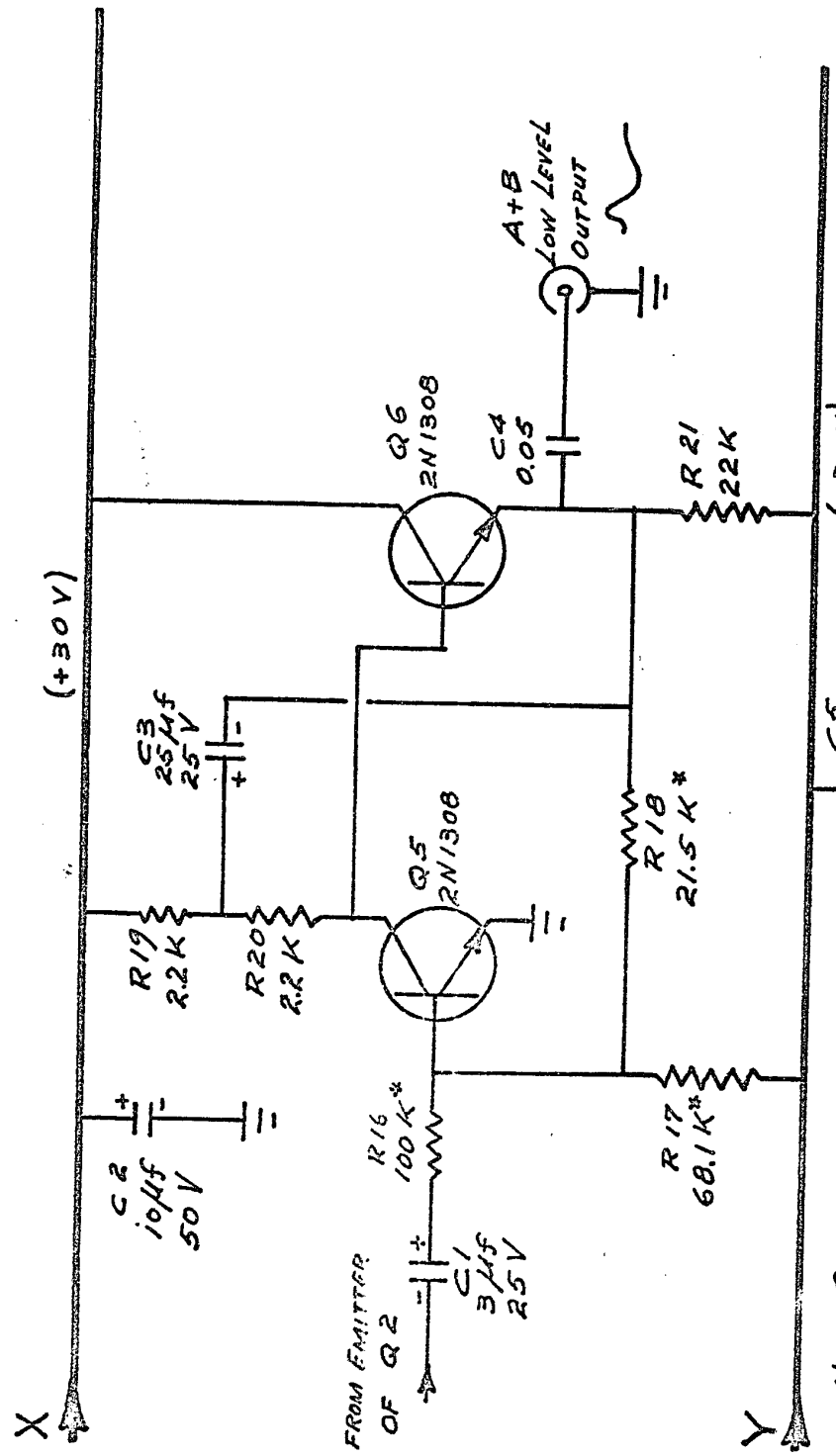

Fig. 7.2 THE LOW LEVEL STAGE OF THE SUM AMPLIFIER

The individual channels may be calibrated on the kicksorter by means of switches S_1 and S_2, without changing the impedance seen at either input. A provision is also made to ground R3 or R5 to prevent stray noise pick-up when that particular input is turned off. Capacitor C5 is used to compensate for the inductance in resistor R7.

Zero to +10 volt bipolar pulses are supplied to the A and B inputs from the Twin Amplifier outputs. The Sum Amplifier adds these pulses linearly and presents their inverted sum at the emitter of Q2.

7.3 The Delay.

The emitter of Q2 drives 3 feet of HH4000, 4000 ohm delay line. This length provides a 3 usec delay for the negative pulse. The delay line is terminated in 4.22 K by resistor R12. Q3 and Q4 are complementary emitter followers designed to drive the A + B HIGH LEVEL OUTPUT with a low impedance. This output is used to feed the kicksorter.

7.4 The Low Level Stage.

In order to compensate for the gain provided by the Franklin TEST INPUT, it was necessary to attenuate and invert the signal from the emitter of Q2. This was achieved

by using the operational amplifier shown in Figure 7.2. This circuit was included in the same chassis. The points X and Y are common points in the two diagrams. The low level stage is an operational amplifier with an input resistance of 100 Kn and a feedback resistor of 21.5 Kn. The gain of this stage is therefore

$$\frac{V_o}{V_i} = -\frac{R_{18}}{R_{16}} = -0.215 \qquad (7.3)$$

Using equation (7.2), the low level output voltage is seen to be

$$V_{o_{LL}} = 0.213\ (V_A + V_B) \qquad (7.4)$$

If, as was suggested earlier, a more appropriate pulse height analyser were built, the low level stage could be replaced with a complementary emitter follower stage identical to the output stage on the delay in Figure 6.2.

As in the Twin Amplifiers, the delay line was attached outside the chassis to prevent stray pulse pick-up from the amplifier itself. The input and output ends of the cable were well separated to prevent feed-through. This precaution is extremely important for a cable of such high impedance.

CHAPTER 8

THE FAST AND SLOW-COINCIDENCE UNIT.

8.1 Introduction.

A fast and slow coincidence system was designed to increase the flexibility of the spectrometer. Applied to the normal sum-coincidence mode, this system permits improving the spectrometer resolving time for cascade coincidences. The price for this improvement, unfortunately, is the loss of some of the information contained in the sum peak. Cross-overs are not observed in the fast coincidence mode. The system may also be operated as a conventional γ-γ spectrometer. One slow channel operates a window for a selected γ-ray energy, while the other channel records, on the kicksorter, all the gamma-rays in coincidence with this selected energy. In this work, the fast coincidence unit was used to gate the kicksorter when analysing the Sum Amplifier output. This technique yields all the energy peaks corresponding to the sums of two or more cascading gamma-ray energies.

For the sake of flexibility, the fast coincidence circuit was designed as a unit separate from the pre-amplifiers. A resolving time suitable for NaI(Tl) detectors was chosen.

The main building blocks for the unit were: (1) a pair of limiters operating a fast coincidence circuit, (2) a delay flip-flop, (3) a slow coincidence unit for use with a single channel analyzer pulse, and (4) a 5 μsec flip-flop to operate the kicksorter gate. All parts were built into a single chassis.

8.2 The Fast Coincidence Circuit.

Figure 8.1 shows the circuit for the fast coincidence. This is a transistorised design similar to a tube circuit designed by Bell, Graham and Petch[21]; although in their circuit the unit was fed directly from the photomultiplier anodes. Consequently, their fast coincidence output required further amplification by distributed amplifiers. On top of this, the rise time of the output pulse was strongly dependent on the pulse height at the photomultiplier anode.

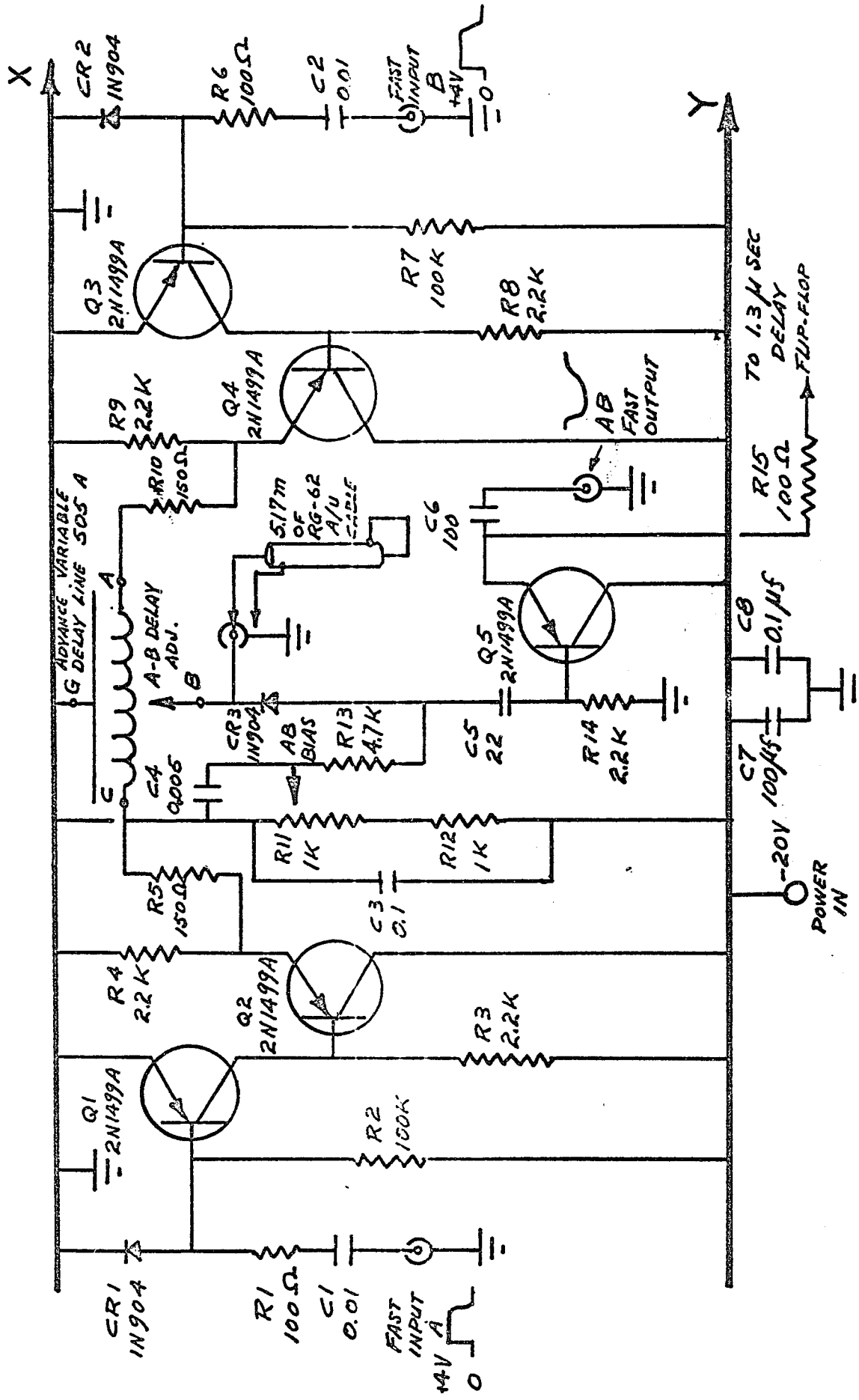

Fig. 8.1 THE FAST COINCIDENCE STAGE

In the transistorized system presented here, the input pulses provided for the fast coincidence unit have already been amplified by the limiter preamplifier. They are consequently characterized by a relatively standard rise time. No further amplification is required at the coincidence output.

The first stage of the fast coincidence is a pair of limiters. On input A this consists of transistors Q1 and Q2; on input B, Q3 and Q4 form an identical set. The purpose of the limiter is to define a standard pulse shape regardless of the input.

Transistor Q1(Q3) is held in saturation by the 0.2 ma current flowing in resistor R2(R7). A positive pulse applied to the FAST INPUT causes the supply of this current to switch from the base of Q1(Q3) to the resistor R1(R6). Consequently, Q1(Q3) turns off, giving a negative 16 volt pulse at its collector. Since only 0.02 volts is required at the input to switch Q1(Q3) off, the 4 volt pulse from the preamplifier turns Q1(Q3) off very quickly, and the pulse shape at the collector is independent of the input pulse. The rise time of the pulse at the collector of Q1(Q3) is the inherent turn off time of the transistor. Transistor Q2(Q4) is an emitter follower designed to drive this pulse into the variable 150 Ω delay line.

Resistors R1 and R6 are included to terminate the RG-62 cables coming from the preamplifiers. When Q1(Q3) is turned off, CR1(CR2) shorts the junction of R1(R6) to ground. This action prevents damaging the transistors with a reverse bias on the base. Since the diode CR1(CR2) is initially turned off, all the current from R1(R6) is used in turning the transistor off. A high gain results.

Resistors R5 and R10, added to the output impedances of transistors Q2 and Q4, match the 180 Ω input impedance of the Advance Variable Delay Line. The input pulse height becomes 9 volts at the delay line.

A 5.17 meter, 90 ohm, RG-62 shorting stub is hung on the delay line wiper. Provision is made for attaching different lengths of cable through a B.N.C. connector. Pulses arriving at the point B from either input are clipped to a standard 40 nsec length by the 5.17 meter shorting stub. Since the RG-62 cable sees the 180 ohm impedances from both ends of the variable delay line in parallel, its impedance is matched at the input. When a single pulse arrives at B from either input, it sees the 90 ohm impedance of the stub in parallel with the 180 ohms of the remainder of the delay line. The resultant impedance is 60 ohms. The pulse height seen at B for a

single input is therefore 4.5 volts. When two pulses arrive simultaneously from the two inputs, they add to give a 9 volt negative pulse. The coincidence event is therefore marked by twice the pulse height of the single event at B. The diode CR3 whose bias is set by resistors R11 and R12 can be adjusted to pass only the coincident events.

The emitter follower Q5 is included to drive a low impedance output. Q5 also drives the delay flip-flop through R15.

The AB FAST OUTPUT was primarily used for observing the addition of coincident pulses. The variable delay line A-B DELAY ADJ. control permits compensation for differences in the delays in the two input channels. The delays can be matched in two ways using the 0.511 MeV annihilation gamma-rays from Na^{22}. The coincidence counting rate can be plotted as a function of the variable delay position and the peak selected, or the addition can be observed on the AB FAST OUTPUT and the delay adjusted until the maximum pulse height and rate is observed. The second method is quicker, but the first method is more accurate.

If the pulse shape were exactly rectangular, one would expect the resolving time to be independent of the AB BIAS, above the bias required to reject single events. It would be determined solely by the clipping time of the shorting stub. Actually, the pulse seen at B has a rise time of about 8 nsec and does not have a flat top. Consequently, the resolving time of the circuit turns out to be a function of the AB BIAS. Figure 8.2 is a graph of the resolving time τ as a function of the AB BIAS. The AB BIAS readings are approximately 10 times the actual bias voltage. It is obvious that smaller resolving times than the basic 40 nsec can be obtained for higher values of the AB BIAS. Figure 8.2 also shows a curve for a 1.93 m. shorting stub. This is about the minimum practical length for use in the unit. The curve was measured using 4 volt pulses from a pulse generator with a 10 nsec rise time. If two pulses reach the point B within the time interval τ with respect to each other, they will register a coincidence according to Figure 8.2.

It will be noticed in Figure 8.2 that the bias voltage is lower than what one would expect to be necessary to differentiate between single and coincident events. This discrepancy is due to the loss of pulse height as the pulse travels through the circuitry to the delay flip-flop.

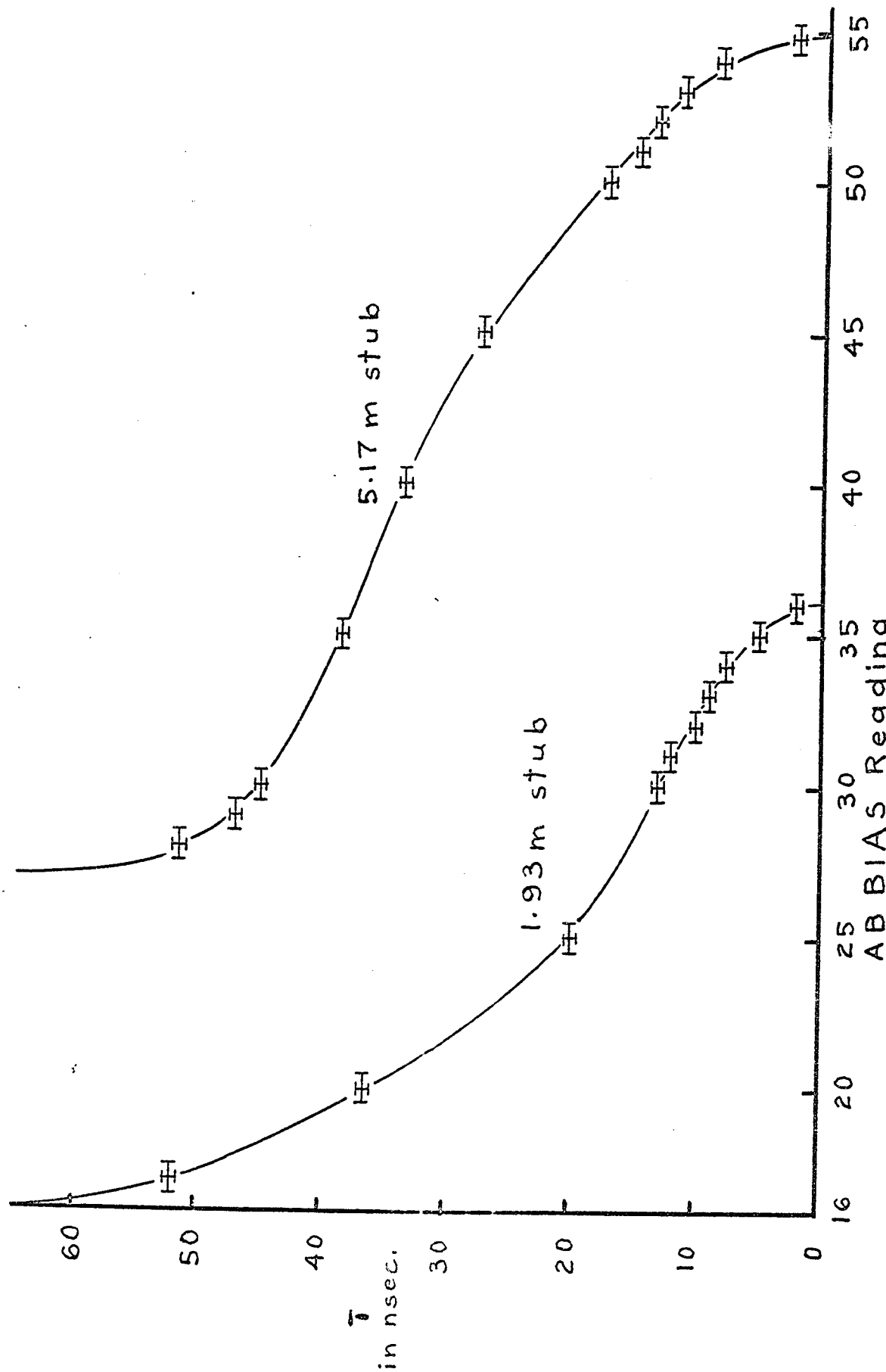

Fig. 8.2 The resolving time, $\bar{T}$, of the fast coincidence.

A much faster circuit could be built if shorter resolving times were required. For a faster design the limiter transistors should be replaced with a faster transistor such as the 2N976. The collector load should be changed to 180 ohms and the variable delay driven directly from this load. For higher speed the biasing should be changed so that the limiters were not held in saturation. For a faster response, the biasing arrangement with CR3 and Q5 including the delay flip-flop could be replaced by a fast trigger similar to the one given by Tomlinson and Fraser[19]. With a careful, fast design, no doubt, the resolving time of this circuit could be reduced by a factor from 5 to 10.

8.3 The Delay Flip-Flop.

The AB FAST OUTPUT is fed through resistor R15 to the delay flip-flop shown on the left side of Fig. 8.3. The circuit performs two functions. First of all, it provides a standard triggered pulse initiated by the fast coincidence pulse. Secondly, by differentiating the output pulse and selecting the trailing edge, a delay is obtained. This delay can be adjusted to match the delay in the rest of the logic circuits.

Transistor Q6 is normally held off by resistor R19. Consequently transistor Q7 is held on hard by resistors R16, R17 and R20. A negative pulse at the base of Q6 causes Q6 to turn on, turning off Q7. The

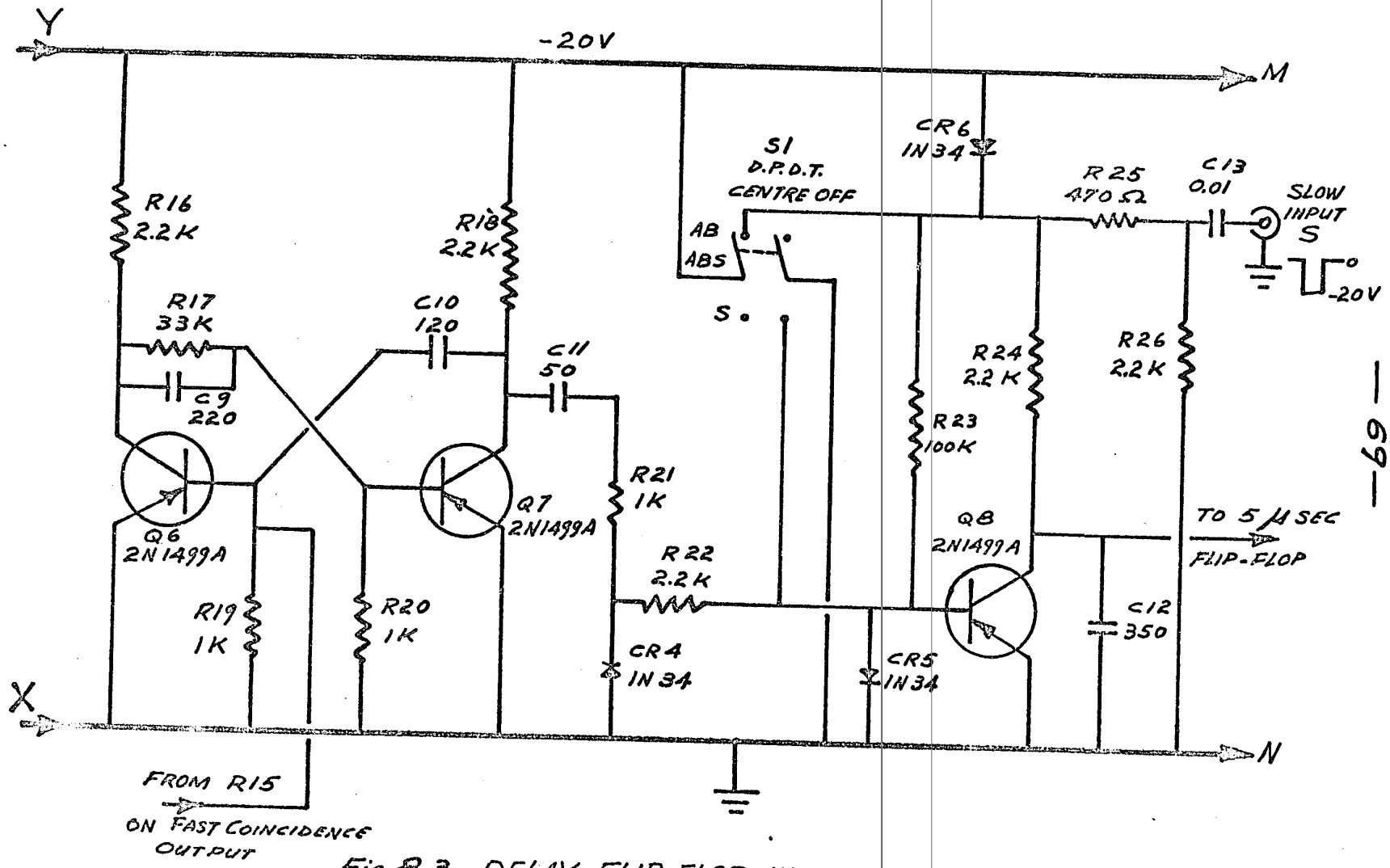

Fig. 8.3 DELAY FLIP-FLOP AND SLOW COINCIDENCE

regenerative feedback through the capacitor C10 makes the switching fast and keeps transistor Q7 off for 1.3 μsec. At the end of this period the circuit quickly returns to its original state. The output seen at the collector of Q7 is a negative 20 volt rectangular pulse of 1.3 μsec duration.

Capacitor C11 and resistor R21 differentiate the output giving a negative spike followed, 1.3 μsec later, by a positive spike. Diode CR4 clips off the negative pulse and allows the positive pulse to pass on to the slow coincidence. By changing C10, the delay can be adjusted to match the arrival time of the slow logic pulse at the SLOW INPUT S.

8.4 The Slow Coincidence.

The remainder of the circuit in Figure 8.3 is associated with the slow coincidence unit. The switch S1 selects one of three different modes of operation. In the position S, the negative 20 volt pulse from the SLOW INPUT S (usually driven by the sum window logic pulse) is allowed to pass through resistor R24 to the 5 μsec flip-flop. This mode is used to operate the equipment in the sum-coincidence configuration. When the switch is in the AB position, the fast coincidence circuit

feeds the 5 usec flip-flop. This allows operation in the fast coincidence mode. When the switch is in the ABS position, the transistor Q8 allows a pulse to pass on to the 5 usec flip-flop only when there is a slow coincidence between the fast coincidence pulse and the SLOW INPUT S.

Consider first the operation in the ABS mode. Suppose that a negative 20 volt pulse arrives at the SLOW INPUT without a fast coincidence pulse arriving at the base of Q8. The negative pulse will be applied to the collector through resistor R24. On the other hand, resistor R23 also applies this pulse to the base of Q8, turning the transistor on hard. As a result, no pulse is observed at the collector of Q8. The capacitor C12 is included to compensate for the delay caused by the turn on time of the transistor.

In order to have a negative pulse appear at the collector of Q8, a positive pulse must arrive at the base to turn the transistor off at the same time that the negative pulse arrives at the junction of R23 and R24. Hence, a negative output registers a coincidence between the SLOW INPUT and the fast coincidence pulse.

CR5 prevents the base of Q8 from being excessively back biased. CR6 limits the input pulse to 20 volts. A 4 volt pulse at the SLOW INPUT was found to be the minimum required pulse height.

When the switch S1 is in the AB position, Q8 operates as a switching transistor, giving a negative pulse at the collector every time a positive fast coincidence pulse is fed to the base.

In the S mode, transistor Q8 is simply held off so that every SLOW INPUT pulse drives the 5 usec flip-flop.

6.5 The 5 usec Flip-Flop.

Figure 6.4 shows the 5 usec flip-flop used to drive the kicksorter gate. Both plus 6 volt and minus 15 volt output pulses are available. The +6 volt output is used for the Tullamore, Victoreen kicksorter, while the -15 volt pulse accommodates the C.D.C., 100 channel kicksorter.

Transistor Q10 is normally held on hard by R32 and R34. This keeps transistor Q9 off. A negative pulse from the collector of Q8 causes Q9 to turn on, turning Q10 off. Due to C17, the circuit stays in this state for 5 usec, then sharply returns to its original state.

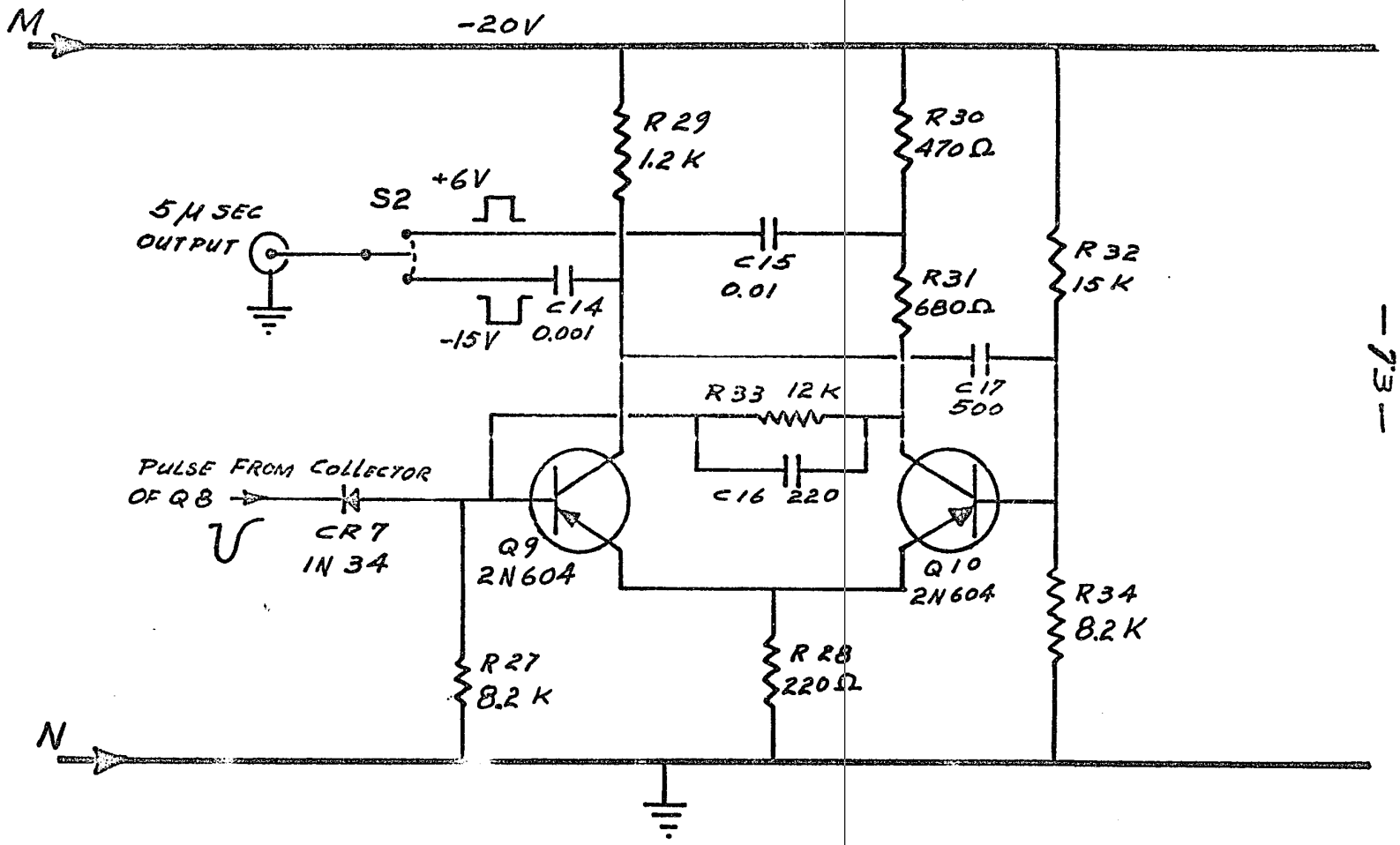

Fig. 8.4 - 5 μ SEC. OUTPUT FLIP-FLOP

The switch S2 permits driving either +6 volt or -15 volt, 5 usec pulses into the output. The diode CR7 is included to prevent the trailing edge of the input pulse from turning off the flip-flop.

CHAPTER 9

TIME RESOLUTION STUDIES.

9.1 Aim of the Study.

Since such a low level of limiting was achieved with the preamplifier fast limiter, it was decided that it would be interesting to see what time resolution was obtainable. Information on time resolution as a function of the γ-ray energy should provide a guide to the selection of the optimum resolving time in the fast coincidence unit.

Unfortunately, the time during which equipment was available for these experiments was limited. As a result, the quality of the measurements could be improved. However, they provide a rough indication of what is involved, and give some support to a theoretical argument.

9.2 The Method.

Figure 9.1 shows a block diagram of the equipment employed. The preamplifier fast limiter outputs were fed into a time-to-amplitude convertor (T.A.C.) similar in design to that of Tomlinson and Fraser[19]. The output of

the T.A.C. was processed by a 200 channel analyser.

The slow outputs of the preamplifiers were passed through linear amplifiers to single channel analysers (S.C.A.). A slow coincidence between the two S.C.A. outputs was used to gate the kicksorter. In this way, the time spectrum could be observed on the kicksorter for selected γ-ray energy ranges in each detector.

A Co^{60} γ-ray source was used. The photomultipliers were operated with high voltages between 1500 and 1600 volts. For a better analysis a source with energies available up to 3 MeV, and down to about 30 KeV should be used. These experiments should also be repeated for lower photomultiplier voltages.

9.3 The Time Measurements.

Figure 9.2 shows the ungated time spectrum where all energies were allowed to operate the T.A.C. The peak marks zero time, where both γ-rays were of the same energy. The shoulder on the extreme right marks the case where a low energy γ-ray was accepted in detector A while one of high energy was detected in channel B. The shoulder on the left represents the opposite case. The half width for 90% of the counts is seen to be 12.7 nsec.

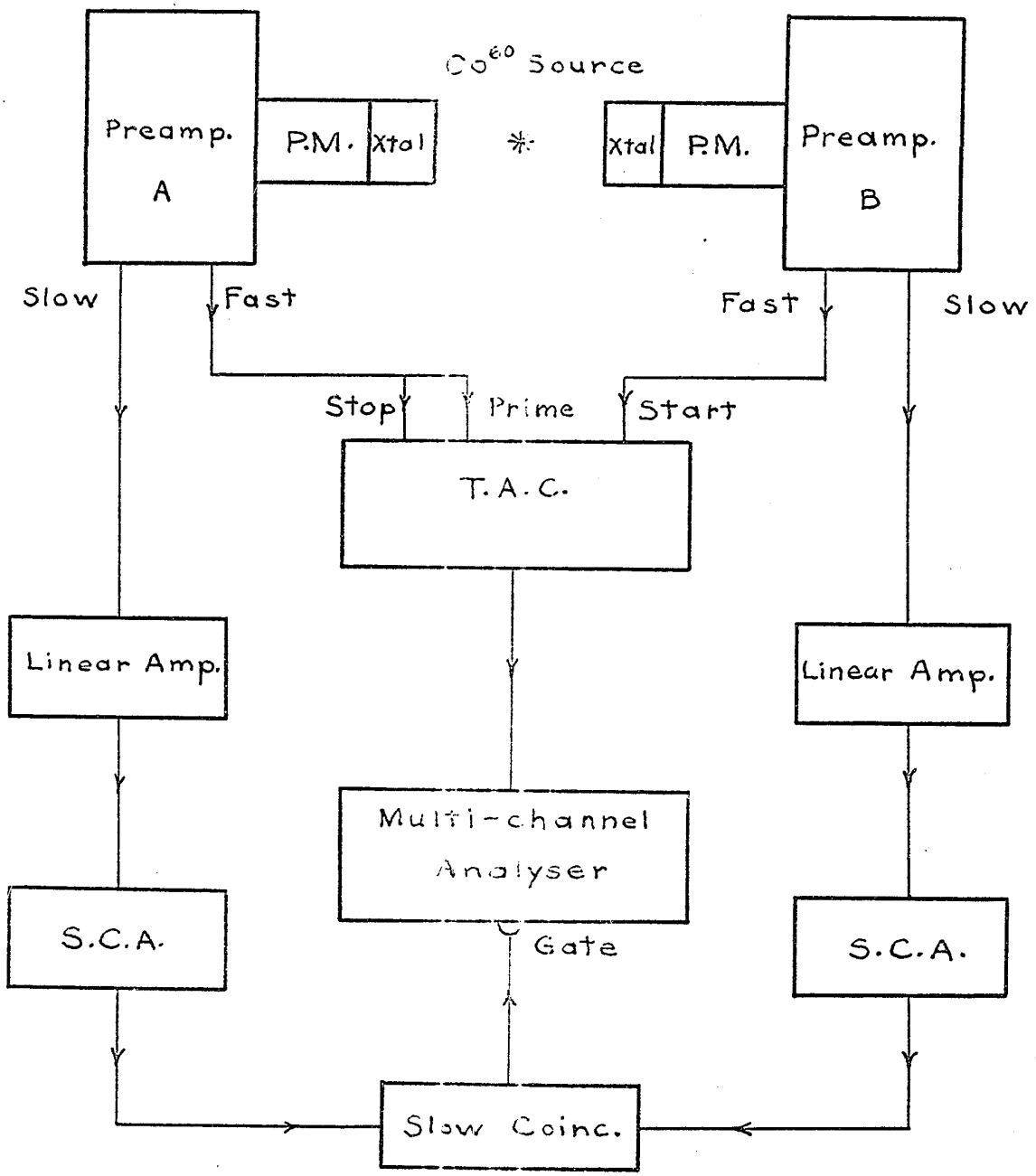

Fig. 9.1. The circuit for time resolution studies.

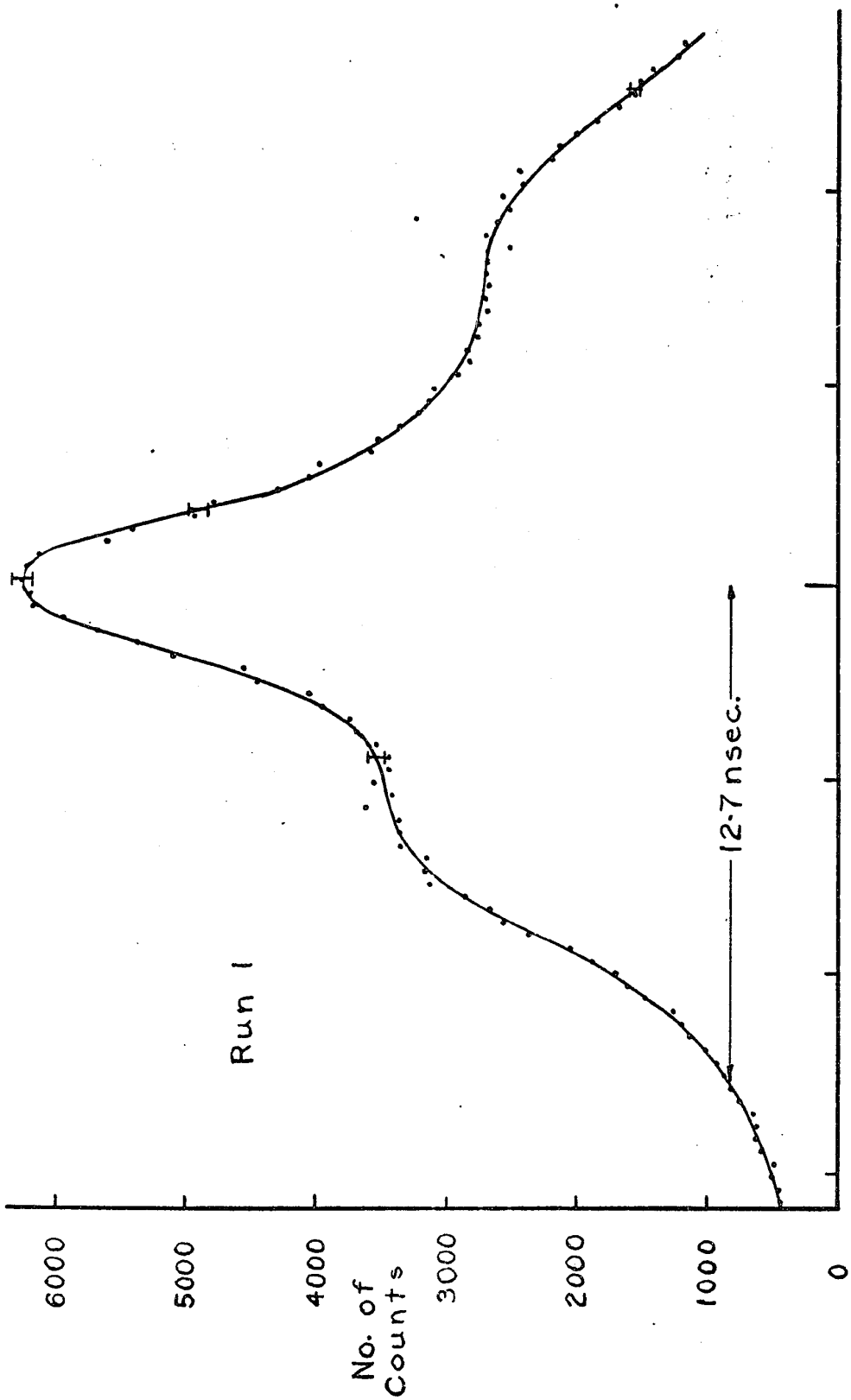

Fig. 9.2. The time spectrum for Co^{60} γ-rays.

For Figures 9.3 to 9.7 the single channel analyser in channel B was set on the Co^{60} 1.33 MeV peak while a series of lower energy settings were selected in channel A. Each peak obtained represents the time relationship between a 1.33 MeV γ-ray in detector B, and a lower energy absorbed in detector A.

Several features are noticeable in these spectra.

(1) As the energy of the gamma-ray decreases, the width of the time peak increases.

(2) As the γ-ray energy decreases, the centroid of the peak shifts.

(3) The time shift is not linear with energy.

It should be noted that the width of the time peak, within which 90% of the counts fall, varied from 4.79 nsec for a 1.33 MeV and 1.17 MeV pair up to 6.25 nsec for a 1.33 MeV and 0.28 MeV pair. This should be compared to a shift in the peak for the same energy range of from 0.33 nsec to 9.63 nsec. This indicates that the shift in the statistical time peaks was the major contribution to the width of the peak in Figure 9.2. For this reason it is desirable to take steps to eliminate this contribution in order to improve the operation of the fast coincidence circuit.

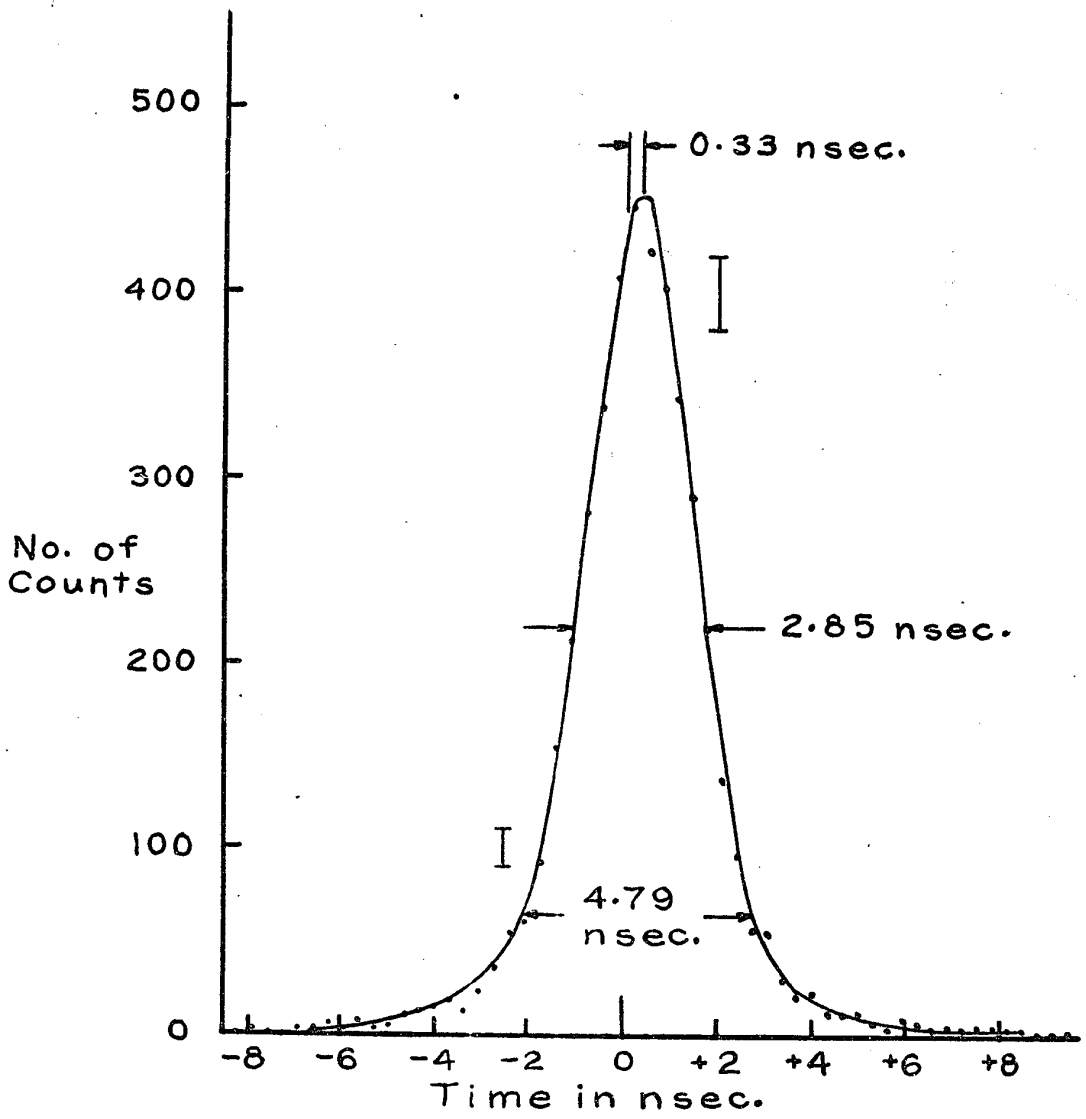

Fig. 9.3. Time spectrum for Co^{60}, 1.33 MeV and 1.17 MeV energies.

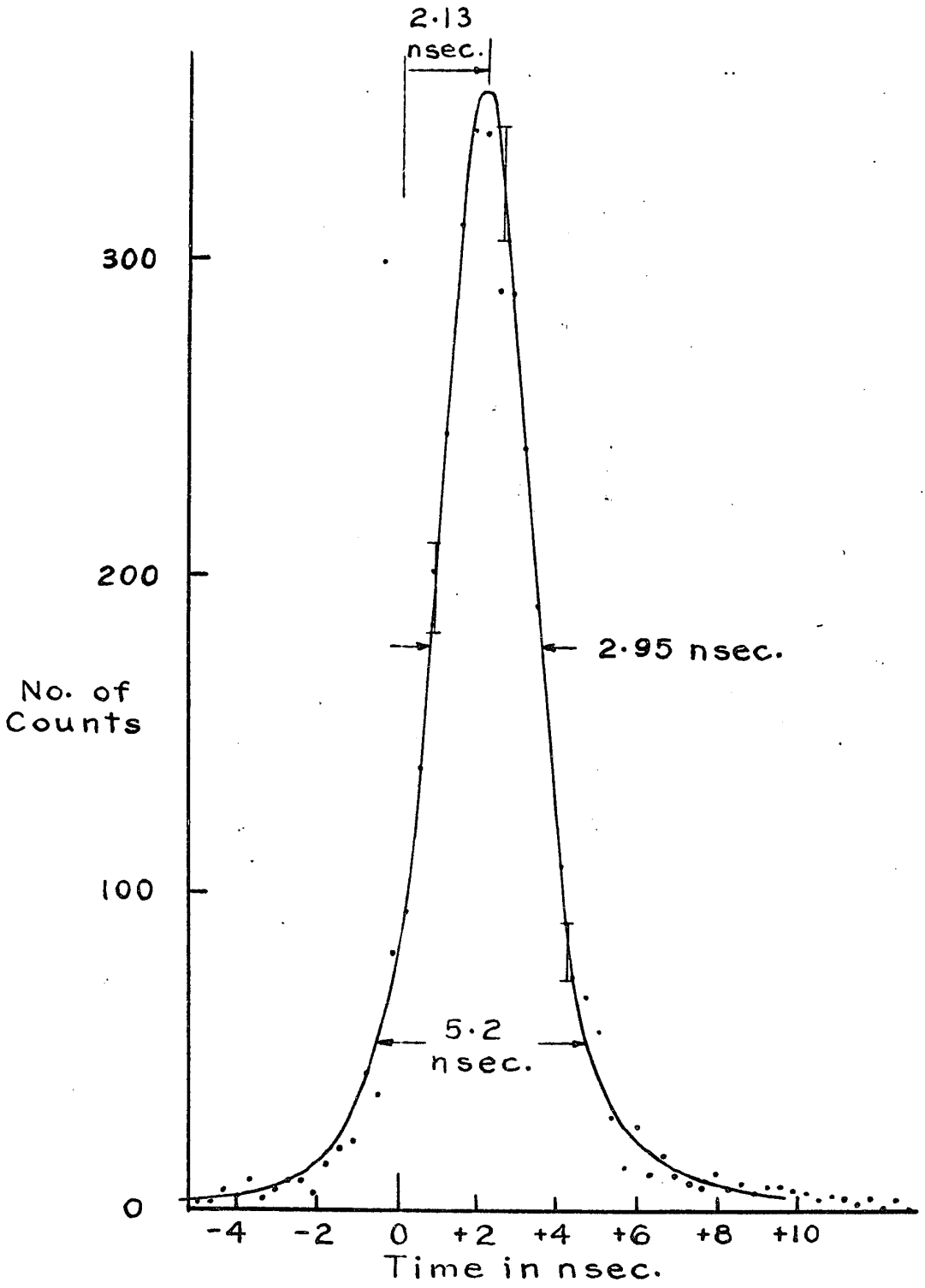

Fig. 9·4. Time spectrum for Co^{60}, 1.33 MeV and 0.85 MeV energies.

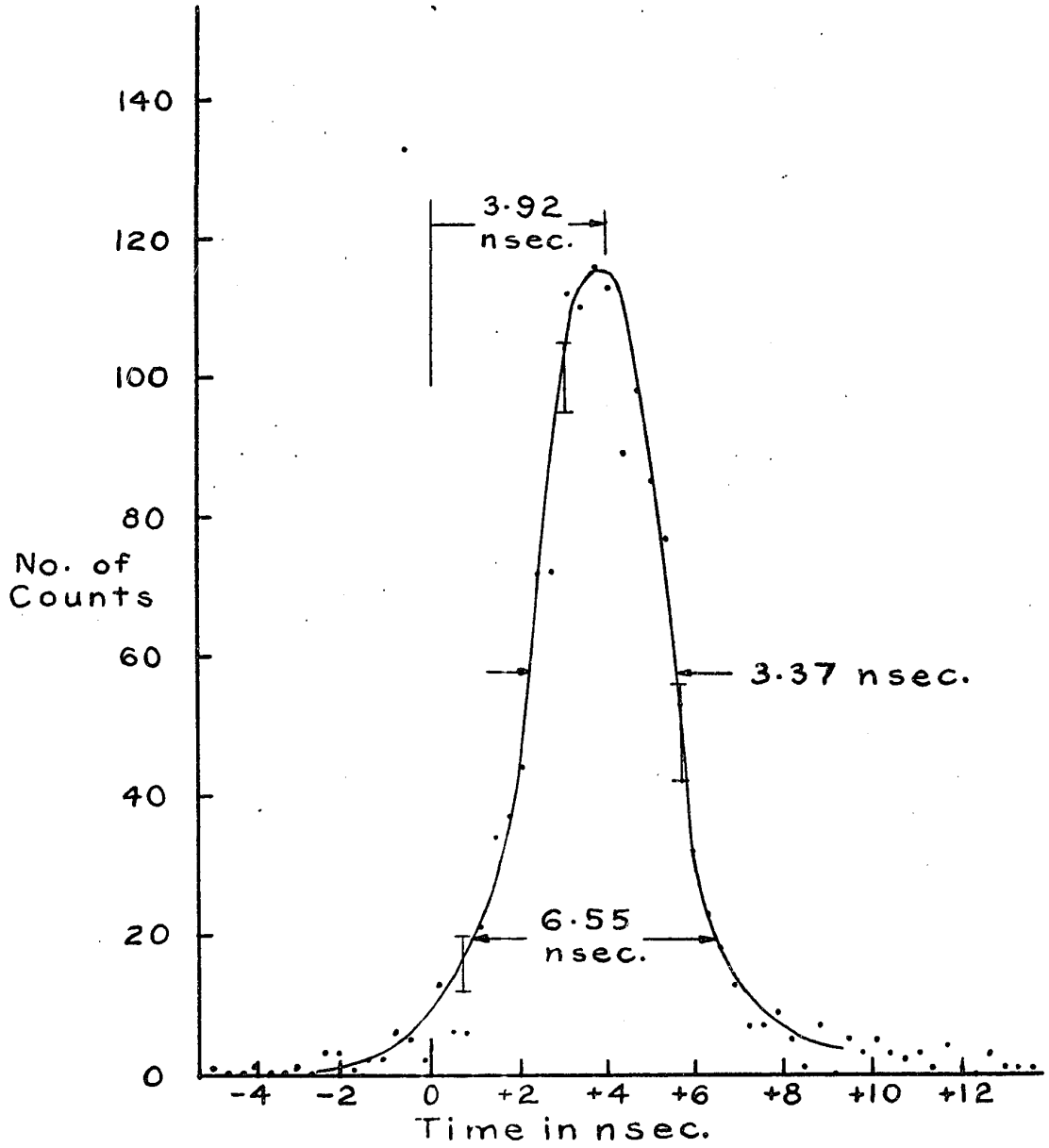

Fig. 9.5. Time spectrum for Co^{60}, 1.33 MeV and 0.62 MeV energies.

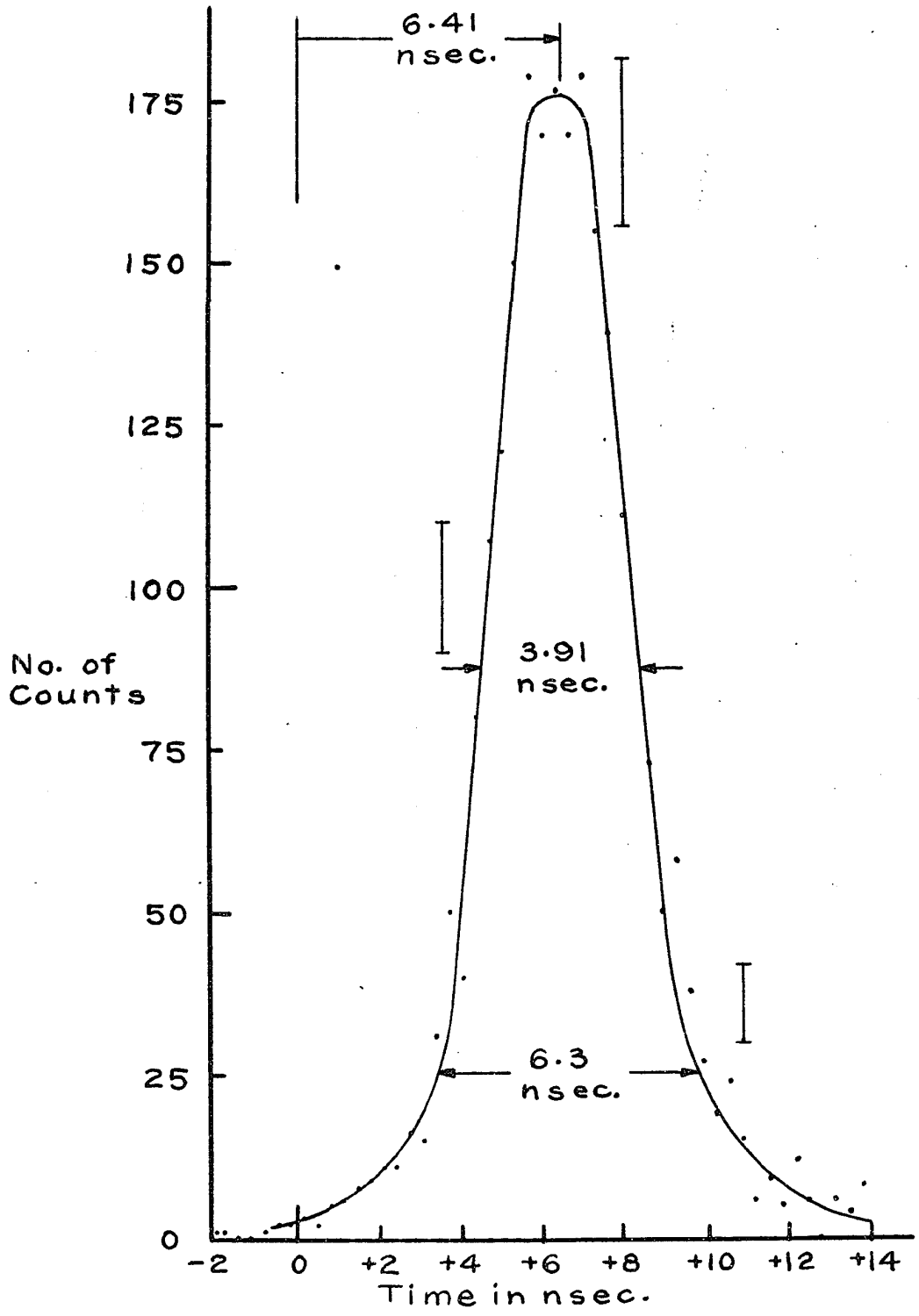

Fig 9.6. Time spectrum for Co^{60}, 1.33 MeV and 0.537 MeV energies.

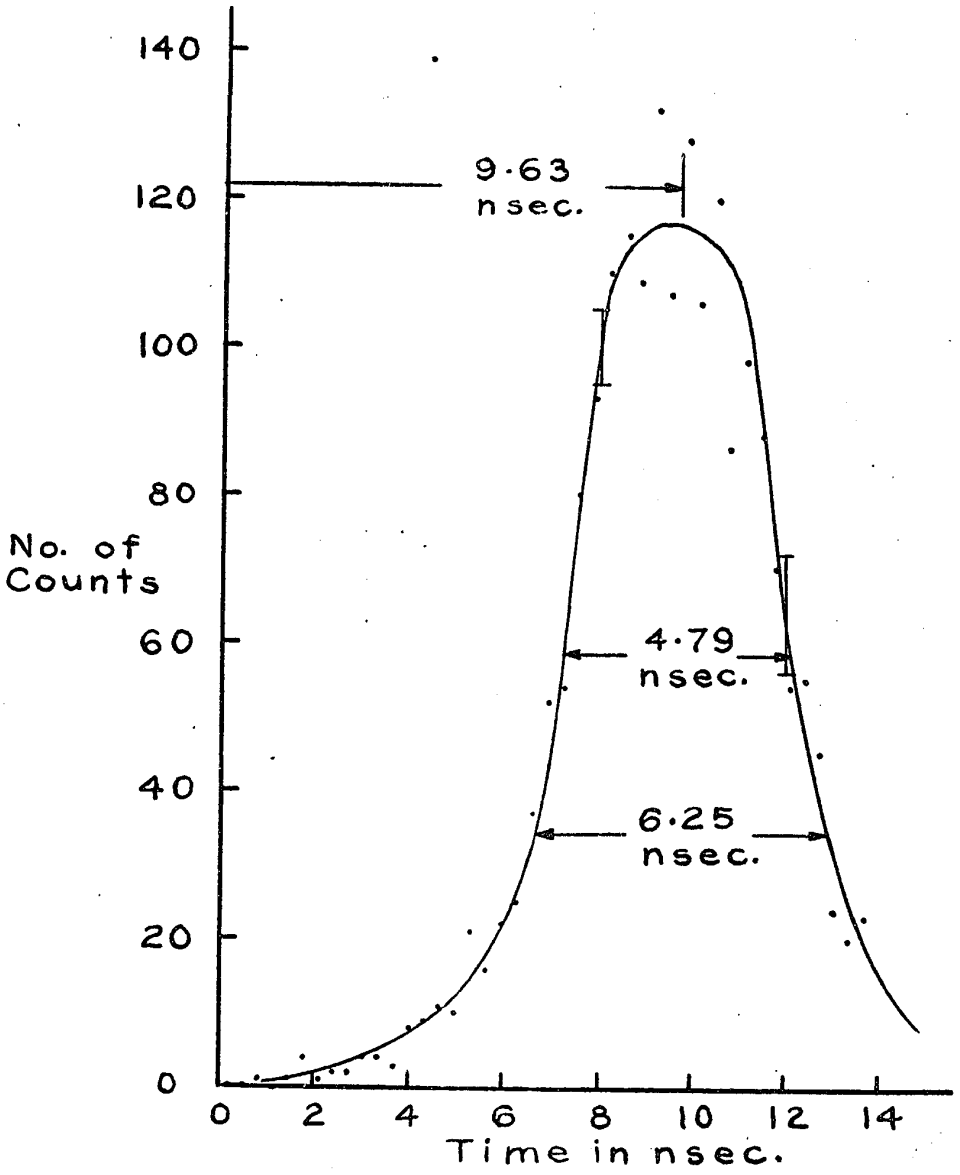

Fig. 9.7. Time spectrum for Co^{60}, 1.33 MeV and 0.28 MeV energies.

9.4 The Theory of Post and Schiff.

Post and Schiff were the first workers to consider the theory of time resolution in photomultipliers[22]. They developed expressions for the variance, v, and the average value, $\bar{t}$, of the machine time. The machine time is defined as the time interval between the interaction of the radiation with the scintillator, and the time defined by the electronic trigger mechanism. In their analysis they effectively considered contributions from the decay time of the scintillator, and fluctuations in photoelectron emission. Their model assumes that the output current of the photomultiplier is integrated on stray capacitance. A charge C is presumed necessary to trigger the electronic time marker device. Their results are given in equations (9.1) and (9.2).

$$\bar{t} = \tau\left(\frac{C}{R}\right)\left[1 + \left(\frac{C+1}{2R}\right) + \ldots\ldots\ldots\right] \qquad (9.1)$$

$$v = \tau^2 \frac{C}{R^2}\left[1 + \frac{2(C+1)}{R} \ldots\ldots\right]$$

$$= \frac{\bar{t}^2}{C}\left[1 + \frac{(C+1)}{R} + \ldots\ldots\ldots\ldots\right] \qquad (9.2)$$

where τ is the scintillator decay time, and R is the average charge in a pulse for the γ-ray energy E. C and R are expressed in terms of the number of photoelectrons initiating the pulse.

The full width at half maximum (F.W.H.M.) of the time peak for two γ-rays in two detectors is given by

$$W_{1/2T} = \sqrt{(W_{1/2(1)})^2 + (W_{1/2(2)})^2}$$

$$= 2.36\sqrt{v_1 + v_2} \qquad (9.3)$$

Equation (9.2) predicts that a minimum F.W.H.M. should be obtained if C, the limiting level, is made to approach zero. For this case, or for very small values of C/R, $\bar{t}$ is proportional to $\frac{1}{R}$ or to $\frac{1}{E}$. Figure 9.8 shows a plot of $\bar{t}$ versus 1/E. The fact that the straight line through the experimental points does not pass through the origin indicates that the choice of zero time reference was incorrect. Note also the large experimental errors in the points representing lower values of E. The two points for the lowest E values do not fit well with a straight line. This discrepancy reflects the precision of the experiment.

Equations 9.2 and 9.3 predict that a plot of $W^2_{1/2T}$ against $(\frac{1}{E})^2$ should be a straight line for values of E where $C/R \ll 1$. Figure 9.9 is a graph of $(W_{1/2T})^2$ against $(1/E)^2$. The points fall reasonably well on a straight line within experimental error. The intercept

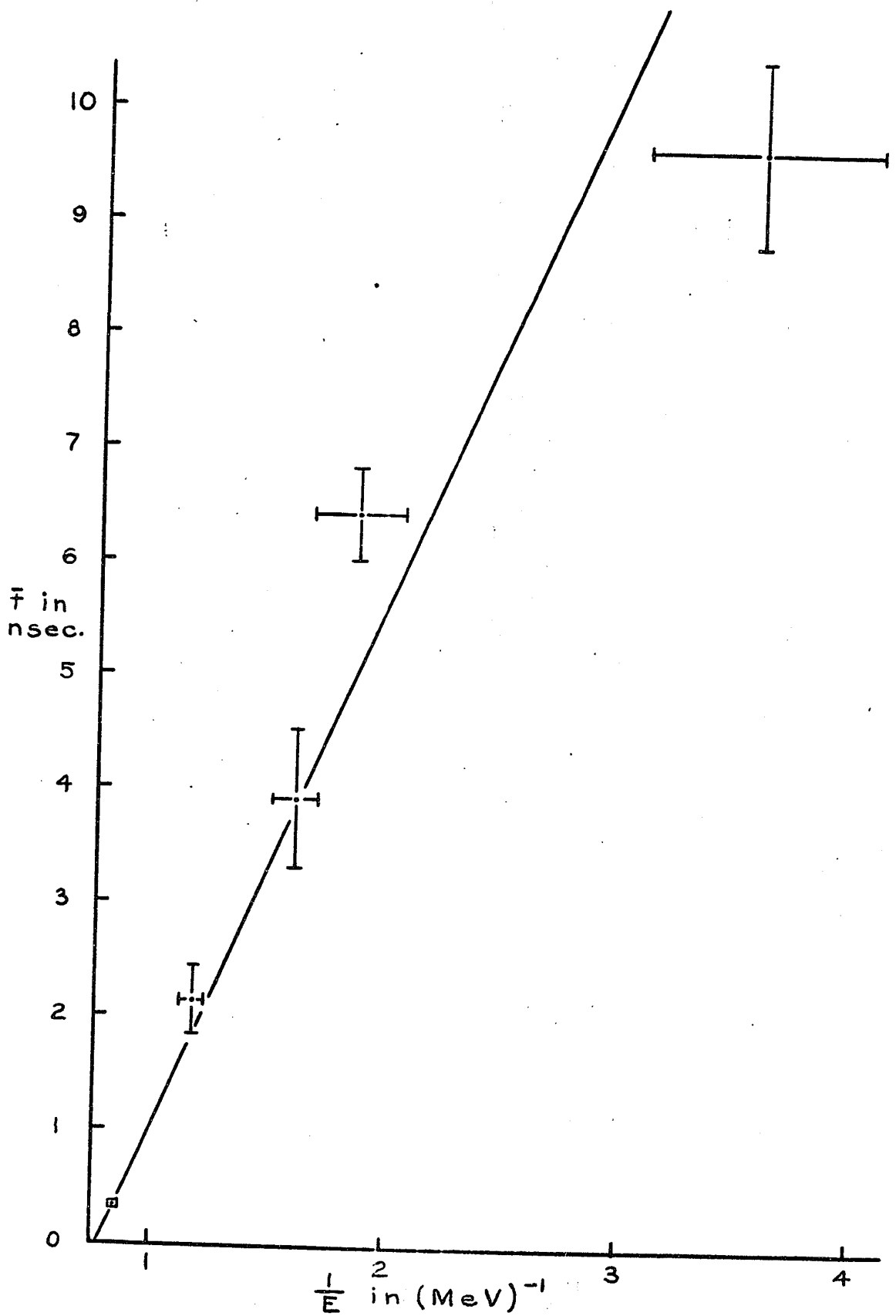

Fig 9.8. $\bar{t}$ versus $\frac{1}{E}$.

on the $(W_{1/2T})^2$ axis gives the contribution to the half-width of the time peak due to the fixed 1.33 MeV energy accepted in detector B. Again the low energy points have large errors.

For fast coincidence measurements $W_{90\%T}$, the width of the time peak which envelops 90% of the total counts for the energy E, is of more interest. Figure 9.10 shows $W_{1/2T}$ and $W_{90\%T}$ as functions of E. Note that below 0.6 MeV the two curves do not reflect the same shape, possibly because the counting statistics were not very good in the low energy range.

Energy resolution measurements at low energies indicated that C was of the order of 2 or 3 photoelectrons. The relationship between E and R was found to be 0.43 photoelectrons per KeV.

Because the measured results were neither extensive enough nor precise enough, a critical test of the Post and Schiff theory was not possible. However, the measured curves give a rough idea of the magnitude of $W_{1/2T}$ and $\bar{t}$, and an indication of their trend as a function of energy. A more refined treatment of the theoretical prediction for $W_{1/2}$ will be discussed in section 9.6.

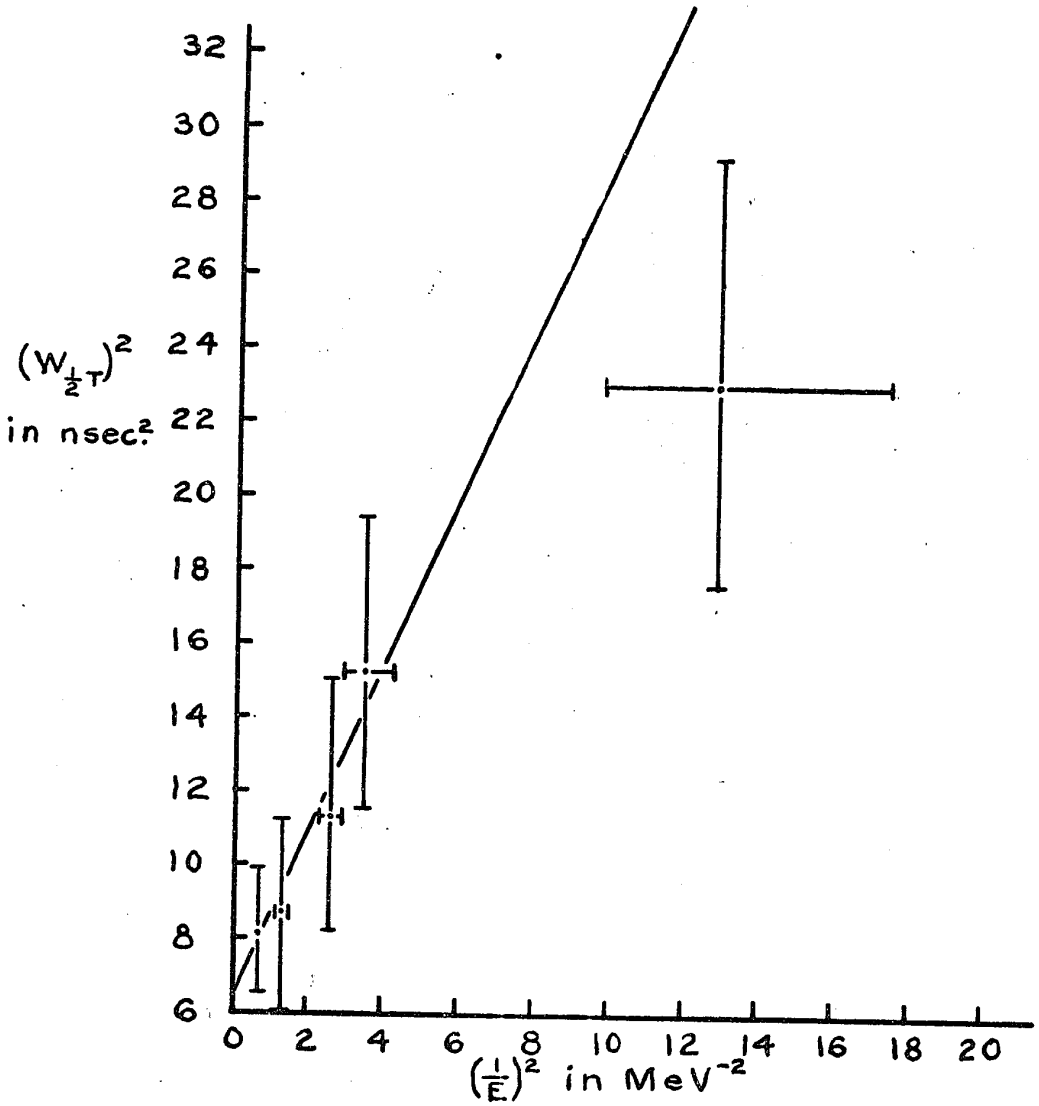

Fig. 9.9. $W^2_{\frac{1}{2}T}$ versus $(\frac{1}{E})^2$.

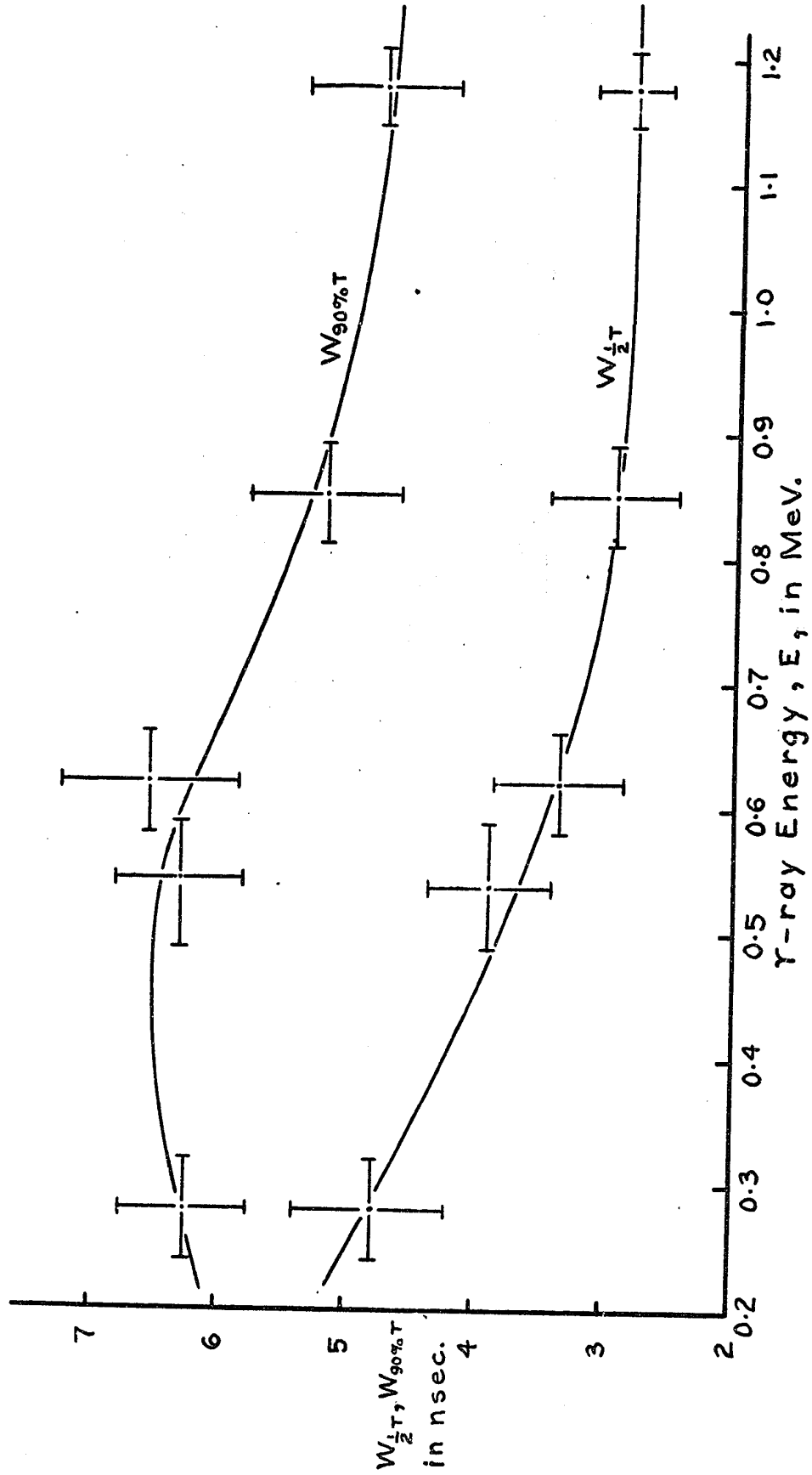

Fig. 9.10. A comparison of $W_{\frac{1}{2}T}$ and $W_{90\%T}$.

9.5 Compensation Networks.

One method for eliminating the contribution to the resolving time arising from the variation of $\bar{t}$ with energy involves the use of a compensation circuit. A pulse height proportional to the start pulse γ-ray energy is subtracted from the T.A.C. output, and a pulse height proportional to the stop pulse energy is added on to the T.A.C. output. If the delay of the time pulse is a linear function of the energy pulse height, these corrections will completely eliminate the $\bar{t}$ dependence.

Figure 9.11(a) shows the system required. The triangular T.A.C. output pulse is fed into one input of an operational amplifier whose gain is 1. An energy pulse from the slow channel is fed into the second input. The resistance R_2 is variable so that the amount of voltage subtracted from the T.A.C. pulse can be adjusted. R_2 is tuned until the time shift with energy disappears. To correct for the stop pulse an identical stage follows, but the energy pulse is added instead of subtracted.

These linear compensation networks would be satisfactory if $\bar{t}$ were a linear function of energy. $\bar{t}$ is, unfortunately, closer to a function of $1/E$. To approximate the function $1/E$, it is possible that the circuit of figure 9.11(b) could be employed. Use is

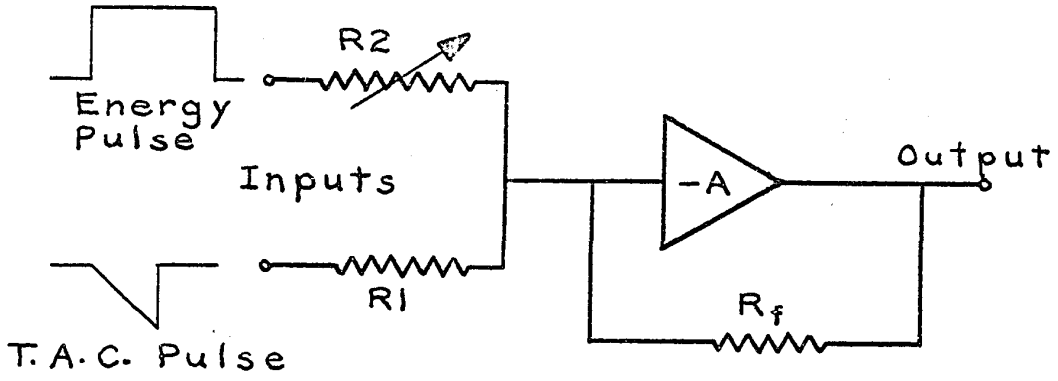

(a)

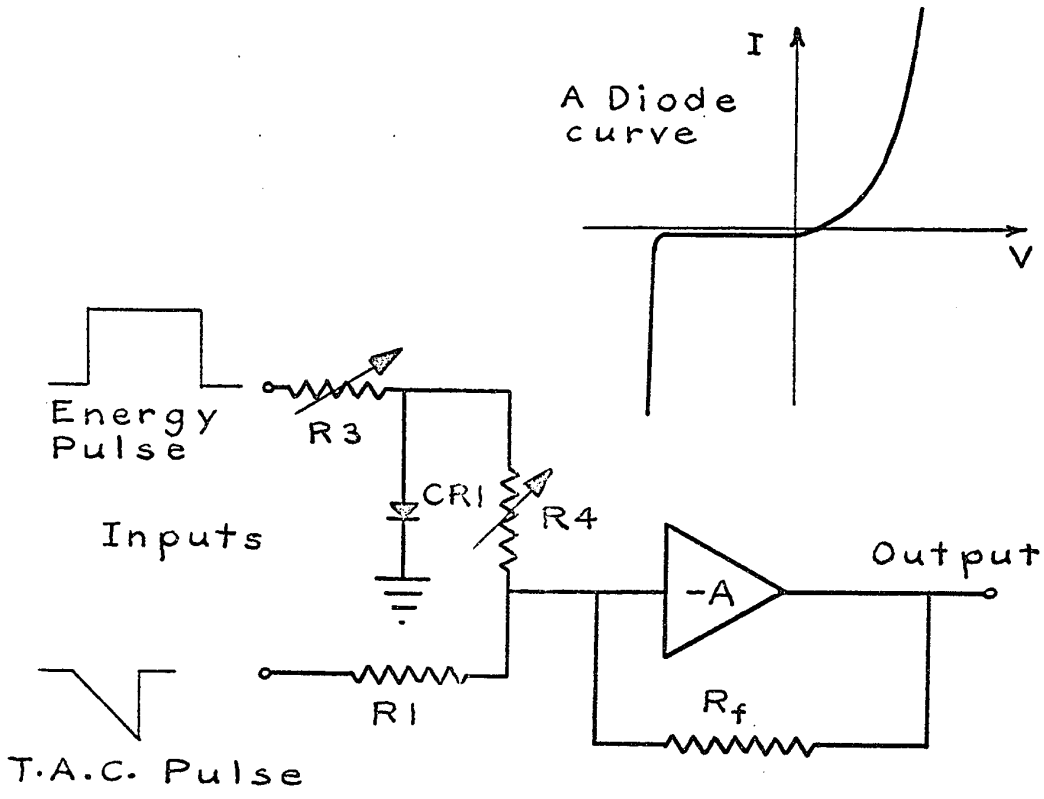

(b)

Fig. 9.11. Compensation circuits.
(a) linear. (b) non-linear.

made of the fact that the voltage across a diode has a non-linear relation to the current it passes.

$$I = I_o(e^{V/V_T} - 1) \qquad (9.4)$$

where I is the current through the diode when the voltage V is applied, I_o is the reverse leakage current, and V_T is a constant.

Resistor R_3 is used to choose the operating range on the diode curve, while R4 selects the magnitude of the correction applied to the T.A.C. signal by the voltage across CR1. By adjusting these two resistors, a non-linear compensation could be achieved. The compensation applies a stronger correction per unit energy for low energy pulses than for high energy pulses. The result should be an improvement over the linear circuit.

Since a linear circuit was available, its effect on the time spectrum was checked. Figure 9.12 shows the spectrum obtained when channel B was gated on the 1.33 MeV peak of Co^{60}, and channel A accepted any energy. A F.W.H.M. of 4.04 nsec and a width containing 90% of the events of 15.4 nsec were measured. In Figure 9.13 linear compensation has been applied from channel A. The amount of compensation was adjusted to get the best F.W.H.M. The 90% width was reduced to 8.0 nsec and the F.W.H.M. to 3.0 nsec. This represents a large improvement: a factor of 1.35 for the F.W.H.M., and more important, a factor of 1.92 for the

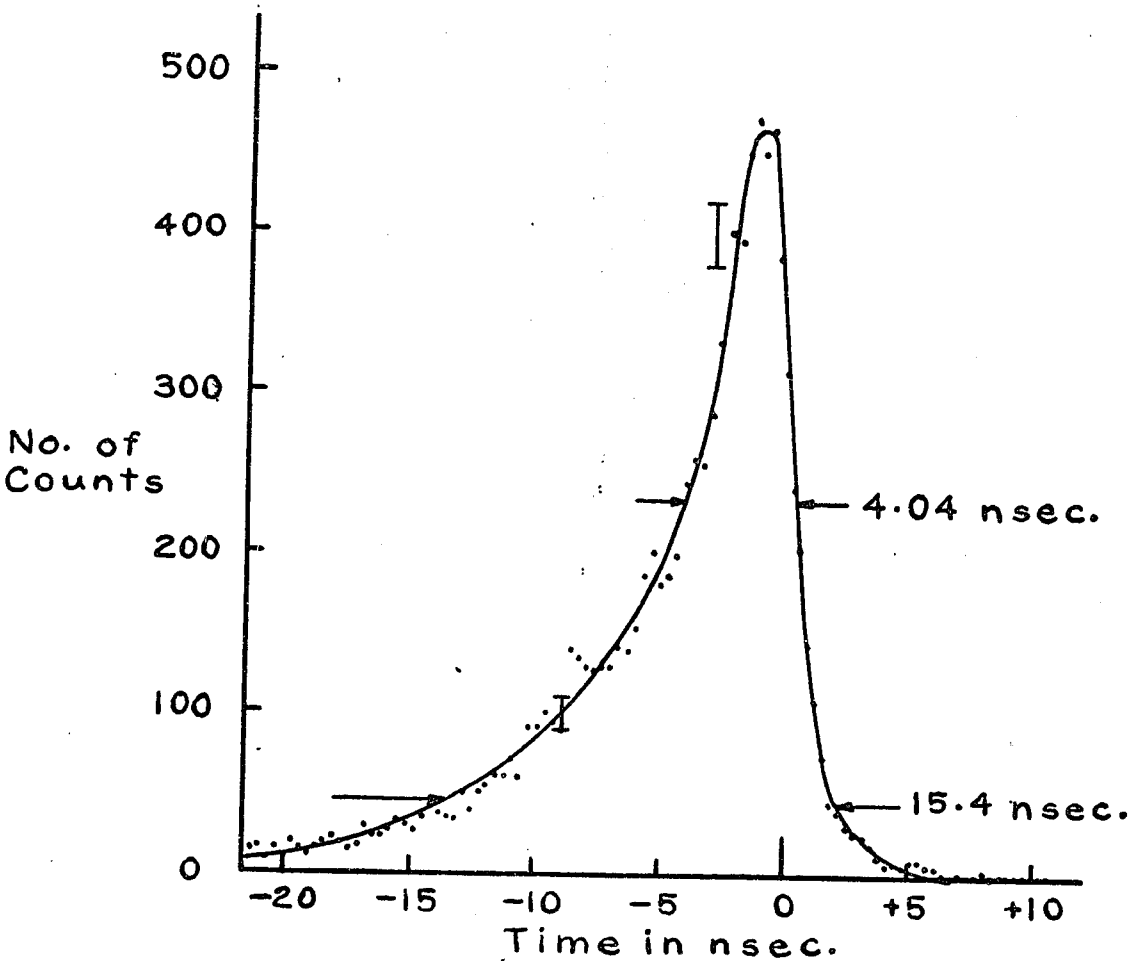

Fig. 9·12. Time spectrum for Co^{60} without compensation. 1·33 MeV accepted in channel A, 0 → 1·17 MeV in channel B.

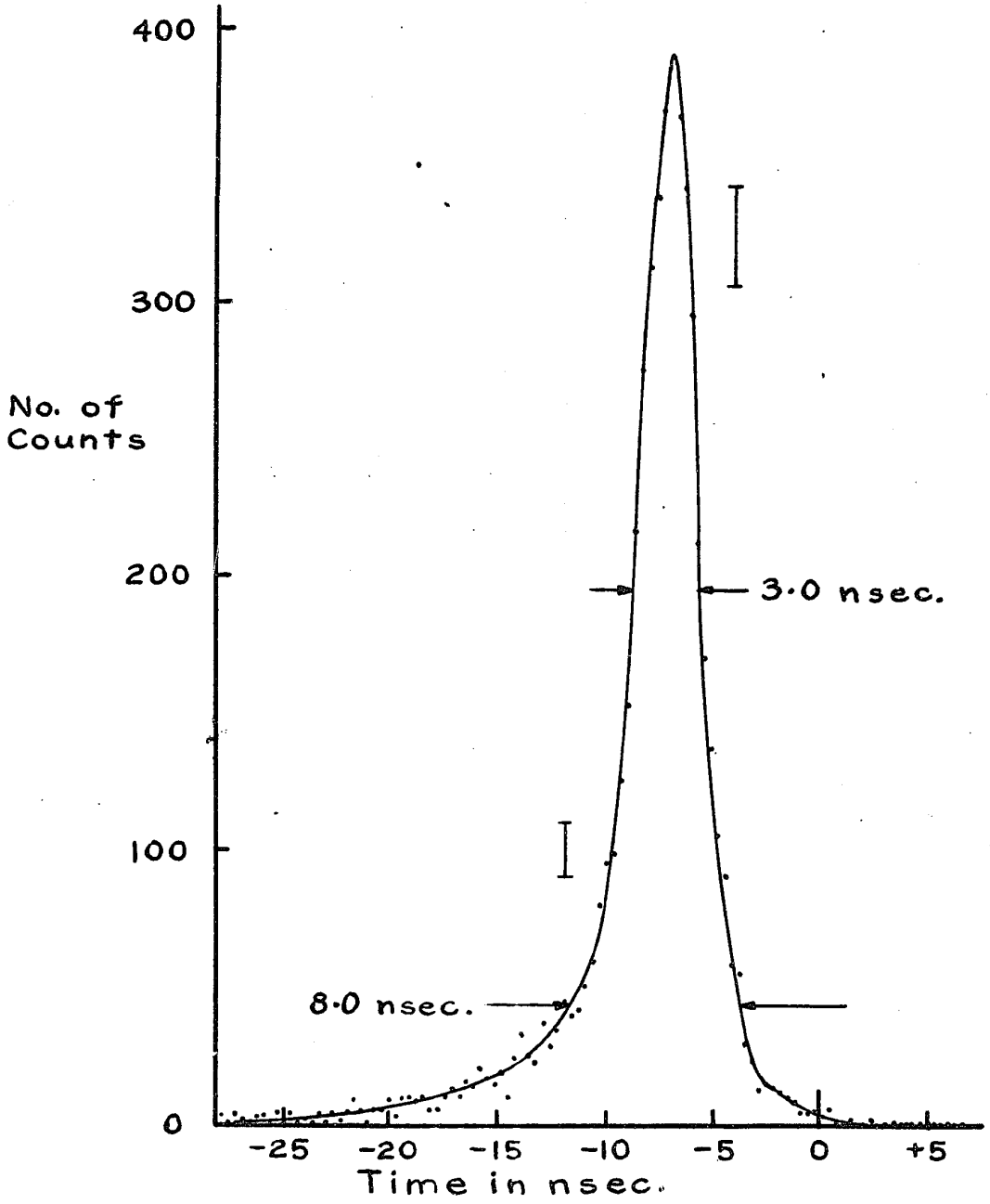

Fig. 9.13. Time spectrum for Co^{60} with linear compensation on channel B. 1.33 MeV accepted in channel A, 0→1.17 MeV in channel B.

90% width. The long tail to the left of the peak results from the low energy γ-rays which have been insufficiently compensated. A properly designed non-linear circuit would shift the events in the tail into the main peak.

These results suggest that a far better fast coincidence circuit could be constructed by using a time-to-amplitude converter, followed by a non-linear compensation circuit. The compensated output would have the annoyingly large $\bar{t}$ contribution removed. Subsequently the output could be fed to a single channel pulse height analyser, which would define the resolving time. Judging from the Figures 9.8 and 9.10, this would reduce the resolving time for a 290 KeV γ-ray from 25.6 nsec down to 6.3 nsec. This is a significant improvement.

9.6 The Theory of Gatti and Svelto.

More recently, Gatti and Svelto have considered the time resolution problem for photomultipliers in much greater detail[23]. In their excellent analysis, they show that previous workers have neglected several important contributions to the resolving time. They, in fact, have shown that the best resolving time is not obtained when C = 0. This result has recently been confirmed experimentally by Schwarzschild[24].

Gatti and Svelto define three sources contributing to the variance of the machine time:

(1) The variance due to statistical fluctuations in photoelectron emission, spread in photoelectric yield, and spread in the current gain.

(2) Variance due to spread in the device delay time (transit time of the electrons).

(3) The variance due to the spread in the single electron response (S.E.R.) width, λ.

Each of these sources affects the resolving time in a different way.

Curves from their work are given in Appendix III. An analysis of their curves shows that, for a given R, the minimum resolving time is obtained for C/R somewhere in the range of 0.2 to 0.02. In addition, the optimum value of C/R is the same for all R. This indicates that, for best operation, a trigger mechanism should be devised to trigger at a fixed fraction of the total charge in the pulse.

In any case, it would be of interest to remeasure the resolution for different values of C/R and attempt to fit this data to the theory of Gatti and Svelto. The characteristic constants applying to the particular detectors in use should be determined, and an appropriate set of curves devised from the theory. The presently

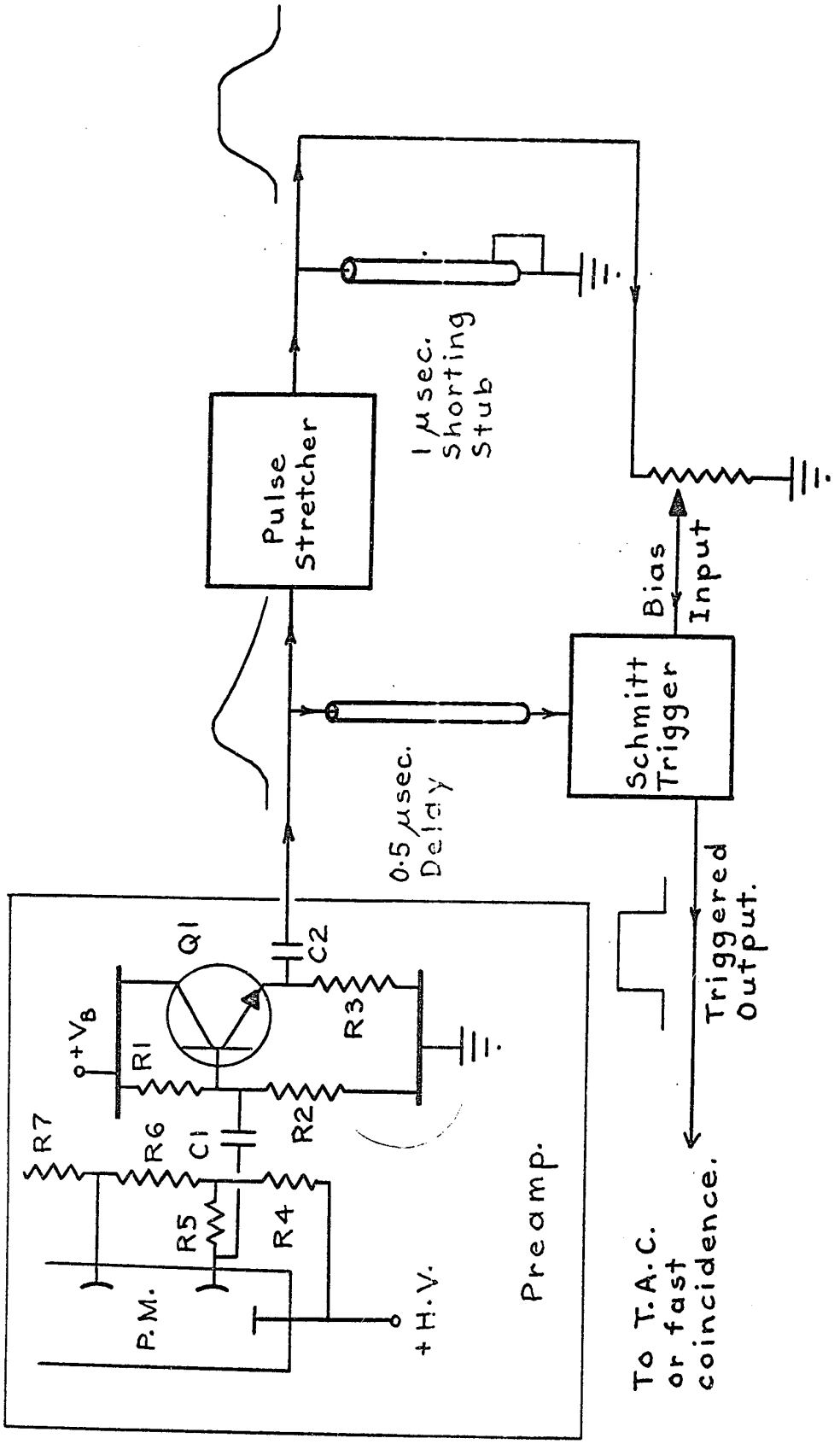

Fig. 9.14. Preamplifier and fractional pulse height discriminator block diagram.

available curves apply more aptly to fast scintillators.

9.7 A Fractional Pulse Height Trigger.

From the predictions made by Gatti and Svelto, it would seem advantageous to design a trigger circuit which triggers at the same value of C/R for each value of R. In addition to permitting a fixed choice of C/R, it would eliminate the $\bar{t}$ dependence on R. Thus the difficult problem of non-linear compensation circuits would be circumvented.

Figure 9.14 shows a proposed scheme for a fractional pulse height trigger system. The complicated limiter circuit is removed from the preamplifier and replaced by a fast emitter follower Q1. The emitter follower drives a 100 Ω cable to the trigger unit. At the trigger unit the pulse is fed through two paths. In one channel the input pulse is stretched, and clipped by a shorting stub. This produces a flat-top pulse whose height is proportional to the original pulse height. The other channel passes the input pulse through a delay. The length of delay is adjusted so that the input pulse arrives at the Schmitt trigger after the clipped pulse has reached its maximum voltage. The Schmitt trigger is biased, in the quiescent state, to trigger as soon as the input rises above zero.

The clipped pulse is attenuated to between 0.02 and 0.2 of the input pulse height. This attenuated pulse is applied to the quiescent bias of the Schmitt trigger to provide an additional bias, v_B. Hence, the triggering occurs when the input pulse rises above v_B. The attenuation factor, K, is related to the input pulse height, v_i, by the equation

$$v_B = K v_i$$

It is clear that the circuit triggers at a fixed fraction K of the input pulse height. Since K = C/R, the attenuator can be adjusted to choose the optimum value of C/R for a minimum resolving time.

In Appendix XXI a circuit is proposed for the Schmitt trigger with a bias control. A major advantage of this trigger system is that, by changing to the appropriate delay and clipping time, the unit can be adapted to a variety of photomultiplier-scintillator combinations. As previously mentioned, no compensation is required for $\bar{t}$ and the optimum C/R ratio can be selected simultaneously for all pulse heights.

Although a time-to-amplitude convertor followed by a single channel pulse height analyser is a rather complicated way to achieve a fast coincidence circuit, certain factors recommend its use for this work. In the first instance, a T.A.C. is usually capable of achieving better resolving times. Secondly, it is extremely useful to be able to observe the time spectrum before setting the appropriate resolving time of the coincidence circuit.

CHAPTER 10

GAIN STABILITY.

10.1 The Gain Stability of the System.

It has been pointed out in section 2.5 that gain stability in the sum-coincidence spectrometer is of vital importance. The measured stability is presented here. In all cases the room temperature fluctuations were held to a minimum.

The counting rate dependence arises primarily from the photomultipliers. Tests using Cs^{137} γ-rays showed that counting rates up to 1.2×10^4 counts per second were possible with a gain shift of less than 0.1%. When a gain shift of 0.5% resulted from exceeding this rate, it took from 5 to 15 minutes for the gain to relax to its original value.

Several long term drift studies were conducted. The random drift in gain over a period of from 4 to 6 days was found to be within ± 0.4% for temperatures held to within ± $1F^o$, and within ± 0.5% for room temperature fluctuations of ± $2.3F^o$. The two Sum Amplifier outputs were found to track together within 0.2%.

These stabilities should be compared to the stability of the Victoreen kicksorter, as measured by its internal pulse generator. The kicksorter calibration was found to vary by ± 0.2% for temperatures held within ± 1F°, and ± 0.3% for room temperature changes of ± 2.3F°.

The error in reading the peak positions on the kicksorter was estimated to be no less than ± 0.2 channels. In 190 channels this gives an error of ± 0.11%.

Most of the runs on Ge^{69} lasted for no more than 5 days. Consequently no opportunity arose to check the stability for longer periods. It may prove worthwhile to study the stability for a period of the order of one month, since longer runs will likely be required in the future.

The gain stability obtained is remarkable for a photomultiplier. Earlier experiments with other photomultipliers and amplifiers, under similar conditions, gave gain fluctuations from ± 2% to as high as ± 5.3%. These earlier results were the factor that launched a complete redevelopment towards the stable system presented in this thesis. Many workers have been forced by such instabilities to use gain stabilizers with the Hoogenboom sum-coincidence spectrometer. For most of the work done to the present date,

the ± 0.4% fluctuation in gain has been reasonably acceptable. However, for cases where a 3% sum window is desired, an improvement by a factor of 2 or 3 in the stability would be advantageous.

9.2 The Principle of Gain Stabilisers.

Before the redesigned spectrometer was completed, it was not known whether sufficient gain stability would be achieved. For this reason, the design of a gain stabilizer was thoroughly investigated, in anticipation of the need for a more powerful solution to the problem. It turned out that the spectrometer gain had sufficient stability for runs as long as 5 days, and sum window widths $\geq$ 5%. For many experiments this stability is adequate. In view of these results, and the fact that the construction of a stabilizer would be a sizeable project in itself, the plans were set aside. It is anticipated, however, that for narrower windows and longer runs, a stabilizer will be found necessary. In addition, as the photomultipliers age, their stability may degenerate, requiring the use of a stabilizer. A great deal of thought was channelled into the stabilizer design, and some of the parts were purchased. For this reason, and because of the expected need for this apparatus, some of the more important design aspects are presented here.

Several good articles have been published on gain stabilisers[25,26,27,28,29,30], and one model is commercially available*. The better features of each have been selected and adapted to a design more suitable for use with the sum-coincidence spectrometer. The general principle of operation is discussed with reference to Figure 10.1.

The output of the photomultiplier and amplifier is fed to a dual channel analyser (D.C.A.). The D.C.A. sets two adjacent windows of equal width across a suitable peak formed by γ-rays from the radioactive source. Following the D.C.A. is an analog scaler (usually a capacitor-type storage counter) which generates a correction voltage proportional to the scaler content. The correction voltage is applied between the photomultiplier cathode and ground, thus affecting the anode to cathode voltage of the tube. When the two channels are set symmetrically on the peak, the counting rates from the two windows are equal. Since the counts in the upper window (U) are added to the scaler

*Model 1001 - Spectrastat, Cosmic Radiation Labs, Inc., Bellport, Long Island, New York.

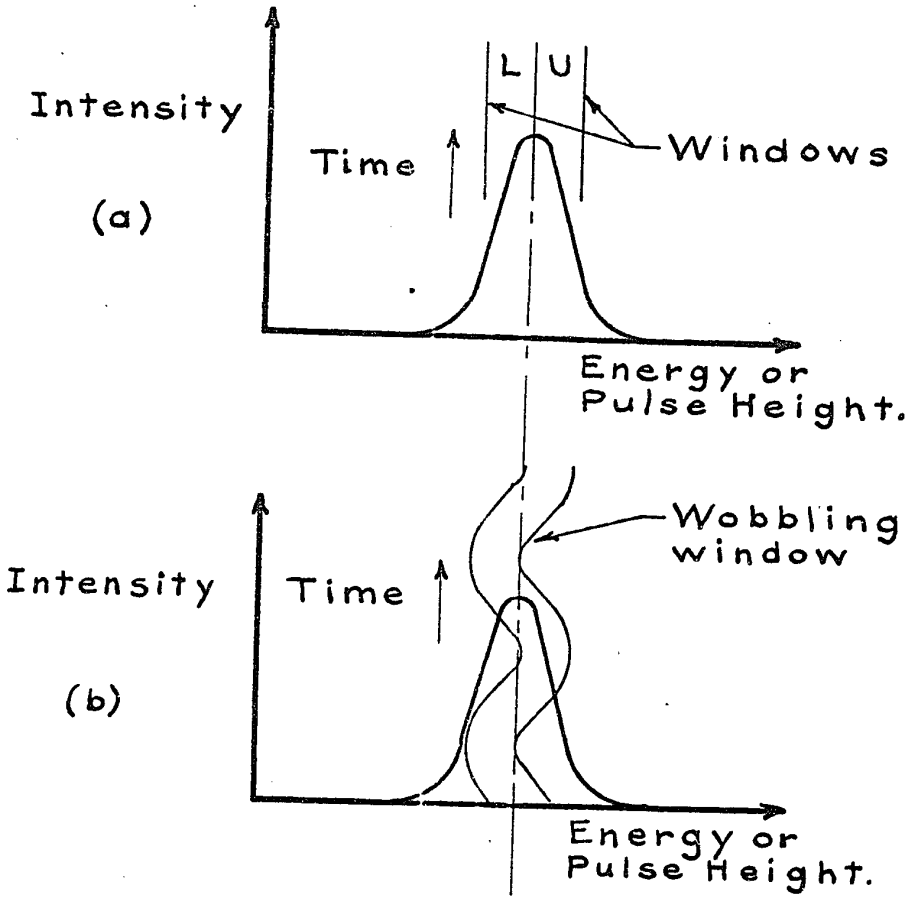

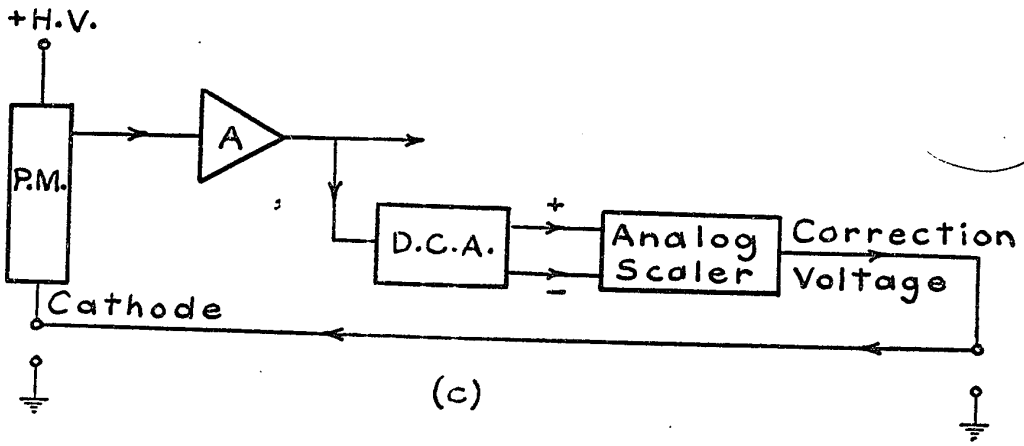

Fig. 10.1 The de Waard gain stabilizer system. (a) The dual window system. (b) The wobbling window. (c) The servo circuit.

content, while the lower window (L) counts are subtracted, the correction voltage will remain the same, on the average. Suppose the gain should increase. The counting rate in the upper window will increase relative to the lower window. The content of the scaler will therefore increase, increasing the correction voltage, until the new anode to cathode voltage of the photomultiplier returns the gain to its original value. A similar correction takes place when the gain decreases. In the deWaard system[25] the stability is improved by using a wobbling single channel analyser window. The wobble can be provided by the 60 cycle/sec AC line voltage. A trigger circuit generates the add command when the window is above the AC zero, and the subtract command when the window is below the AC zero bias. In practice this system is easier to build than the dual window system.

Figure 3.1 shows the gain stabilization loops. Clearly, two loops are required, one for each channel. The reason for including the Twin Amplifiers in the loops has been discussed by Demuynck and Segaert[31]. If a commercial stabilizer were used, the spectrometer would require two independent stabilizers; one for channel A, and one for channel B. This introduces the possibility of drift, or discrepancy between the two stabilizer settings. A method for eliminating this difficulty is presented in Figure 10.2. A single gain stabilizer is used with the de Waard wobbling

window. The window is preceeded by two linear gates with high gain stability[32]. An electronic switch is used to alternate in opening the two gates. The switch allows the stabilizer to analyse each channel through the same window settings. This facility ensures that both channels will be stabilized to the same gain calibration.

Boxes 3, 4, 6, 7, 8 and 9 form the single channel analyser (S.C.A.). The 60 c.p.s. wobble is applied, through a capacitor, to the D.C. bias of the difference amplifier, which sets the lower level of the window. The output of the S.C.A. is fed to an electronic switch, which alternates between sending the pulse to scaler A and to scaler B. The electronic switch also controls the linear gates, 1 and 2, so that when gate 1 is open the S.C.A. pulse is delivered to scaler A, and when gate 2 is open, it is fed to scaler B. Every time a pulse enters the electronic switch, it switches the circuitry to accept the next pulse from the opposite channel. As previously mentioned, the 60 cycle wobble also drives the add/subtract command, which sets the scalers to appropriately add or subtract the pulse they receive from the S.C.A.

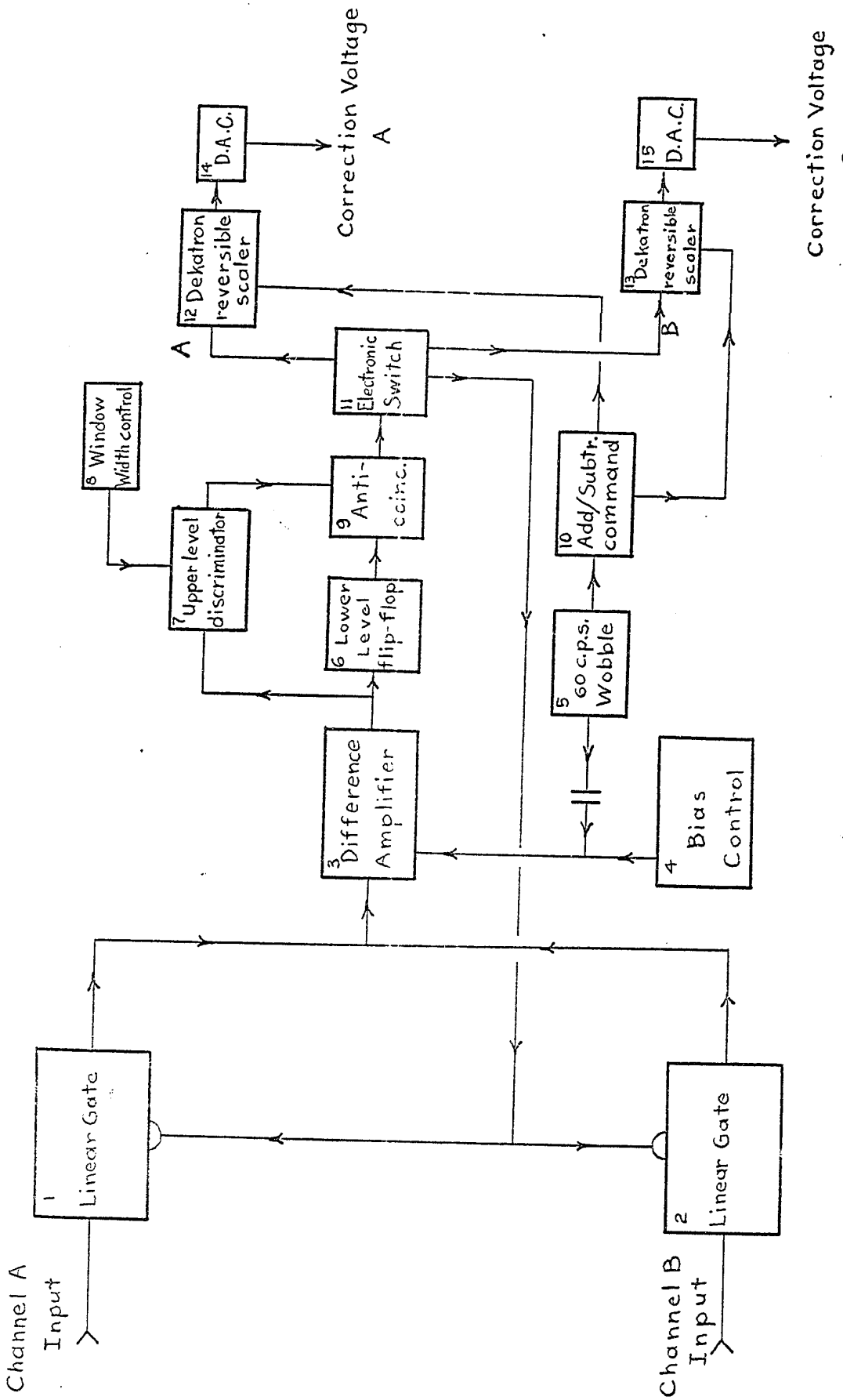

Fig. 10.2 The proposed gain stabilizer design.

In the Spectrastat, and in the original de Waard system, the scaler is a capacitive storage counter. The correction voltage is generated by the charge stored on a capacitor. A big difficulty with this scheme is that the correction voltage decays if the counting of the source ceases. In the design by Ladd[26], this disadvantage is eliminated, at the expense of simplicity, by using a reversible digital scaler.

In Figure 10.2 a Dekatron reversible scaler is used. It is composed of a DK103 Bidirectional Counting Circuit, 3 Bidirectional GSA100 Selector Dekatrons, and two DK101 Reversible Interstage Drivers*. The scaler has a content of 10^3 counts. The analog voltage can be derived from the individual cathode loads on the Dekatron tubes. The scalers are followed by a correction voltage generator (A.E.C.L. Stabilizer H.T. Control Amplifier A-EB3751-F-1) or digital to analogue convertor (D.A.C.). The +20V to +120V correction voltage so generated is applied to the photomultiplier cathode (see Figure 5.1).

*Manufactured by Baird-Atomic, Inc.

Conventional circuitry is used throughout the stabilizer, so that its construction should prove to be straight forward. With a little care, the instrument could be designed to be flexible enough to be used with a variety of detectors. The improvement in gain stability offered by this stabilizer should be substantial. The limit of the stability is set only by the stability of the S.C.A. window.

With this prediction in mind, construction of the stabilizer should fall high on the priority list for further improvement of the spectrometer.

CHAPTER 11

DECAY SCHEMES FOR Ge^{69} PROPOSED BY PREVIOUS WORKERS.

11.1 Introduction.

Previous work has been done on Ge^{69} decay by two groups. Their proposed decay schemes are included here as a prologue for the measurements presented in this thesis. A complete discussion of their results would be far beyond the scope of this thesis, so only those points which are of immediate interest are discussed.

11.2 The Work of Nussbaum and Suri[33].

In 1956 Nussbaum and Suri studied the decay of Ge^{69} using γ-ray and β-ray scintillation detectors. Their work was limited by the use of single channel analysers (multi-channel analysers were not available), poor resolution, and poor gain stability. Prior to the commencement of this thesis, the Nussbaum and Suri paper was the most recently published work on Ge^{69}.

A decay scheme based primarily on their work is shown in Figure 11.1. Ge^{69} decays with a 40 hour half-life into Ga^{69}. The lower levels in Ga^{69} are fed by β^+ decay, while the transitions to the upper levels proceed by electron capture. The intensities of the transitions are given in Figure 11.1. Note the weak intensities of the γ-ray transitions de-exciting the top two levels.

The numerous dotted lines indicate transitions whose positions in the decay scheme were felt by Nussbaum and Suri to be ambiguous. They point out in their paper that their measurements on the top two levels were not highly reliable. These levels were thought to be ideal candidates for study with the sum-coincidence spectrometer.

11.3 Results by Schwerdtfeger et al.

Figure 11.2 shows a decay scheme recently published by Schwerdtfeger, Ramayya, and Mitchell[34]. Their data was collected using a conventional γ-γ spectrometer, but with the aid of a multi-channel analyser. It will be noticed that their proposed scheme differs somewhat from the one in Figure 11.1; primarily in that it is greatly simplified.

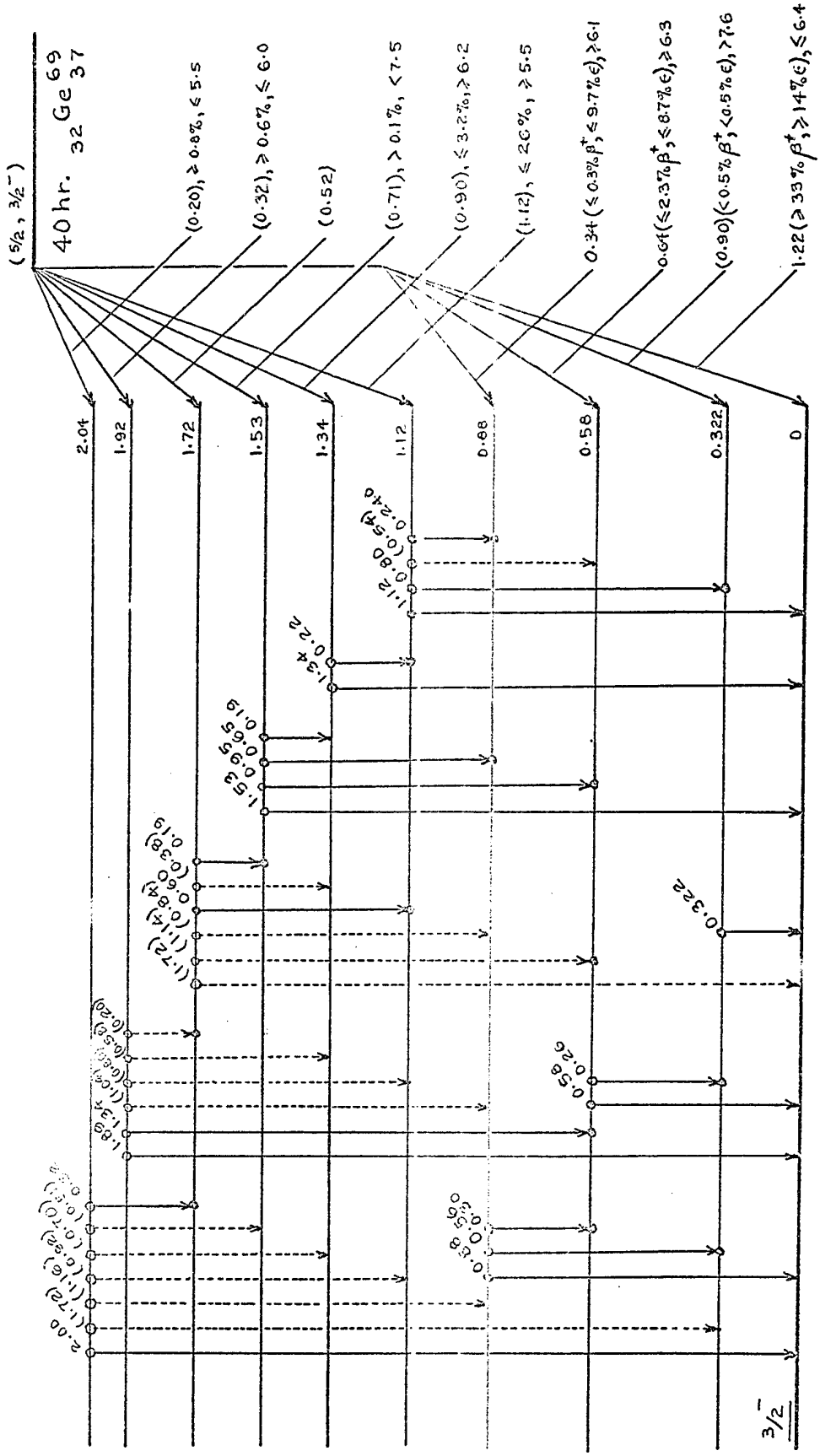

Fig. 11.1 The decay scheme from Nussbaum and Suri.

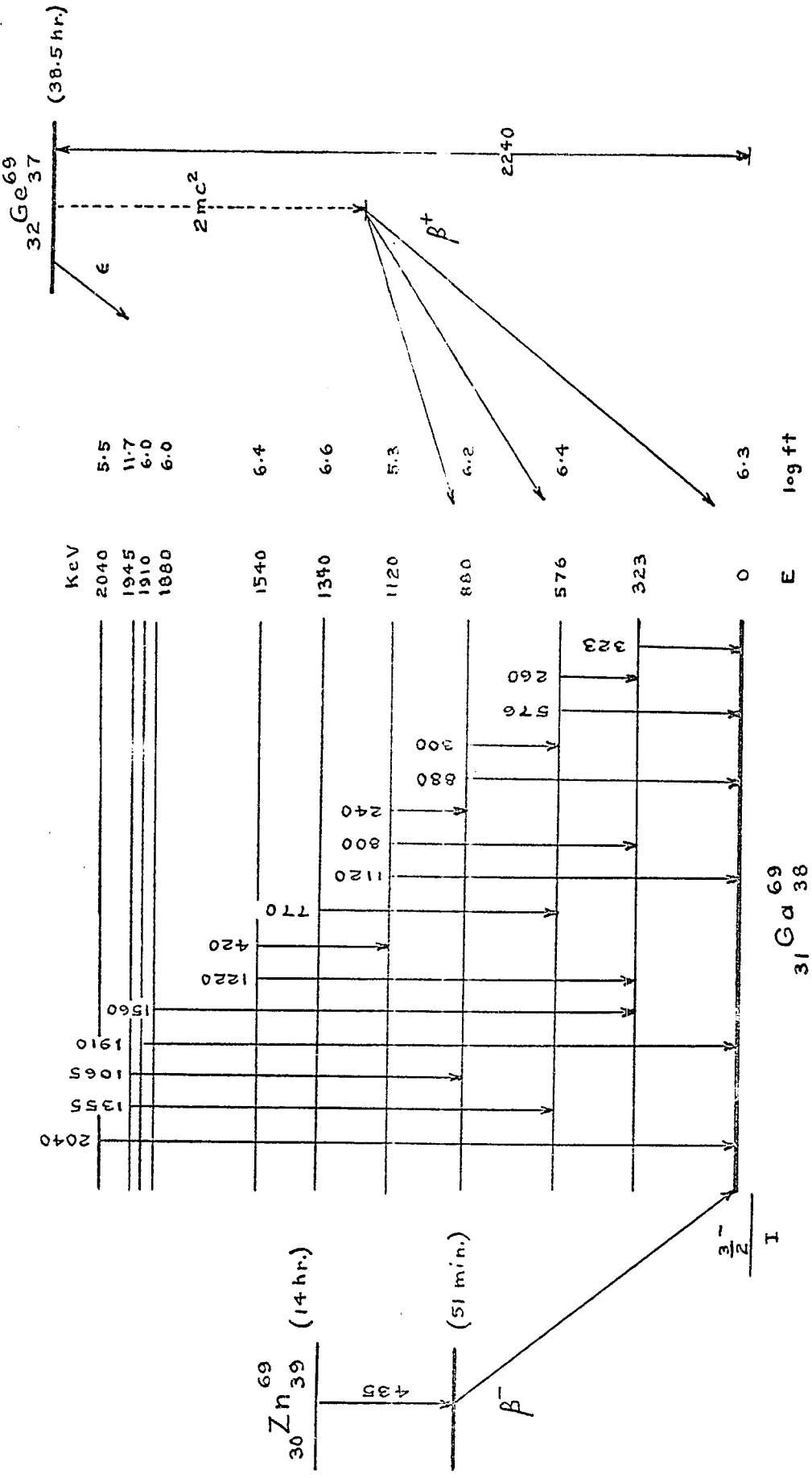

Fig. 11.2. The decay scheme of Schwerdtfeger *et al.*

Schwerdtfeger's analysis, however, suggests that much of the simplification has been achieved by selecting the most probable of several possible assignments for the position of a γ-ray of a given energy in the decay scheme. Some of the assignments chosen have not been shown to be the only possible choice. For this reason a more detailed investigation should prove fruitful. None of the spins or parities of the excited states of Ga^{69} have been measured to date. Hence angular correlation measurements with the sum-coincidence spectrometer would be desirable for the evaluation of these spins.

Schwerdtfeger does not confirm the presence of the 1.72 MeV level proposed by Nussbaum and Suri. This is not surprising, since Nussbaum and Suri found only weak evidence to support the proposal. Schwerdtfeger also differs from the previous paper when he proposes that the 1.94 MeV level is actually three levels very close together. It is interesting to note that the effect of the non-linearity in pulse-height response of NaI(Tl)[35] on the summing of γ-ray cascades could produce energy differences of this order. Schwerdtfeger has not indicated that he took account of this non-linearity. Therefore, it is of great interest to check the "1.94 MeV level" de-excitation. The sum-coincidence spectrometer is a good instrument for checking whether this level is, in fact, three levels.

Nussbaum and Suri stated that, in several cases, small but definitely reproducible energy shifts were found when certain γ-rays were measured in coincidence with different cascade γ-ray partners. This is the evidence which led them to conclude that some of the weak lines are double in the γ-ray spectrum. Hence, they showed several dotted transitions which could explain the similar energies obtained in these peaks. Schwerdtfeger makes no mention of this effect, and it is not known whether he studied it in his work. It would seem worthwhile to resolve this ambiguity.

The analyses of both groups employed spectrum subtraction techniques to separate the peaks of interest from the large background of other interfering transitions. In the case of such a complicated spectrum, this method might easily give rise to serious errors. Schwerdtfeger selected 17 peaks from the singles spectrum, and had of the order of 7 peaks in most of his coincidence spectra. Keeping in mind the large contribution from the Compton background from each of these peaks, it is obvious that

the accuracy of this technique must be seriously limited by the large and complicated corrections this spectrum subtraction required. The Hoogenboom sum-coincidence spectrometer is capable of giving a much more accurate and direct analysis of the Ge^{69} spectrum; particularly for the weaker transitions from the upper levels of Ga^{69}. For this reason it is well worthwhile to reinvestigate the decay scheme.

CHAPTER 12

THE PREPARATION AND COUNTING OF THE RADIOACTIVE Ge^{69} SOURCE.

12.1 Activation.

The radioactive Ge^{69} was produced by an (n,2n) reaction on the Ge^{70} contained in a 99.99% pure sample of natural germanium. The samples were cut to 1.5 cm x 1.5 cm x 2.3 cm, and weighed 27 gm. 14 MeV neutrons from a Texas Nuclear Neutron Generator were used for the activation. The natural abundance of Ge^{70} in these samples is 20.6% by weight.

Table 12.1 shows the possible reactions produced by the irradiation. The interfering γ-ray emitting radionuclide produced along with Ge^{69} which has the longest half-life is Ga^{72}. Ga^{72} has a half-life of 14.2 hours. To minimise the interference from Ga^{72} in the Ge^{69} spectrum, the germanium sample was irradiated for 120 hours (three Ge^{69} half-lives). This brings the Ga^{72} and the Ge^{69} activities close to saturation. Following this period, the sample was removed from the activation area and allowed to decay for 40 hours. This reduced the Ge^{69} activity by a factor of 2, and the Ga^{72} activity

Table 12.1

Neutron Reactions for Germanium†

Element	% Abundance	$\sigma(n,\gamma)$	Product Nuclide	$t_{1/2}$ of Product	Radiation from Product	$\sigma(n,2n)$	Product Nuclide	$t_{1/2}$ of Product	Radiation from Product
$_{32}Ge^{70}$	20.55	3.5b	$_{32}Ge^{71}$	11d	EC 0.22 end point	600 mb	$_{32}Ge^{69}$	40.0 h	1.22^{*}, 0.61^{*} <u>1.1,0.9,0.6</u>
$_{32}Ge^{72}$	27.37	940 mb	$_{32}Ge^{73}$	Stable					
$_{32}Ge^{73}$	7.67	13.7 b	$_{32}Ge^{74}$	Stable					
$_{32}Ge^{74}$	36.74	600 mb	$_{32}Ge^{75}$	48 s 82 m	<u>0.14</u> 1.1<u>4</u>,0.6<u>14</u>; <u>0.26,0.19</u>				

Key:

β^{-} decay energies: regular type

β^{+} decay energies: *

γ-ray energies: underlined

Electron capture: EC

"End point": end point energy of internal Bremsstrahlung.

σ : cross-section for the reaction.

$t_{1/2}$: half-life

$\sigma(n,\gamma)$ is for thermal neutrons; all other σ's are for 14 to 15 MeV neutrons.

†Taken from: Table of Cross Sections for Fast Neutron Reactions, Texas Nuclear Corporation, 1960.

Table 12.1 (cont'd)

Neutron Reactions for Germanium

Element	σ(n,p)	Product Nuclide	$t_{1/2}$ of Product	Radiation from Product	σ(n,α)	Product Nuclide	$t_{1/2}$ of Product	Radiation from Product
$_{32}Ge^{70}$	130 mb	$_{31}Ga^{70}$	21 m	1.65				
$_{32}Ge^{72}$	65 mb	$_{31}Ga^{72}$	14.2 h	0.64,0.96, 1.5,2.5; 0.8,2.2 etc				
$_{32}Ge^{73}$	140 mb	$_{31}Ga^{73}$	5.0 h	1.19,0.4; 0.295				
$_{32}Ge^{74}$					15 mb (2.2 m)	$_{30}Zn^{71}$	3 h 2.2 m	1.5;0.38, 0.49,0.61 2.4;0.51

by a factor of about 8. Thus, the interference from Ga^{72} was effectively reduced. Any residual activity due to Ga^{72} in the beginning of each run on Ge^{69} was easily recognized by its 14.2 hour decay time. In practice, very little interference was encountered.

The counting equipment was located in the same room as the neutron generator. Consequently, great difficulty was encountered in keeping down the counting rate in the sum-coincidence spectrometer during irradiation due to the neutron background. For this reason continuous activation of new samples and simultaneous counting of irradiated samples could not be carried out. Instead two samples were used with their activation times staggered by 40 hours. The second sample was placed in the neutron flux 40 hours after the first, and removed again 40 hours after the removal of the first sample. In this way, each sample received 120 hours of activation, and was allowed to decay 40 hours before counting. The neutron generator was shut off during the counting of the sources.

A simple calculation shows that, if a counting rate of the order of 10^3 c.p.s. is desired (for a detector-source distance of 8 cm), then a neutron flux of from 10^7 to 5×10^7 neutrons/cm^2/sec is required. This flux must

be maintained for a total of 160 hours to irradiate both samples. The tritium target assembly provided with the neutron generator was capable of delivering this flux for only 15 hours. Consequently, a larger, oscillating, tritium target was designed. Appendix IV describes the target built to accommodate the 160 hour, high flux requirement.

An improvement in the efficiency of the runs could be achieved if the detectors were operated in a room which was not near the neutron generator. This change would permit continuous activation and counting of the germanium samples. This arrangement was not feasible for the work to date.

12.2 Counting Geometry and Detector Shielding.

Runs were conducted with θ, the angle between the source and each of the two detectors, set to 90° and to 180°. For most of the runs, the distance between the source and each detector was 8 cm. In some cases a higher counting efficiency was desired, and the distance was reduced to 1/2" with $\theta = 180^{\circ}$. This configuration brought the efficiency close to that of a 4π counter.

To prevent backscattering, the source was mounted in a 1.5 cm x 2.3 cm hole in a 1/4" plate of lead. The lead formed a wall of shielding between the two detectors, with the germanium sample visible to both crystals. The

detectors were set up in a horizontal position, with the germanium sample sitting on the centre line of their cylindrical axes. The crystals were shielded with 1" to 2" of lead, and the whole chamber containing the source and the detectors was shielded with 2" of lead. During the activation period, the lead shielding was surrounded by sheets of cadmium. Around this, one foot thick walls of paraffin were erected. This shielding was used to reduce the background of neutrons reaching the detectors.

CHAPTER 13

MEASUREMENTS ON Ge^{69} DECAY

13.1 Introduction.

Several types of experiments were carried out with the spectrometer, with particular attention being given to the de-excitation of the "1.92 MeV level" and the 2.04 MeV level in Ga^{69}. First, a singles spectrum was taken. This was later compared with the spectrum obtained by Schwertfeger. Secondly, channel A plus channel B, or "cascade sum" spectra were accumulated using the fast coincidence unit. These spectra are used to locate all the peaks representing the sums of the energies in the γ-γ cascades. Lastly, sum-coincidence measurements were made on the "1.92 MeV level", with and without a fast coincidence.

Due to running time limitations, there was not sufficient source activity to make a sum-coincidence run on the "1.92 MeV level" at the 8 cm detector-source distance with $\theta = 180^{\circ}$. This run is necessary for more accurate intensity calculations. Approximate intensity values were calculated for a run with the detector source distance, $r_{ds} = 1/2"$, and $\theta = 180^{\circ}$. Intensity and energy measurements

were made more difficult in two of the runs because the sum window was set slightly low.

An earlier run using the original low stability spectrometer has been included. Although this spectrum was made on an unmatched system, it provides valuable information about the decay of the 1.12 MeV level.

13.2 The Singles Spectrum.

Figure 13.1 shows the singles spectrum obtained with the germanium sample against the detector crystal face. This spectrum is identical to that given by Schwerdtfeger, except for the 2.22 MeV and the 2.52 MeV peaks. These peaks are due to the 14 hour Ga^{72} activity. Ga^{72} did not interfere with the sum-coincidence spectra. The γ-rays listed by Schwerdtfeger have been marked for reference in Figure 13.1.

The high energy region of the singles spectrum is shown in Figure 13.2, with improved statistics. The 1.92 MeV and 2.04 MeV peaks are both quite prominent, as found by Schwerdtfeger. A 1.72 MeV γ-ray proposed by Mussbaum and Suri is not obviously visible; the hump at channel 127 being likely due to the Compton edges of the 2.04 MeV and the 1.92 MeV peaks.

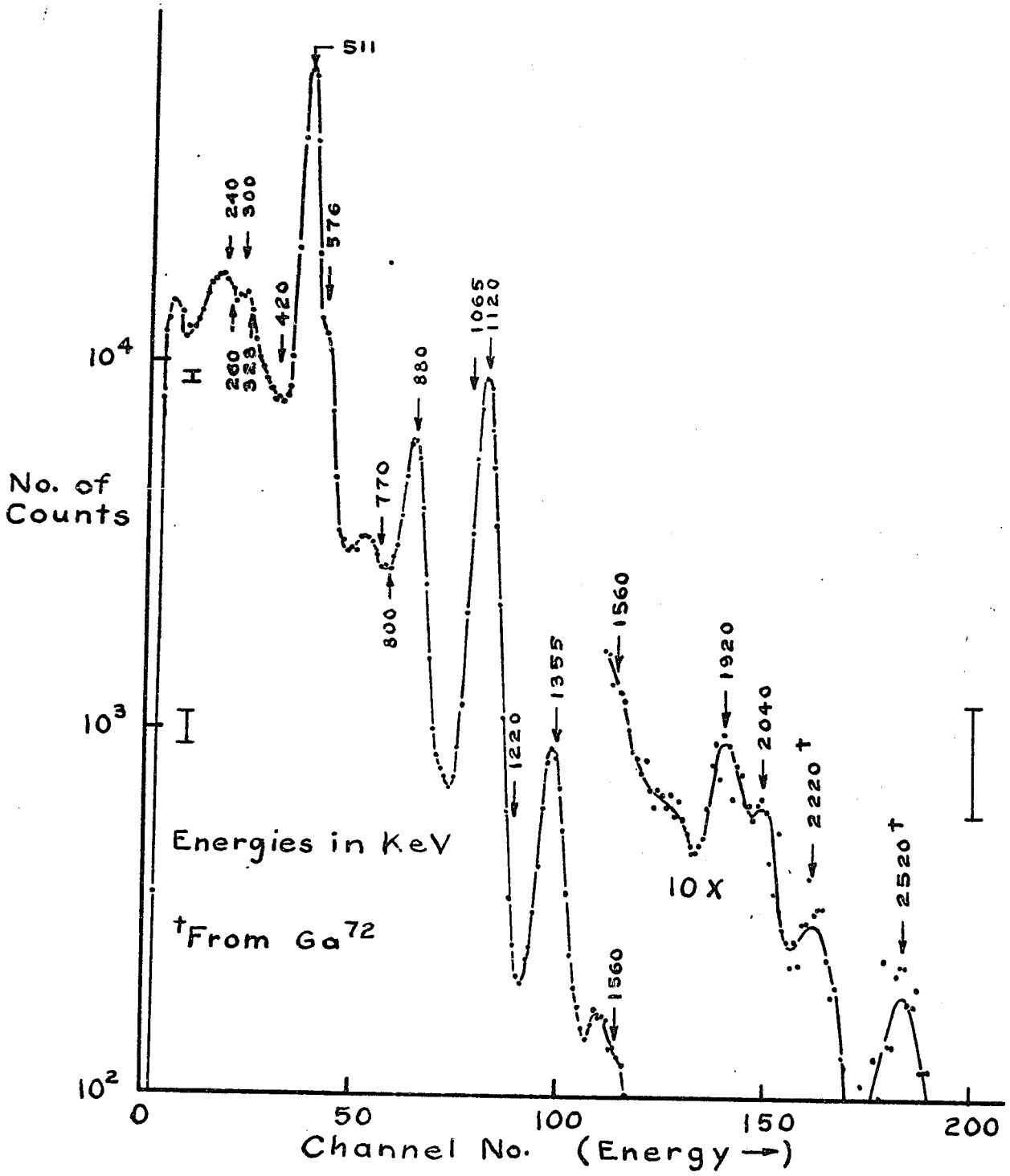

Fig. 13.1. A singles spectrum on Ge^{69}.

Run 23: Source against crystal face;
Counting rate at start of run, 747 c.p.s.;
Total counting time, 8 min.

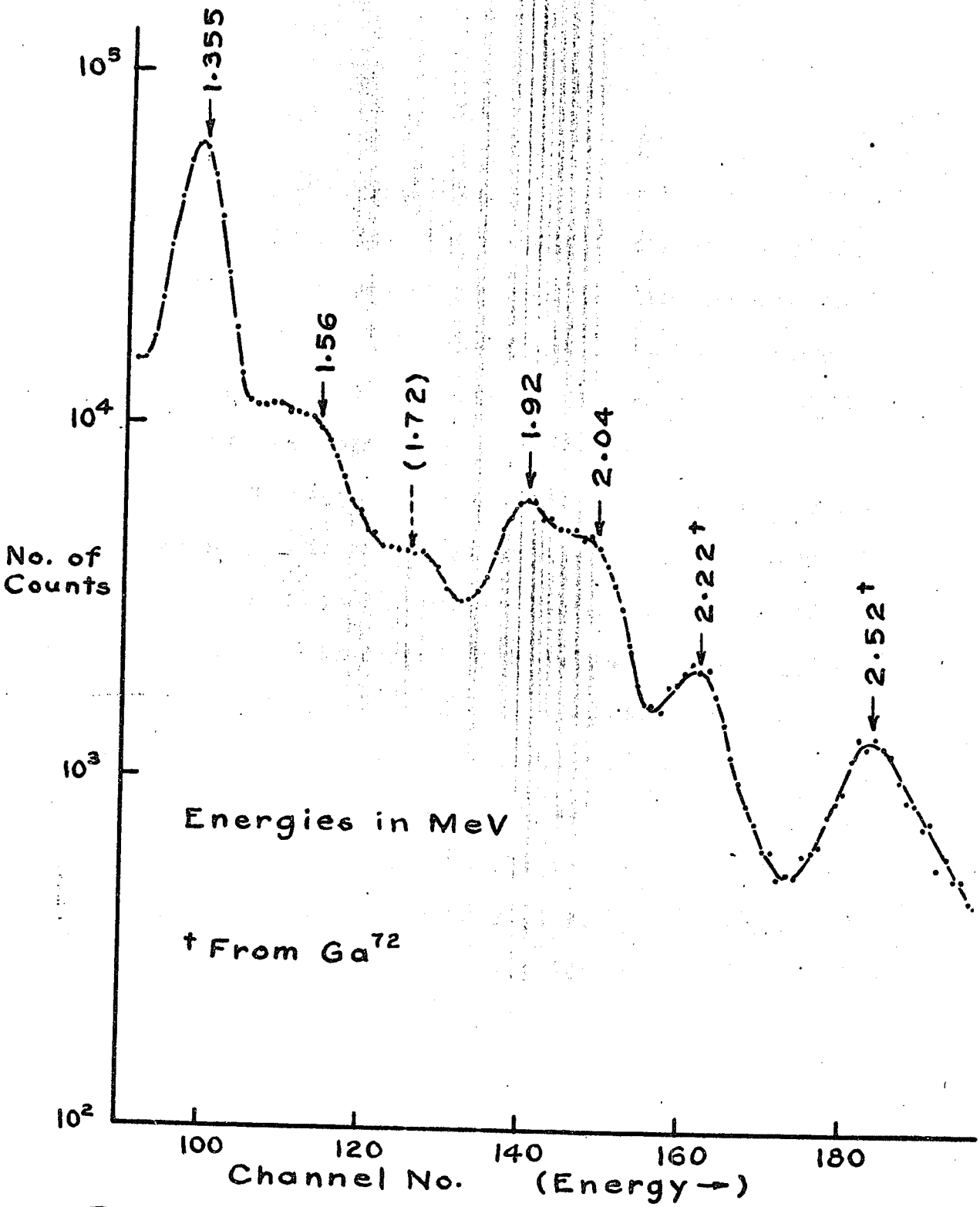

Fig. 13.2. A singles spectrum on Ge^{69}.
Run 24: Source against crystal face;
Counting rate at start of run, 747 c.p.s.;
Total counting time, 10.5 hr.

13.3 The Cascade Sum Spectra.

The Sum Amplifier A + B output was analysed with a fast coincidence demanded between the two detectors. Figures 13.3, 13.4 and 13.5 show the results obtained. These spectra represent the sum of the cascade energies for each prompt γ-γ cascade.

It must be kept in mind that the apparent energy of the experimentally measured sum peak for a cascade is shifted upward by a small amount with respect to the numerically calculated sum. This effect is due to the non-linearity in the pulse height response from NaI(Tl). Where it was of particular interest, the predicted energies have been corrected from data by Devare and Tandon[35] for comparison with the experimentally measured value.

The spectrum in Figure 13.3 was taken with $r_{ds} = 1/2"$ and $\theta = 180^{\circ}$, and with a fast coincidence resolving time $2\tau = 77$ nsec. A well-defined shoulder appears at an energy slightly over 0.576 MeV. This shoulder is interpreted as being partly due to the summing of the 0.511 MeV annihilation radiation, and partly due to the 0.260 MeV - 0.323 MeV cascade.

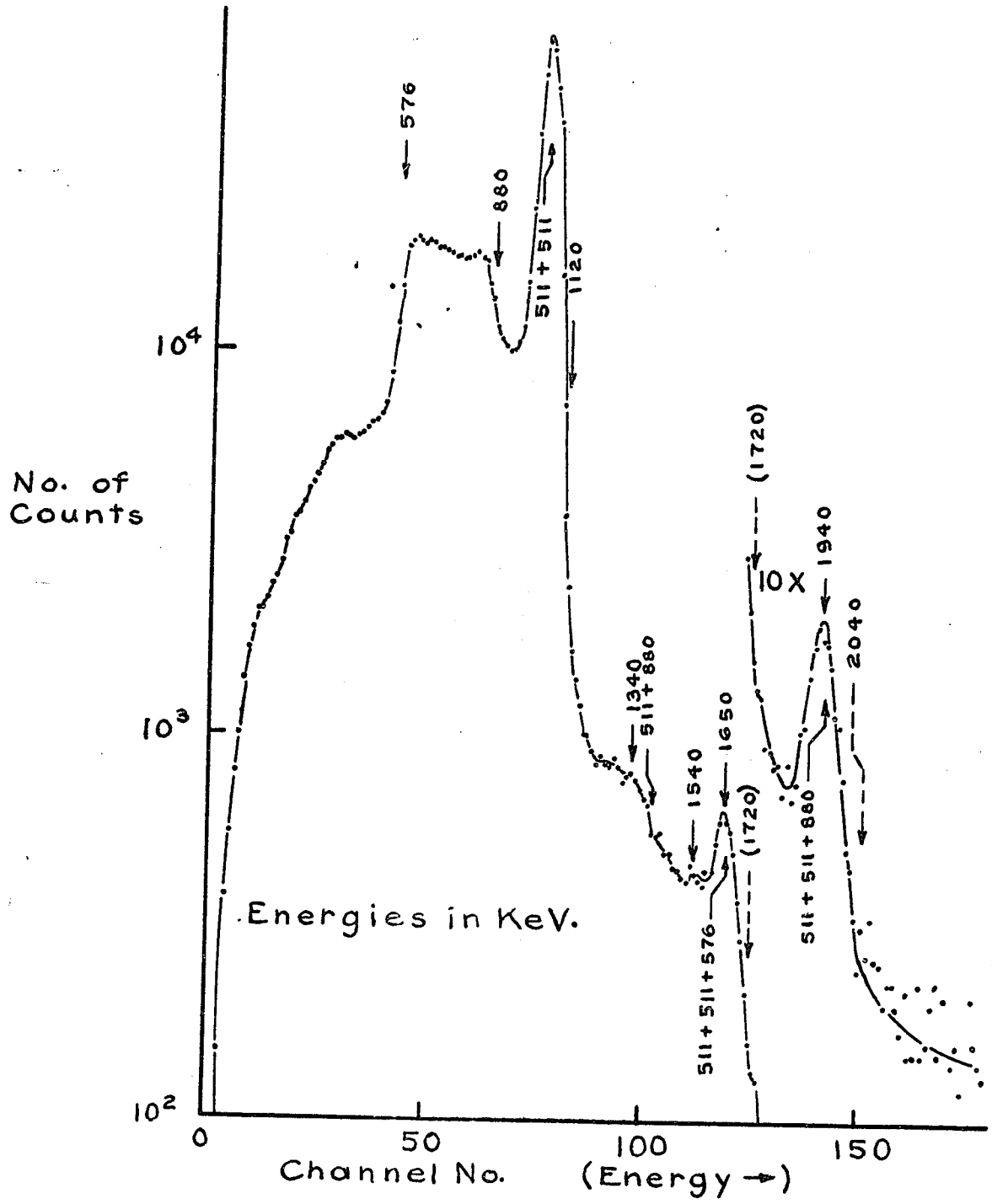

Fig. 13.3. A cascade sum spectrum on Ge^{69}. Run 27: Sum Amplifier A+B output with fast coincidence. $r_{ds} = \frac{1}{2}"$, $\theta = 180°$. Fast coincidence resolving time, $2\tau = 77$ nsec. Single crystal counting rate at start of run: 747 c.p.s. Counting time 74 min. Bent arrows show expected energy shifts due to summing cascades.

Peaks at 0.880 MeV and 1.12 MeV, due to the cascades from these levels, are too weak to be observed. The peak at 1.04 MeV is due to the summing of two 0.511 MeV annihilation γ-rays. The expected position for the sum of the 0.880 MeV γ-ray with a 0.511 MeV annihilation γ-ray has been marked; although, at 180° a summing of two 0.511 MeV γ-rays with a 0.880 MeV γ-ray is much more probable.

Figure 13.4 shows the higher energy region with better statistics. A slight hump is observed at a position corresponding to the 1.34 MeV level, and there is a slight disturbance where the 1.54 MeV peak is expected. However, the spectrum does not conclusively indicate cascades from these levels. No indication is observed here for the 1.72 MeV level proposed by Nussbaum and Suri. The 1.647 MeV peak is attributed to the sum of two 0.511 MeV annihilation γ-rays and a 0.576 MeV γ-ray. This assignment is supported by the fact that the peak disappears when the detectors are set to $\theta = 90^{\circ}$.

A substantial peak is evident at 1.94 MeV. This peak is mainly due to cascades from the "1.92 MeV level". The remainder should be contributed by the sum of two 0.511 γ-rays with a 0.880 MeV γ-ray. Evidence for cascades from

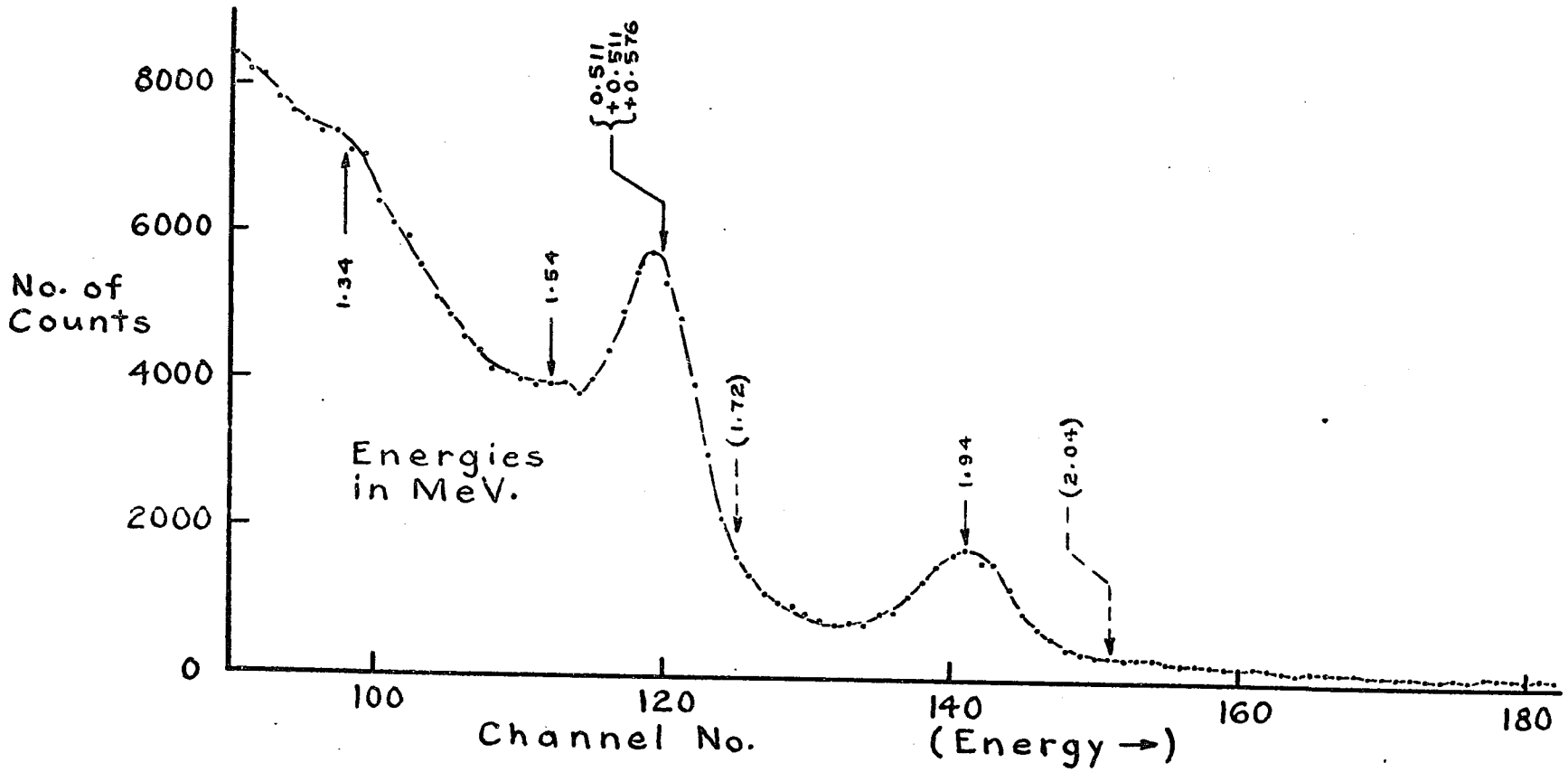

Fig. 13.4. A cascade sum spectrum on Ge^{69}.

Run 28: Sum Amplifier A+B output with fast coincidence. $r_{ds} = 1/2"$. $\theta = 180°$. $2\tau = 77$ nsec. Single crystal counting rate at start of run, 747 c.p.s. Counting time, 13 hr 24 min. Bent arrows show expected energy shifts from NaI(Tl) response.

the 2.04 MeV level should appear at about 2.03 MeV (i.e. channel 151). There is no indication of these transitions. It is estimated that the cascade intensity from the 2.04 MeV level must be less than 1/100 of the total cascade intensity for the "1.92 MeV level".

Figure 13.5 shows the cascade sum spectrum for r_{ds} = 8 cm and $\theta = 90^{\circ}$. In this geometry, all the events are eliminated to which two coincident 0.511 MeV annihilation γ-rays contribute. A peak corresponding to the 0.576 MeV level is clearly visible, confirming the existence of the 0.260 MeV - 0.323 MeV cascade. The assignment of this cascade sum peak to a transition between the 1.92 MeV and the 1.34 MeV levels is regarded as unlikely on the basis of intensity considerations. The next peak is at 0.760 MeV. The most probable cascade causing this peak would be a 0.320 MeV transition between the 1.87 MeV level and the 1.54 MeV level, followed by a 0.420 MeV transition between the 1.54 MeV level and the 1.12 MeV level. Including the non-linear response of NaI(Tl) these transitions add to 0.759 MeV. Schwerdtfeger has conclusive evidence for the above assignment of a 0.420 MeV γ-ray, but he did not propose a 0.320 MeV transition between the 1.87 MeV and the 1.54 MeV levels. There is some evidence to support this assignment of the 0.320 MeV γ-ray.

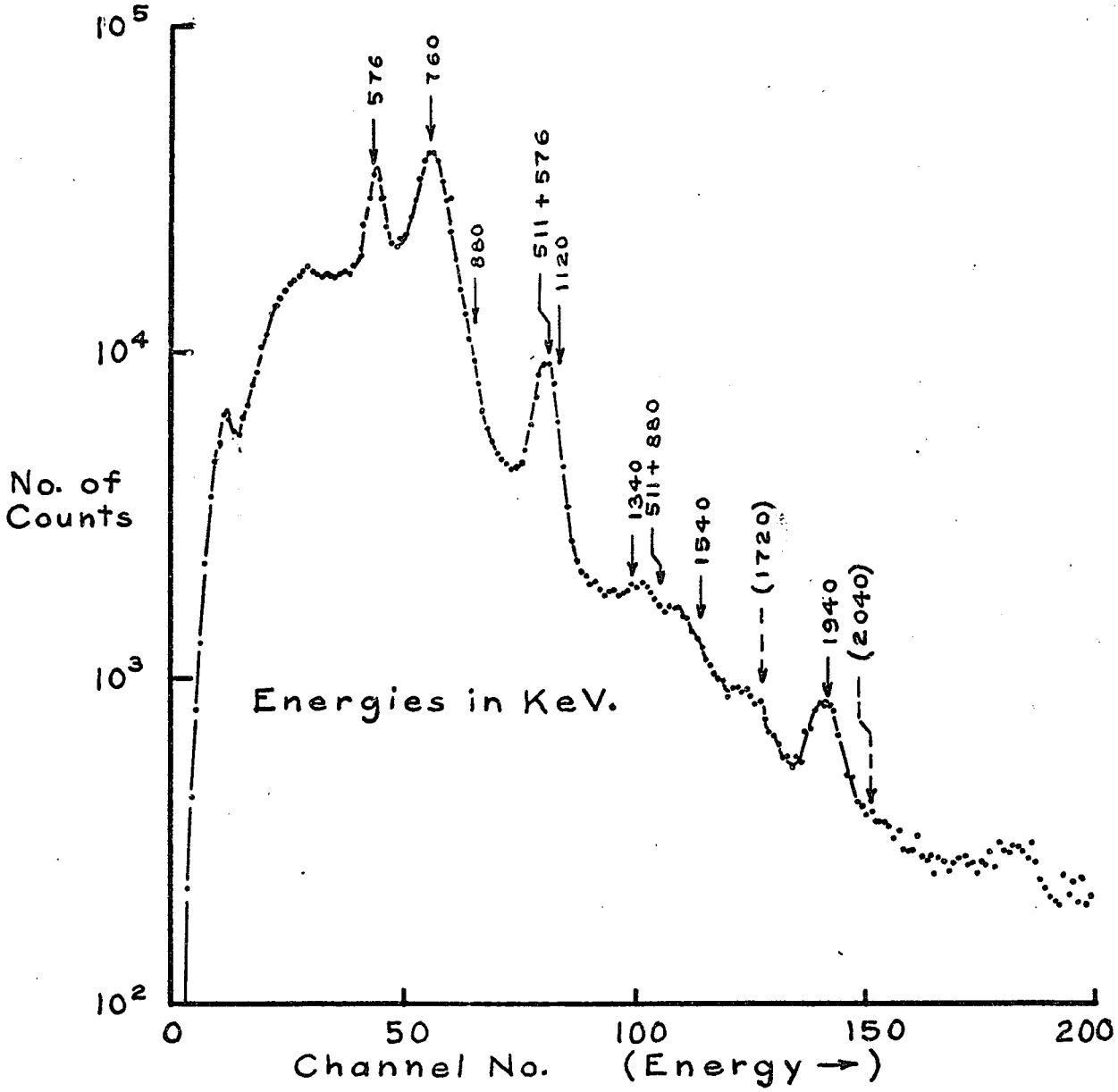

Fig. 13.5 A cascade sum spectrum on Ge^{69}.

Run 2.3: Sum Amplifier A+B output with fast coincidence. r_{ds} = 8 cm. $\theta = 90°$. $2\tau = 77$ nsec. Counting time; 44 hr.

A peak due to the 0.880 MeV level is not evident. The next peak corresponds to the sum of 0.511 MeV and 0.576 MeV with some contribution from cascades from the 1.12 MeV level. No well-defined peaks are observed for the 1.34 MeV and the 1.54 MeV levels. A peak due to 0.511 MeV + 0.880 MeV is not clearly defined, nor is there conclusive evidence for a 1.72 MeV level. Again, the 1.94 MeV peak is evident, and the 2.04 MeV cascade sum is absent.

13.4 The "1.92 MeV Level" Sum-coincidence Spectra.

Figures 13.6, 13.7 and 13.8 show sum-coincidence spectra taken with a relatively wide (~ 8%) sum window set across the 1.92 MeV region. A wide window is preferable in the first set of runs on a level, in order to minimize the problem of sum peak shifts due to the NaI(Tl) non-linear response.

The spectrum in Figure 13.6 was accumulated with r_{ds} = 1/2" and θ = 180°. The following cascades are evident:

0.310 MeV - 1.56 MeV

0.580 MeV - 1.34 MeV

0.880 MeV - 1.047 MeV

0.511 MeV - (0.511 + 0.880) MeV

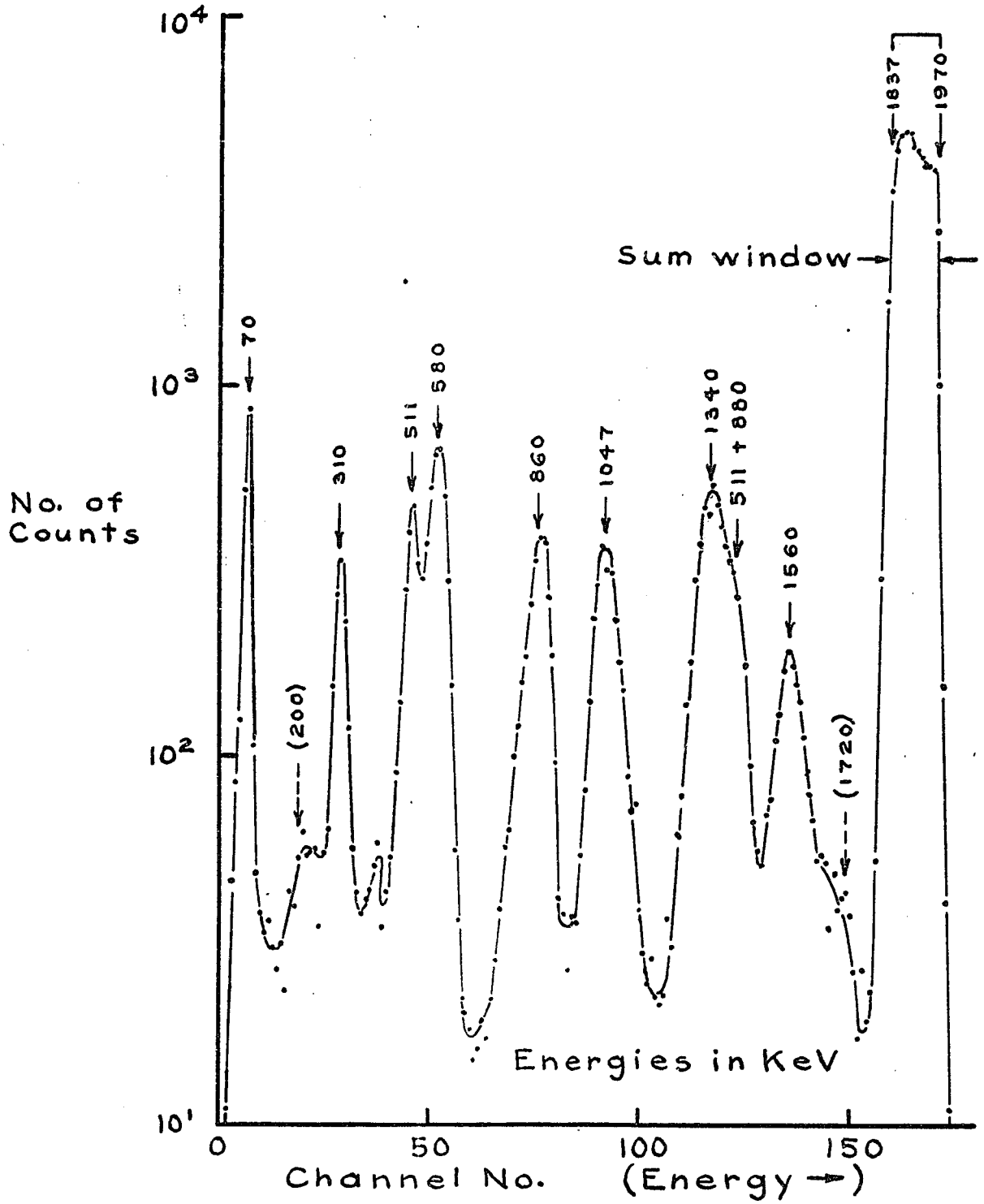

Fig. 13.6. A sum-coincidence spectrum for 1.92 MeV in Ga^{69}.

Run 28.4: $r_{ds} = \frac{1}{2}''$. $\theta = 180°$. Counting time, 29 hr.

The last transition listed does not de-excite the "1.92 MeV level", but arises from annihilation radiation from positrons feeding the 0.880 MeV level. Two peaks, which could correspond to a 0.200 MeV - 1.72 MeV transition, are very weakly indicated. No explanation was found for the 70 KeV peak.

The run in Figure 13.7 is the same as in Figure 13.6 except that a fast coincidence was added. The sum window pulses were counted on a scaler. The window extended from 1.865 MeV to 2.025 MeV. Note that the 70 KeV peak has disappeared, indicating that it is spurious. There is still a suggestion of a 0.200 MeV - 1.72 MeV cascade, but this proposal is not well established. Mussbaum and Suri recorded a 0.190 KeV γ-ray in strong coincidence with a 0.324 MeV γ-ray. If the 0.190 MeV transition occurs between the 1.54 MeV and 1.34 MeV levels, then the 1.72 MeV energy could be a sum of a 0.323 MeV transition between the 1.87 MeV level and the 1.54 MeV level with a 1.34 MeV transition to ground. This would be a 3-γ-ray sum and would therefore appear very weak in intensity. The corresponding 2-γ-ray sums for these transitions may be too weak to be easily detected against other background. The 200 KeV energy is too low to be a backscatter peak from either a 1.92 MeV or a 2.04 MeV γ-ray. If the 0.200 MeV - 1.72 MeV transition does exist, its intensity would have to be less than 1/10 the intensity of the 0.875 MeV - 1.055 MeV cascade. The

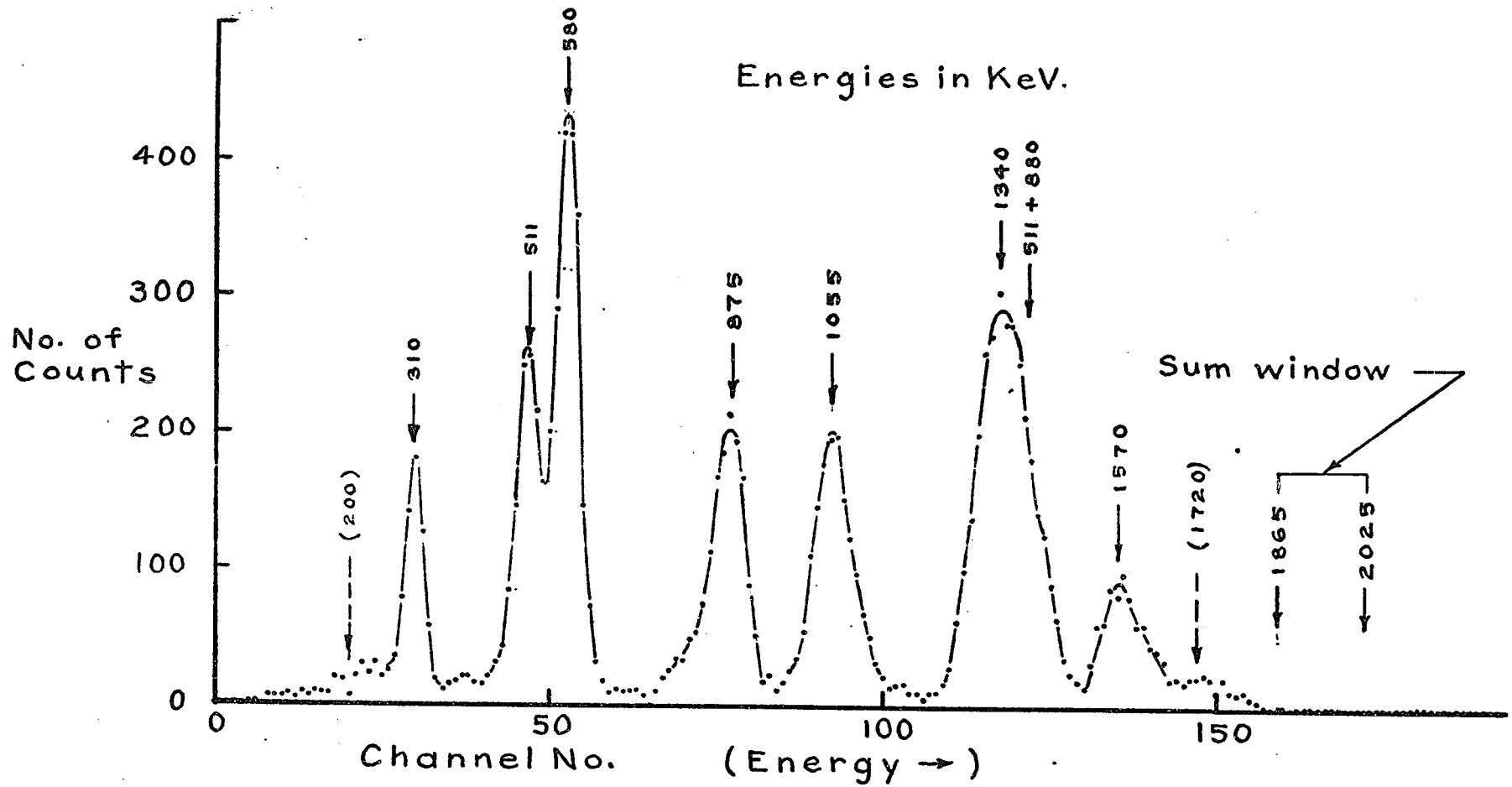

Fig. 13.7. A sum-coincidence spectrum on 1.92 MeV in Ga^{69}, with a fast coincidence.

Run 1.1: $r_{ds} = \frac{1}{2}$". $\theta = 180°$. $2\tau = 77$ nsec. Single crystal counting rate at start of run, 400 c.p.s. Counting time, 21 hr. 26 min. Counts in sum window, 73392.

0.310 MeV - 1.570 MeV, the 0.580 MeV - 1.34 MeV, and the 0.875 MeV - 1.055 MeV transitions are again evident in this spectrum.

Figure 13.8 is a sum-coincidence spectrum taken at $\theta = 90^{\circ}$ and $r_{ds} = 8$ cm. Note that the 0.511 MeV ——— (0.511 + 0.880)MeV transition has vanished, substantiating the proposal that it arises from annihilation radiation combined with the 0.880 MeV γ-ray. The transitions which remain are the 0.315 MeV - 1.57 MeV, the 0.570 MeV - 1.34 MeV, and the 0.876 MeV - 1.04 MeV cascades.

It will be noticed in Figure 13.8 that the peaks are asymmetric. This effect is caused by the sum window being set too low[31]. In Figure 13.6 the asymmetry is still noticeable, but not as pronounced. In Figure 13.6 the sum window is set higher than in Figure 13.8. In Figure 13.7 there is no asymmetry because the sum window is set at the proper energy. This run was the main one used to determine the energies in the transitions. The transitions and the sums of their energies in MeV are:

(1) $(0.310 \pm 0.005) + (1.560 \pm 0.006) = 1.87 \pm 0.011$ MeV

(2) $(0.580 \pm 0.005) + (1.34 \pm 0.011) = 1.92 \pm 0.016$ MeV

(3) $(0.875 \pm 0.006) + (1.055 \pm 0.006) = 1.93 \pm 0.011$ MeV

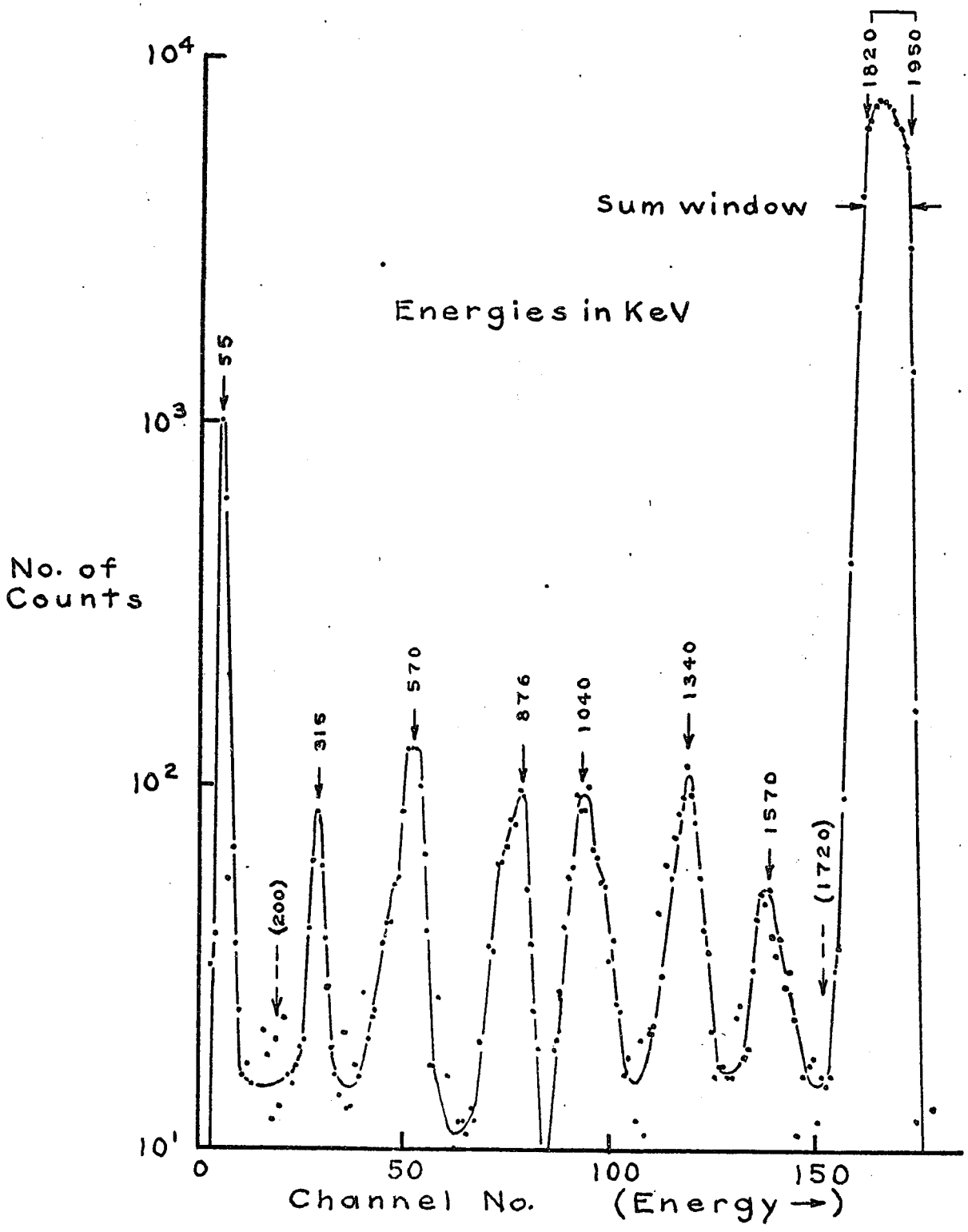

Fig. 13·8. A sum-coincidence spectrum on 1·92 MeV in Ga^{69}.

Run 3·6: r_{ds} = 8 cm. θ = 90°. Single crystal counting rate at start of run, 480 c.p.s. Counting time, 71 hr. 42 min.

Transitions (2) and (3) appear to de-excite the 1.92 MeV level, while it is clear that transition (1) proceeds from a lower level at 1.87 ± 0.011 MeV. It is proposed that the "1.92 level" is actually two levels, and not three, as suggested by Schwerdtfeger. The proposed decay scheme for the 2.04 MeV, the 1.92 MeV and the 1.87 MeV level is given in Figure 13.9. The 2.04 MeV level is de-excited only by a direct transition to ground. A 1.92 MeV cross-over transition occurs from the 1.92 MeV level. In competition with this transition are two cascades: a 0.580 MeV - 1.34 MeV cascade, and a 1.055 MeV - 0.875 MeV cascade. Two different assignments are possible for the 0.580 MeV - 1.34 MeV cascade. The one shown in solid lines has been proposed as the more probable since Nussbaum and Suri measured the coincidence intensity for these two γ-rays to be 10% of the 1.34 MeV γ-ray intensity, and the energies are appropriate. There is no strictly conclusive evidence (here or in Schwerdtfeger's paper) to rule out either possibility. The assignment of this transition remains ambiguous. From energy considerations the 1.055 Mev - 0.875 MeV transition must proceed as shown.

The 1.87 MeV level decays by a 0.310 MeV - 1.56 MeV cascade. The assignment of this cascade is also ambiguous, and two possibilities are indicated. Nussbaum found strong evidence of a 0.190 MeV transition in coincidence with a

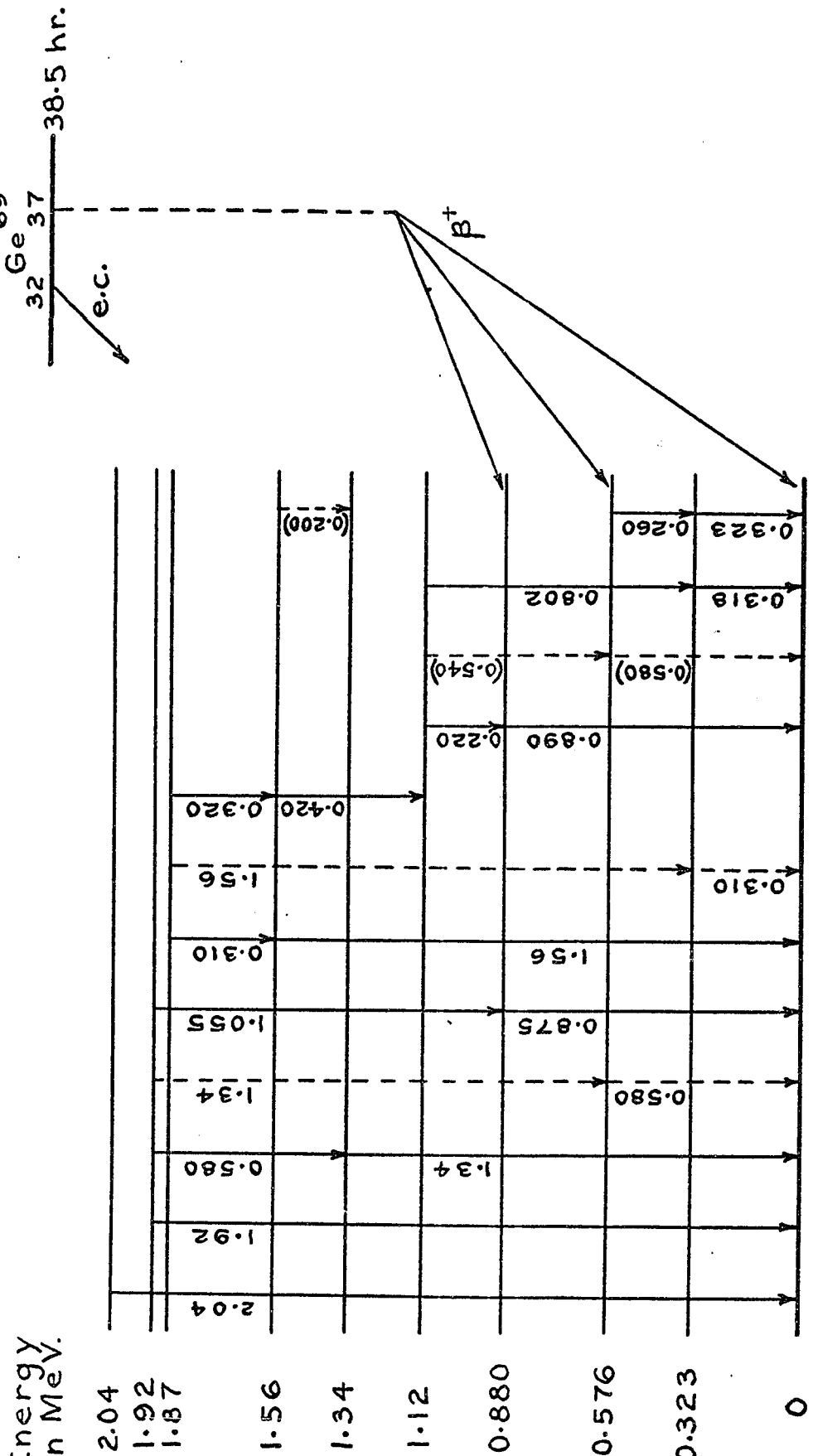

Fig. 13.9. The proposed decay scheme for de-excitation of the 2.04 MeV, 1.92 MeV, 1.87 MeV, and 1.12 MeV levels.

0.324 MeV γ-ray. If the 0.190 MeV transition occurs between the 1.54 MeV and 1.34 MeV levels, then likely a 0.324 MeV transition lies between the 1.87 MeV and 1.54 MeV levels. This possibility should be checked by a sum-coincidence run on the 1.54 MeV level. Previous workers have not presented evidence to conclusively rule out either assignment for the 1.87 MeV level decay.

Approximate intensity measurements have been made on run 1.1 in Figure 13.7. Efficiency curves from Appendix I were used in the calculation. The results are summarized in Table 13.1.

Table 13.1 Transition Intensities

Transition	Intensity I as a % of the cross-over intensity.
0.310 MeV - 1.56 MeV	9.1
0.580 MeV - 1.34 MeV	36
0.875 MeV - 1.055 MeV	19
(0.200 MeV - 1.72 MeV)	<2.1

An error of ± 20% of the values of I has been estimated due to the finite source size and the small detector-source distance. These values should be multiplied by a factor somewhere between 1 and 2 to account for the background in the sum window from the 2.04 MeV cross-over. Even within

the limits of these generous errors it was not possible to find reasonable agreement with intensities listed for the single transitions by Schwerdtfeger. It must be pointed out that the two types of intensity measurements are not strictly comparable until all levels have been analysed.

For more accurate intensity calculations, the detector efficiencies should be measured experimentally and a longer run done at r_{ds} = 8 cms with $\theta = 180^{\circ}$ and 90°.

13.5 The 1.12 MeV Level Sum-coincidence Spectrum.

Figure 13.10 is a sum-coincidence spectrum on the 1.12 MeV level taken with the old spectrometer. Although the old spectrometer had poor gain stability, and its detectors were not matched, this spectrum provides valuable information about the cascades from the 1.12 MeV level. A 0.318 MeV - 0.802 MeV cascade is clearly indicated. These transitions must occur between the 1.12 MeV and the 0.323 MeV level, and between the 0.323 MeV level and ground. A 0.220 MeV - 0.890 MeV cascade is also evident. The 0.220 MeV transition occurs between the 1.12 MeV and the 0.880 MeV level, while the 0.890 MeV transition proceeds to ground from the 0.880 MeV level. The central broad peak is mainly due to background from the 0.576 MeV + 0.511 MeV

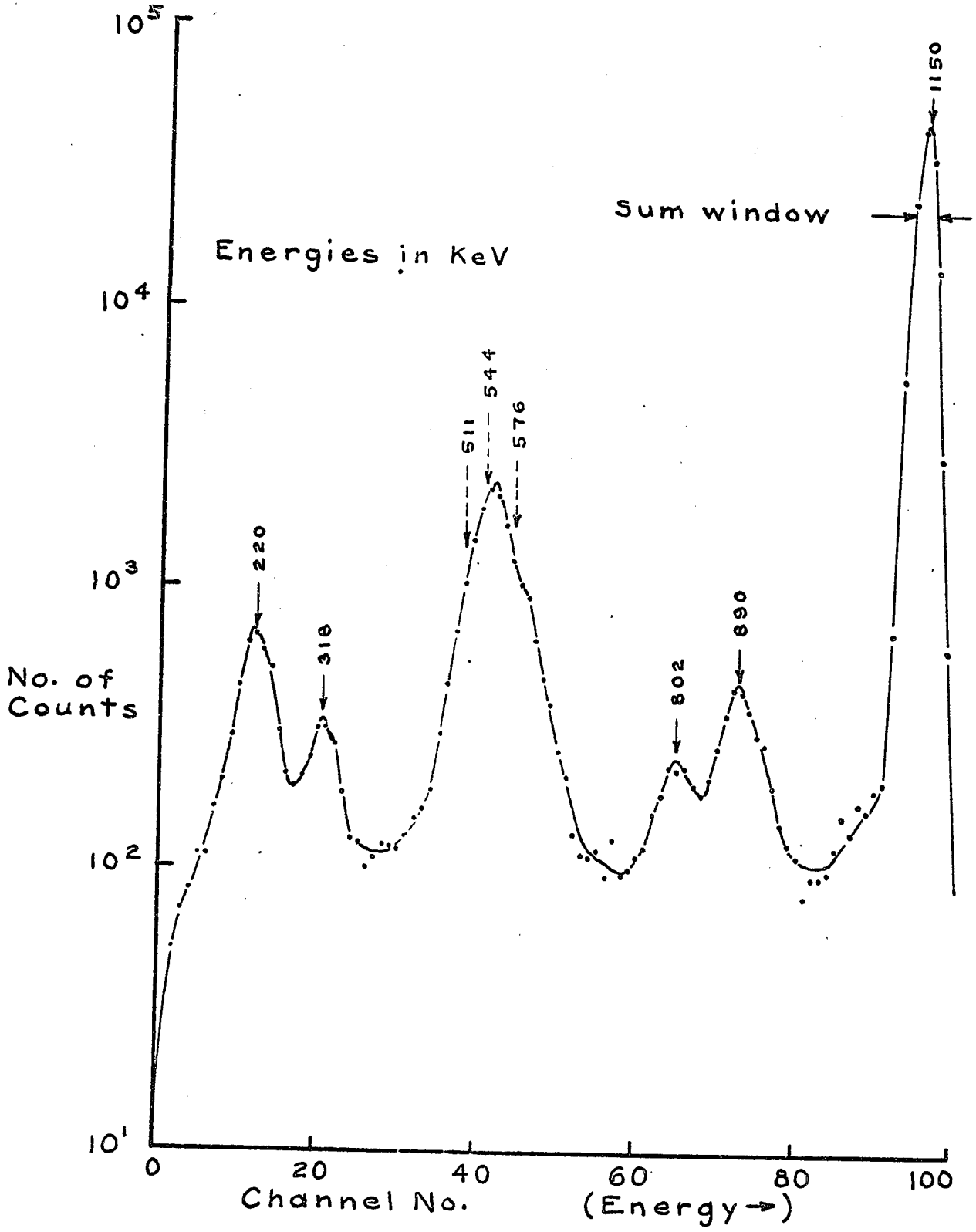

Fig. 13.10. A sum-coincidence spectrum on the 1.12 MeV level in Ga^{69}, taken with the old spectrometer.

sum peak, and does not belong to the 1.12 MeV level. If there is a 0.576 MeV - 0.544 MeV transition, it is obscured by this background. Note that the sum window is too narrow for a first run, and is set a bit too high for the 0.220 MeV - 0.890 MeV cascade.

13.6 Shifts in the Cascade Sum Peaks.

Shifts in the cascade sum peaks have been calculated from data by Devare and Tandon. The values for the studied transitions are presented in Table 13.2. This data should be used for setting the sum window in future runs. It is interesting to note that the weighted averages of the expected sum peak positions for the 1.92 MeV level is 1.946 MeV. This agrees well with the observed value.

Table 13.2

Transition	Energy Sum	Expected Sum Peak Position
0.875 MeV - 1.055 MeV	1.93 MeV	1.962 MeV
0.580 MeV - 1.34 MeV	1.92 MeV	1.951 MeV
0.310 MeV - 1.56 MeV	1.87 MeV	1.898 MeV
0.318 MeV - 0.802 MeV	1.12 MeV	1.150 MeV
0.240 MeV - 0.880 MeV	1.12 MeV	1.139 MeV

13.7 Suggestion for Further Study.

In order to improve the accuracy of the data, longer runs should be made on the 1.92 MeV and 1.87 MeV levels. Measurements should be made at $\theta = 180^{\circ}$ and 90° with $r_{ds} = 8$ cms. Runs with narrower window widths would be helpful. For better intensity calculations, the detector efficiency curves should be measured, and accurate background measurements made for each run. Angular correlation measurements, as previously suggested, should follow.

Many of the observed γ-ray peaks could be composite, consisting of two or more γ-rays of similar energies. To resolve these peaks it would be advantageous to use a Lithium Drift Detector. A study of the non-linearity of response of

the NaI(Tl) detectors should also be made. For further runs a 3-fold increase in the neutron flux is desirable.

The results of the studies on Ge^{69} decay are summarised in Figure 13.9.

CHAPTER 14

CONCLUSIONS

14.1 A Summary of the Results.

The high stability sum-coincidence spectrometer which was developed proved to be a substantial improvement over conventional sum-coincidence spectrometers as described by Hoogenboom. The high stability achieved is demonstrated by typical gain drifts being ± 0.4% for room temperature held to ± 1F° over periods of 4 to 6 days. No gain stabilizers were used. Counting rates up to 1.2×10^4 counts/sec were possible with negligible gain shifts. The addition of a fast coincidence circuit, in conjunction with provision for analysing the Sum Amplifier A + B output greatly improved the versatility of the spectrometer. The technique for analysing spectra that this arrangement allowed is a substantial contribution to the Hoogenboom sum-coincidence method.

In the course of reviewing the theory for the resolution and efficiency of the spectrometer, a new and more versatile expression for the detection efficiency was developed. This expression is based on a more realistic

model for the sum window. It allows efficiency calculations for windows of any width, off-center windows, and for the cross-over intensity in the sum-coincidence spectrum. These calculations were not possible with the Hoogenboom formula.

Several levels were studied in the Ge^{69} decay scheme. The highest energy levels in Ga^{69} following Ge^{69} decay were shown to be 2.04 MeV, 1.92 MeV and 1.87 MeV. A cross-over and two cascades were found to de-excite the 1.92 MeV level, while the 2.04 MeV level was shown to decay only by a cross-over, and the 1.87 MeV level by a 0.310 MeV - 1.56 MeV cascade. Two cascades were found to de-excite the 1.12 MeV level. For the 0.576 MeV level, evidence was found for the existence of a 260 KeV - 323 KeV cascade. The results are given in Figure 13.9.

The runs on Ge^{69} indicated that a higher activity should be used. For more efficient use of the neutron generator, the spectrometer should be operated in a remote location, where continuous sample counting could be carried out. Longer runs on the 1.92 MeV and 1.87 MeV levels are required with narrow sum windows and with $\theta = 180^{\circ}$ and 90° at $r_{ds} = 8$ cms.

14.2 Suggestion for Further Projects.

In the course of this work, several concepts came under consideration which gave rise to ideas that could develop into sizeable projects in themselves. These proposals are given here along with other suggestions for further study.

High on the priority list is a measurement of the non-linearity in pulse-height response of the NaI(Tl) detectors used in the spectrometer. For the present work, data from Devare and Tandon has been used, but their measurements were made on a well crystal, and may not be strictly accurate for the Harshaw 3" x 3" detectors.

As previously described, two single channel analysers should be constructed for use with the spectrometer. The gain stabilizer, a project in itself, should be developed for use in longer runs.

Although a critical test of the time resolution theory was not achieved, several proposals arose. Consideration of the theory by Gatti and Svelto indicate that a "fractional pulse height trigger" should be constructed in order to improve the time resolution of the fast coincidence unit. This trigger is of most importance for analysis of the low energy region, where time resolution is the worst. It would be interesting to re-investigate the

resolving time with the existing equipment for different photomultiplier high voltages, and for energies from 30 KeV to 3 MeV.

A derivation for r_{ls}, using a new method similar to that devised for the calculation of e_{ls} in Appendix I, would be of interest. The basis for this new derivation is more realistic than Hoogenboom's model. The possibility is suggested that this new analysis could predict the shapes and positions for peaks in the sum-coincidence spectrum even when the sum window is off center.

Of course, an extension of the investigation of Ge^{69} decay should be carried out. This study should include angular correlation experiments.

14.3 Conclusion.

It is felt that a large contribution has been made to the development of a versatile and highly stable sum-coincidence spectrometer. Several new ideas have been proposed for improvement of the spectrometer and for the refinement of its theory. Substantial information has been gathered on the decay of Ge^{69}. This thesis should provide a thorough guide for continuation of the research undertaken in this project.

APPENDIX I

RESOLUTION AND EFFICIENCY CALCULATIONS.

I.1 Derivation of the Hoogenboom Formulas.

For derivation of the efficiency and resolution formulas the photopeaks formed by the γ-rays are assumed to be Gaussian in shape. For a γ-ray of energy E_{oi} the spectral shape is given as

$$f_i(E_i - E_{oi}) = I_i e^{-\mu^2 \left(\frac{E_i - E_{oi}}{\Gamma_i}\right)^2} \qquad (I.1)$$

where I_i is the maximum height of the photopeak at energy $E_i = E_{oi}$, and Γ_i is the F.W.H.M. of the peak. From the definition of Γ_i, μ can be shown to be

$$\mu = 2\sqrt{\ln 2} \qquad (I.2)$$

If the area under the photopeak is normalised to give the intrinsic photopeak efficiency, ϵ_i, for the γ-ray of energy E_{oi}, then

$$\epsilon_i = \int_{E_i = -\infty}^{+\infty} f_i(E_i - E_{oi})\,dE_i \qquad (I.3)$$

$$\text{giving} \quad I_1 = \frac{c_1}{\sqrt{\pi}} \left(\frac{\mu}{\Gamma_1}\right) \tag{I.4}$$

Assuming a symmetrical detection system, we can write the probability that γ-ray, γ_1, of energy E_{o1} gives a point of energy E_1 in its photopeak due to absorption in detector A, as

$$f_1(E_1 - E_{o1}) = I_1 e^{-\mu^2 \left(\frac{E_1 - E_{o1}}{\Gamma_1}\right)^2} \tag{I.5}$$

For γ-ray, γ_2, of energy E_{o2}, absorbed in detector B the probability is

$$f_2(E_2 - E_{o2}) = I_2 e^{-\mu^2 \left(\frac{E_2 - E_{o2}}{\Gamma_2}\right)^2} \tag{I.6}$$

These γ-rays add to an energy

$$E_{os} = E_{o1} + E_{o2} \tag{I.7}$$

When the two γ-rays are added, the cascade sum spectrum so obtained is described by the probability function

$$f_c(E_c - E_{oc}) = \int_{E_2 = -\infty}^{+\infty} f_1(E_1 - E_{o1})\, f_2(E_2 - E_{o2})\, dE_2 \tag{I.8}$$

where $$E_1 = E_\sigma - E_2 \qquad \text{(I.9)}$$

and $$E_{o\sigma} = E_{os} = E_{o1} + E_{o2} \qquad \text{(I.10)}$$

Equation (I.8) is evaluated as

$$f_\sigma(E_\sigma - E_{o\sigma}) = I_\sigma e^{-\mu^2\left(\frac{E_\sigma - E_{o\sigma}}{r_\sigma}\right)^2}$$

$$= \frac{\mu}{\sqrt{\pi}} \frac{\epsilon_1\epsilon_2}{\sqrt{r_1^2 + r_2^2}} e^{-\mu^2\left(\frac{E_\sigma - E_{o\sigma}}{\sqrt{r_1^2 + r_2^2}}\right)^2} \qquad \text{(I.11)}$$

Hence, the efficiency for the cascade sum peak*, or the area under this peak is given by

$$\epsilon_\sigma = \epsilon_1 \cdot \epsilon_2 \qquad \text{(I.12)}$$

and the F.W.H.M. of the cascade sum peak is

$$r_\sigma = \sqrt{r_1^2 + r_2^2} \qquad \text{(I.13)}$$

*For actual cascade sum runs this value must be multiplied by 2 to account for each γ-ray being detected in either crystal.

To calculate the F.W.H.M. of the peaks in the sum-coincidence spectrum, Hoogenboom assumed a Gaussian shape for the peak transmitted through the sum window*. This shape is given by

$$f_s(E_s - E_{os}) = I_s e^{-\mu^2\left(\frac{E_s - E_{os}}{\Gamma_s}\right)^2} \qquad (I.14)$$

where Γ_s is the window width. The argument for the derivation of the shape, f_{1s}, of the peak for γ-ray, γ_1 in the sum-coincidence spectrum follows. The probability of detecting a pulse height E_2 due to the detection of γ_2 in detector B is

$$f_2(E_2 - E_{o2}) \qquad (I.6)$$

The probability of the selected sum peak pulse height E_s appearing in the sum window is

$$f_s(E_s - E_{os}) \qquad (I.15)$$

*Hereafter called the "gated sum peak".

The probability that these last two events occur at the same time, such that $E_s = E_1 + E_2$, is

$$f_2(E_2 - E_{o2}) \cdot f_s(E_1 + E_2 - E_{os}) \qquad \text{(I.16)}$$

The total probability for all energies E_2 is

$$\int_{E_2 = -\infty}^{+\infty} f_2(E_2 - E_{o2}) \cdot f_s(E_1 + E_2 - E_{os})dE_2 \qquad \text{(I.17)}$$

The probability that γ-ray γ_1 gives a pulse height E_1 such that $E_s = E_1 + E_2$ at the same time is

$$P = f_1(E_1 - E_{o1}) \int_{E_2 = -\infty}^{+\infty} f_2(E_2 - E_{o2}) \cdot f_s(E_1 + E_2 - E_{os})dE_2 \qquad \text{(I.18)}$$

This is just the probability distribution for the peak for γ-ray γ_1 in the sum-coincidence spectrum; i.e.

$$P = f_{1s}(E_{1s} - E_{o1}) = I_{1s}e^{-\mu^2\left(\frac{E_{1s} - E_{o1}}{\Gamma_{1s}}\right)^2} \qquad \text{(I.19)}$$

Evaluation of equations (I.18) and (I.19) show the F.W.H.M. of the γ_1 peak in the sum-coincidence spectrum to be

$$\Gamma_{1s} = \frac{\Gamma_1\sqrt{\Gamma_2^2 + \Gamma_s^2}}{\sqrt{\Gamma_1^2 + \Gamma_2^2 + \Gamma_s^2}} \qquad \text{(I.20)}$$

and the efficiency for detection of γ_1 in the sum-coincidence spectrum to be

$$\epsilon_{1s} = 2\sqrt{\frac{\ln 2}{\pi}}\,\epsilon_1\epsilon_2\,\frac{\epsilon_s}{\sqrt{\Gamma_1^2 + \Gamma_2^2 + \Gamma_s^2}} \qquad \text{(I.21)}$$

Hoogenboom sets $\epsilon_s = \Gamma_s$ to obtain

$$\epsilon_{1s} = 2\sqrt{\frac{\ln 2}{\pi}}\,\epsilon_1\epsilon_2\,\frac{\Gamma_s}{\sqrt{\Gamma_1^2 + \Gamma_2^2 + \Gamma_s^2}} \qquad \text{(I.22)}$$

This is equivalent to setting the gated sum peak maximum height to

$$I_s = \frac{n}{\sqrt{\pi}} \qquad \text{(I.23)}$$

By interchanging appropriate subscripts, equations (I.20) and (I.22) yield the values for γ_2.

I.2 A Direct Intensity Calculation.

Since it was found difficult to justify the choice of I_s made by Hoogenboom (equation I.23) in a logical fashion, a more direct derivation for an efficiency formula was constructed.

Equations (I.11), (I.12) and (I.13) define the shape of the cascade sum peak $f_\sigma(E_\sigma - E_{o\sigma})$. This peak contains all the events where γ_1 has entered detector A in coincidence with γ_2 entering detector B. The area under this curve represents the efficiency for detection of the coincident events. If a sum window, instead of a Gaussian window, with sharply defined, straight edges and width Γ_s is applied symmetrically to this peak (i.e. from $E_\sigma = E_{o\sigma} - \frac{\Gamma_s}{2}$ to $E_\sigma = E_{o\sigma} + \frac{\Gamma_s}{2}$), then only those events lying within the window contribute to the γ_1 peak in the sum-coincidence spectrum. Consequently, the area under $f_\sigma(E_\sigma - E_{o\sigma})$ between $E_\sigma = E_{o\sigma} - \frac{\Gamma_s}{2}$ and $E_\sigma = E_{o\sigma} + \frac{\Gamma_s}{2}$ represents the efficiency, ϵ_{1s}, for detection of γ_1 in the sum-coincidence spectrum.

$$\epsilon_{1s} = \int_{E_\sigma = E_{\infty} - \frac{\Gamma_s}{2}}^{E_{\infty} + \frac{\Gamma_s}{2}} \Gamma_\sigma (E_\sigma - E_{\infty}) dE_\sigma$$

$$= \int_{E_\sigma = E_{\infty} - \frac{\Gamma_s}{2}}^{E_{\infty} + \frac{\Gamma_s}{2}} I_\sigma e^{-\mu^2 \left(\frac{E_\sigma - E_{\infty}}{\Gamma_\sigma} \right)^2} dE_\sigma \qquad (I.24)$$

Now make the substitution

$$\frac{\epsilon^2}{2} = \mu^2 \left(\frac{E_\sigma - E_{\infty}}{\Gamma_\sigma} \right)^2 \qquad (I.25)$$

$$dE_\sigma = \frac{\Gamma_\sigma}{\mu \sqrt{2}} \, d\epsilon \qquad (I.26)$$

and (I.24) becomes

$$\epsilon_{1s} = \frac{I_o r_o}{\mu \sqrt{2}} \int_{t = -\frac{\mu r_s}{2 r_o}}^{t = \frac{\mu r_s}{2 r_o}} e^{-\frac{t^2}{2}} dt$$

$$= 2\epsilon_1 \cdot \epsilon_2 \, \phi\left(\frac{\mu r_s}{\sqrt{2}\, r_o}\right) \qquad \text{(I.27)}$$

The function

$$\phi\left(\frac{\mu r_s}{\sqrt{2}\, r_o}\right) = \phi(x) = \frac{1}{\sqrt{2\pi}} \int_{t = o}^{t = x} e^{-\frac{t^2}{2}} dt \qquad \text{(I.28)}$$

$$\text{where} \quad x = \frac{\mu r_s}{\sqrt{2}\, r_o} = \frac{\sqrt{2 \ell n 2}\, r_s}{r_o} \qquad \text{(I.29)}$$

is a common and well tabulated integral[36].

Hence the efficiency for detecting γ-ray γ_1, or γ-ray γ_2 in the sum-coincidence spectrum is

$$\epsilon_{1s} = \epsilon_{2s} = 2\epsilon_1 \cdot \epsilon_2 \, \phi\left(\frac{\mu r_s}{\sqrt{2}\, r_\sigma}\right) \qquad \text{(I.27)}$$

This equation is accurate to the extent that the singles spectrum photopeaks can be represented by Gaussian shapes.

Equation (I.27) is also useful in that it predicts the efficiency for detecting the cross-over transition in the sum-coincidence spectrum. For the cross-over, $\epsilon_1 \cdot \epsilon_2$ is replaced by ϵ_c, the efficiency for detecting the cross-over in detector A; and r_σ is replaced by r_c, the F.W.H.M. of the cross-over photopeak. Clearly, the efficiency for detecting the cross-over in the sum-coincidence spectrum is

$$\epsilon_{cs} = 2\epsilon_c \, \phi\left(\frac{\mu r_s}{\sqrt{2}\, r_c}\right) \qquad \text{(I.30)}$$

For an approximate comparison of equation (I.27) with Hoogenboom's formula (equation I.22), the function $\phi(x)$ can be expanded[37].

$$\Phi(x) = \frac{1}{\sqrt{\pi}} \left[\frac{x}{2} - \frac{\frac{x}{2}^3}{1!3} + \frac{\frac{x}{2}^5}{2!5} - \frac{\frac{x}{2}^7}{3!7} + \text{.....} \right] \qquad \text{(I.31)}$$

For $\frac{x}{2} < 1$ we approximate $\Phi(x)$ by

$$\Phi(x) \approx \frac{1}{\sqrt{\pi}} \left(\frac{x}{2}\right) \qquad \text{(I.32)}$$

Using this in equation (I.27) the approximate values of ϵ_{1s} for $r_s / \sqrt{r_1^2 + r_2^2} < 1$ is

$$\epsilon_{1s} = \epsilon_{2s} = 2\sqrt{\frac{\ln 2}{\pi}} \frac{\epsilon_1 \epsilon_2 r_s}{\sqrt{r_1^2 + r_2^2}} \qquad \text{(I.33)}$$

Equation (I.33) differs from Hoogenboom's equation (I.22) only in that the $\sqrt{r_1^2 + r_2^2 + r_s^2}$ term in equation (I.22) becomes $\sqrt{r_1^2 + r_2^2}$ in equation (I.33).

It is felt that equations (I.27) and (I.30) provide a much more accurate estimation of the detection efficiencies in the sum-coincidence spectrum than Hoogenboom's formulas do; particularly for a wide sum window. It would be

interesting to use the same technique developed in this section to obtain more accurate formulas for Γ_{1s} and Γ_{2s}. While accurate values for Γ_{1s} and Γ_{2s} are not extremely important, precise formulas for the efficiencies ϵ_{1s}, ϵ_{2s} and ϵ_{es} are of utmost importance for the analysis of transition intensities in γ-ray spectra.

The same analysis, but with different limits of integration, could be used to calculate the effect of an off-center sum window on the detection efficiency in the sum-coincidence spectrum. The calculation is very simple, and leads to an expression involving the sum of two easily evaluated $\Phi(x)$ terms. Since there are often several competing cascades de-exciting a level, and the non-linearity of NaI(Tl) shifts the cascade sum peak for each cascade by a different value, it is inevitable that the sum window will be set off-center for all but one of these cascades (or the cross-over peak). Hence, it is necessary to calculate detection efficiencies for off-center sum windows. Hoogenboom's formula does not provide for this case, nor for a calculation of the cross-over detection efficiency in the sum-coincidence spectrum. For a sum window shifted off center by an energy interval "a", the efficiency formula becomes

$$\epsilon_{1s} = \epsilon_{2s} = \epsilon_1 \epsilon_2 \left\{ \Phi\left[\frac{2u}{\sqrt{2}\, r_o}\left(\frac{r_s}{2} + a\right)\right] + \Phi\left[\frac{2u}{\sqrt{2}\, r_o}\left(\frac{r_s}{2} - a\right)\right]\right\} \quad (I.34)$$

This function can be easily evaluated from known values of ϵ_1 and ϵ_2, and from tables of the error function, $\Phi(x)$. A similar formula applies for the cross-over detection efficiency.

I.3 Detection Efficiencies for the Singles Spectrum.

Figure I.1 shows the transmission efficiency I/I_o of the aluminum window in the detectors used.

$$\frac{I}{I_o} = 2^{-d/d_{1/2}} \quad (I.35)$$

where I is the transmitted γ-ray intensity, I_o is the incident γ-ray intensity, d is the window thickness and $d_{1/2}$ is the half thickness for the γ-ray energy, E. $d_{1/2}$ is a function of E. Figure I.1 shows that I/I_o can be taken as 1 for energies above 50 KeV.

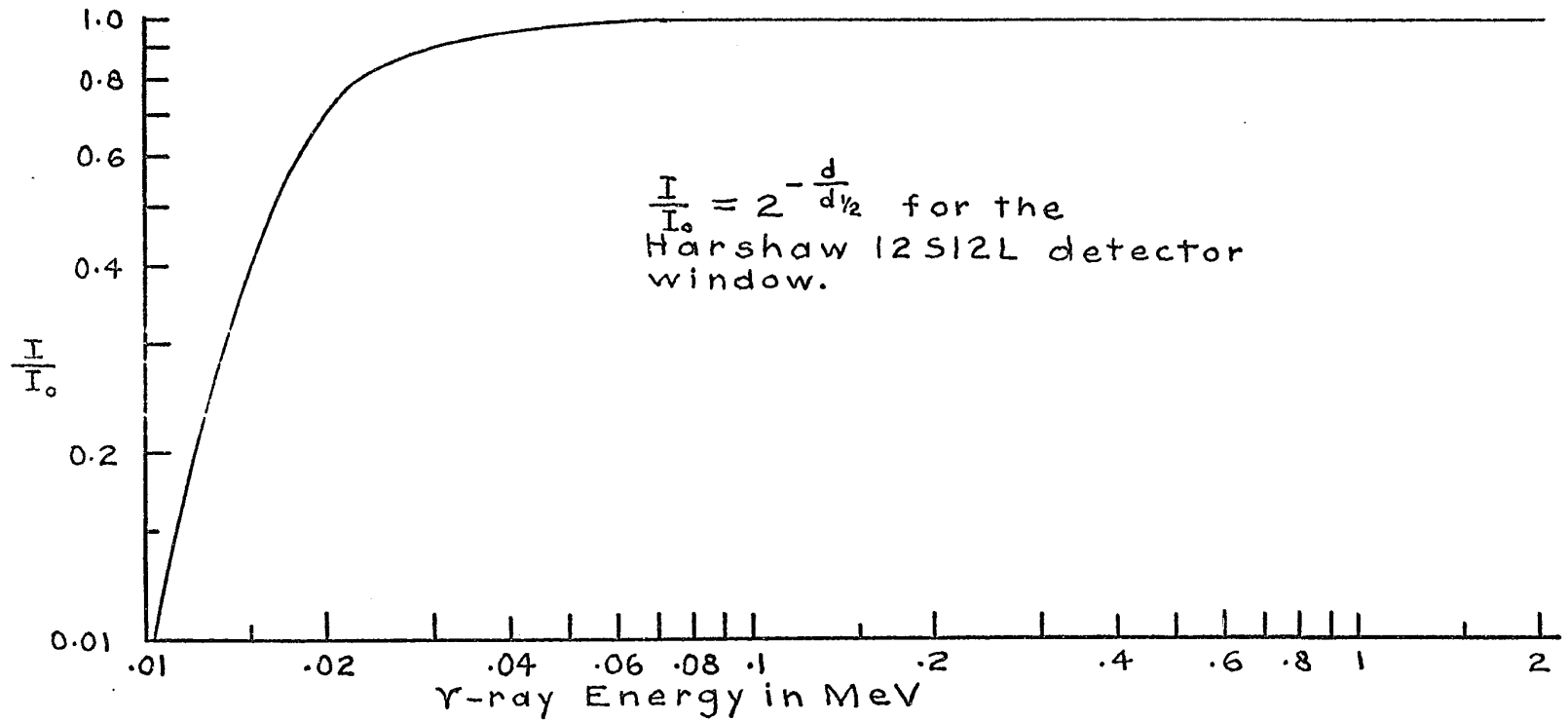

Fig. I.1. The detector window transmission factor.

Figure I.2 gives the total γ-ray detection efficiency, ϵ_t, and the absolute photopeak detection efficiency, ϵ_p, for a γ-ray of energy E in a singles spectrum. The curves are given for a 3" x 3" NaI(Tl) crystal, with a detector-source distance r_{ds} = 8 cms. r_{ds} is the distance from the assumed point source, on the cylindrical axis of the crystal, to the front face of the NaI(Tl) crystal. The curves were calculated from theoretical curves by Wolicki et al[1,38], combined with experimental photofraction measurements by Heath[1,39].

Figure I.3 shows the measured resolution curve for the two detectors used. The resolution is expressed in percent; i.e. $\frac{\Gamma_1}{E_1} \times 100\%$, where Γ_1 is the F.W.H.M. of the photopeak for the gamma-ray of energy E_1.

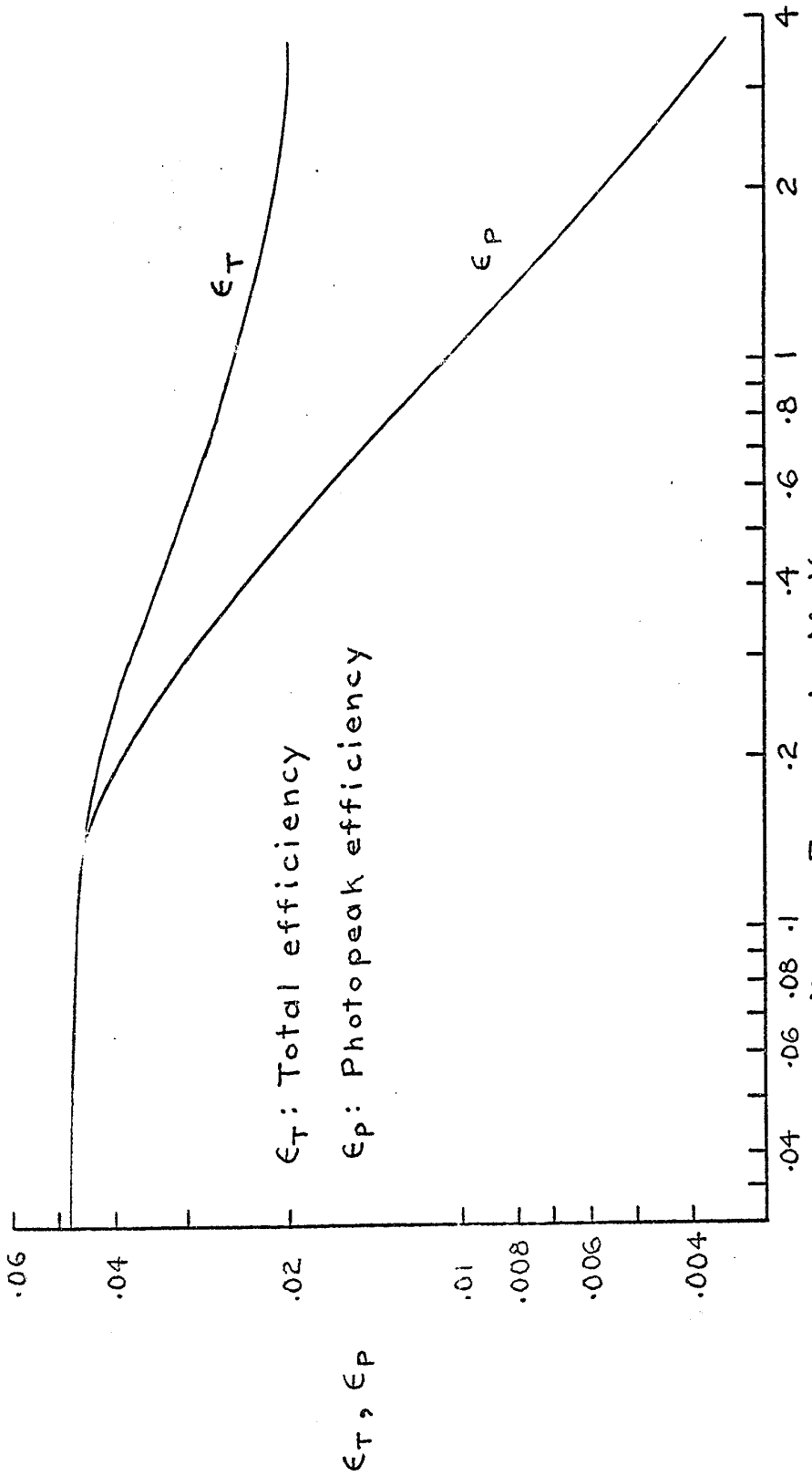

Fig. I·2. Calculated γ-ray detection efficiencies for a 3"X 3" NaI(Tl) crystal with r_{ds} = 8 cm.

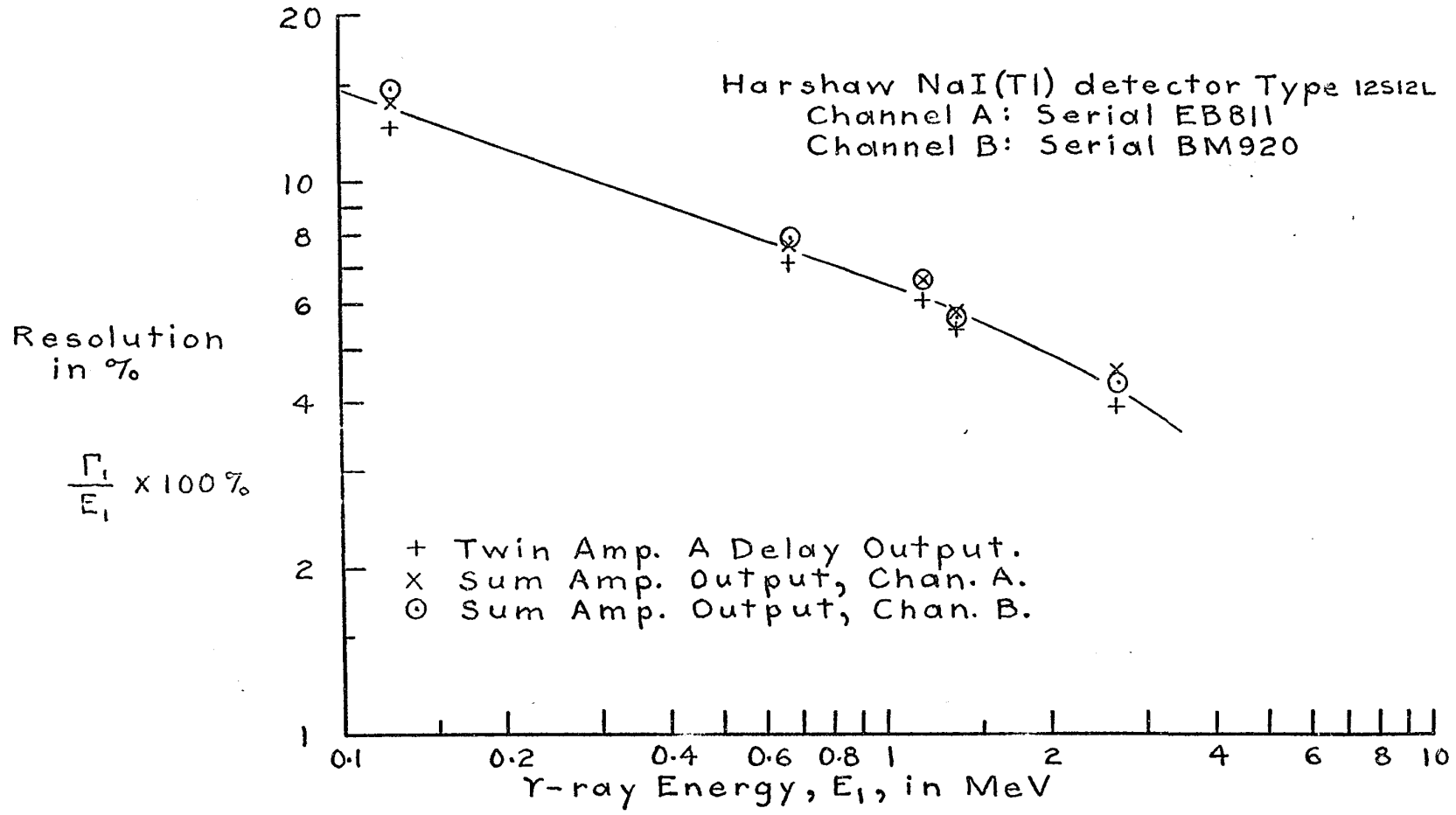

Fig. I-3 The detector resolution curve.

APPENDIX II

CALCULATIONS ON THE OPERATIONAL AMPLIFIER.

II.1 The General Operational Amplifier.

Calculations are made for the voltage and current gains, and the input and output impedances for the general operational amplifier shown in figure II.1. The circuit consists of a transistor amplifier with an open loop current gain -A. The input impedance of this amplifier is the base resistance to ground, R_b, of the first transistor. For generality, an output impedance R_o is shown. The output voltage, V_o, is developed with the output current i_L in the load Z_L. A feedback through the impedance Z_f gives negative feedback to the base of the first transistor V_i is the input voltage developed across Z_i, the input load. The voltage developed across R_b is termed V_I.

The three voltages may be expressed as:

$$V_i = Z_i i_i + V_I \qquad \text{(II.1)}$$

$$V_I = i_a R_b \qquad \text{(II.2)}$$

$$V_o = i_L Z_L = i_f Z_f + V_I \qquad \text{(II.3)}$$

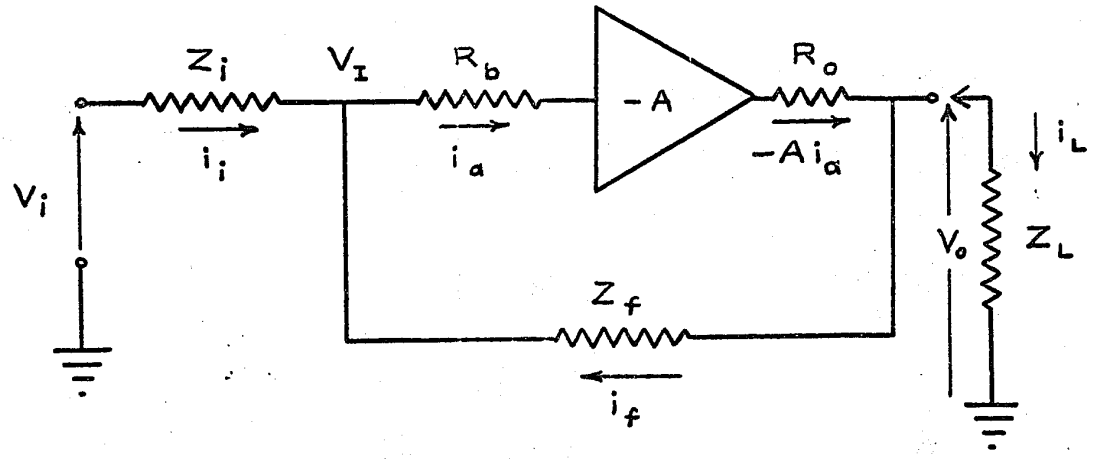

Fig. II.1. The operational amplifier.

The two node equations give:

$$i_i = i_a - i_f \qquad \text{(II.4)}$$

$$-Ai_a = i_f + i_L \qquad \text{(II.5)}$$

II.2 Voltage Gain.

The voltage gain $\frac{V_o}{V_i}$ is calculated as follows. To eliminate i_a, equations (II.4) and (II.5) are combined to give:

$$i_L = -Ai_i - (A + 1)i_f \qquad \text{(II.6)}$$

Also from equations (II.3) and (II.2),

$$i_L = i_f \frac{Z_f}{Z_L} + \frac{i_a R_b}{Z_L} \qquad \text{(II.7)}$$

and substituting for i_a from equation (II.4) equation (II.7) becomes

$$i_L = i_f \frac{Z_f}{Z_L} + \frac{(i_i + i_f)R_b}{Z_L} \qquad \text{(II.8)}$$

Equating equations (II.6) and (II.8) gives:

$$-(A + \frac{R_b}{Z_L})i_i = (A + 1 + \frac{Z_f + R_b}{Z_L})i_f \qquad \text{(II.9)}$$

From equations (II.1), (II.2) and II.3) the voltage gain is

$$\frac{V_o}{V_i} = \frac{i_f Z_f + i_a R_b}{Z_i i_i + i_a R_b} \qquad \text{(II.10)}$$

and from equations (II.4) and (II.9) this is simplified to

$$\frac{V_o}{V_i} = - \frac{A Z_f - R_b}{(A + 1 + \frac{Z_f + R_b}{Z_L}) Z_i + (1 + \frac{Z_f}{Z_L}) R_b} \qquad \text{(II.11)}$$

It will be noticed here that the voltage gain is independent of R_o. Typical values for an amplifier where the impedances are all resistive are:

$$A = 2 \times 10^4$$

$$R_b = 200 \ \Omega$$

$$Z_i = 10K$$

$$Z_f = 10K$$

$$Z_L = 2K$$

Using these values it may be seen that

$$\frac{V_o}{V_i} \approx - \frac{A}{(A + 6)} \quad \frac{Z_f}{Z_i} \approx - \frac{Z_f}{Z_i} \qquad \text{(II.12)}$$

From equations (II.1), (II.2) and II.3) the voltage gain is

$$\frac{V_o}{V_i} = \frac{i_f Z_f + i_a R_b}{Z_i i_i + i_a R_b} \qquad \text{(II.10)}$$

and from equations (II.4) and (II.9) this is simplified to

$$\frac{V_o}{V_i} = - \frac{A Z_f - R_b}{(A + 1 + \frac{Z_f + R_b}{Z_L}) Z_i + (1 + \frac{Z_f}{Z_L}) R_b} \qquad \text{(II.11)}$$

It will be noticed here that the voltage gain is independent of R_o. Typical values for an amplifier where the impedances are all resistive are:

$$A = 2 \times 10^4$$

$$R_b = 200\ \Omega$$

$$Z_i = 10K$$

$$Z_f = 10K$$

$$Z_L = 2K$$

Using these values it may be seen that

$$\frac{V_o}{V_i} \approx - \frac{A}{(A + 6)} \qquad \frac{Z_f}{Z_i} \approx - \frac{Z_f}{Z_i} \qquad \text{(II.12)}$$

The voltage gain is clearly independent of the amplifier open loop gain, $-A$, and depends only on the ratio of the feedback impedance to the input load.

In general for an operational amplifier the conditions

$$A \gg 1$$

$$AZ_f \gg R_b$$

$$A \gg \frac{Z_f + R_b}{Z_L}$$

and $$(A + 1 + \frac{Z_f + R_b}{Z_L})Z_1 \gg (1 + \frac{Z_f}{Z_L})R_b$$

are met and equation (II.12) is valid to a very small error.

II.3 Current Gain.

The current gain $\frac{i_L}{i_1}$ is calculated in the following manner. From equations (II.2), (II.3) and (II.4) V_I and i_a are eliminated to give

$$i_f(Z_f + R_b) = i_L Z_L - i_1 R_b \qquad \text{(II.13)}$$

Equations (II.13) and (II.6) are combined to eliminate i_f and give

$$-(\frac{Z_f + R_b + (A + 1)Z_L}{A + 1})i_L = \left[\frac{A(Z_f + R_b) - (A + 1)R_b}{A + 1}\right] i_1$$

(II.14)

Hence

$$\frac{i_L}{i_1} = -\frac{A Z_f - R_b}{(A+1)Z_L + (Z_f + R_b)} \qquad \text{(II.15)}$$

Here typical values are

$$A = 10^4$$

$$Z_f = 5K$$

$$R_b = 200\ \Omega$$

$$Z_L = 500\ \Omega$$

and again it is guaranteed that

$$AZ_f \gg R_b$$

and $$(A+1)Z_L \gg (Z_f + R_b)$$

so that

$$\frac{i_L}{i_1} = -\left(\frac{A}{A+1}\right)\frac{Z_f}{Z_L} = -\frac{Z_f}{Z_L} \qquad \text{(II.16)}$$

The current gain depends only on the ratio of the feedback impedance to the load impedance.

II.4 Input Impedance.

The impedance of the virtual ground seen at the junction of Z_f and R_b is easily derived. i_f from equation (II.4) is substituted in equation (II.9) which reduces to

$$i_i = \frac{(A + 1 + \frac{Z_f + R_b}{Z_L})}{(1 + \frac{Z_f}{Z_L})} i_a \qquad \text{(II.17)}$$

The input impedance at the virtual ground is

$$Z_I = \frac{V_I}{i_i} = \frac{i_a R_b (1 + \frac{Z_f}{Z_L})}{(A + 1 + \frac{Z_f + R_b}{Z_L}) i_a}$$

$$= \frac{R_b (1 + \frac{Z_f}{Z_L})}{(A + 1 + \frac{Z_f + R_b}{Z_L})} \qquad \text{(II.16)}$$

Usually, $\frac{Z_f}{Z_L} \gg 1$

and $A \gg 1 + \frac{Z_f + R_b}{Z_L}$

so that (II.18) may be simplified to

$$Z_I = \frac{R_b \frac{Z_f}{Z_L}}{A} \qquad \text{(II.19)}$$

For

$A = 10^4$

$R_b = 200\ \Omega$

$Z_f = 10K$

$Z_L = 2K$

$Z_I = 0.1\ \Omega$

For

$A = 10^4$

$R_b = 200\ \Omega$

$Z_f = 5K$

$Z_L = 500\ \Omega$

$Z_I = 0.2\ \Omega$

It is evident that Z_I is extremely small and the junction of Z_1, Z_f and R_b may be considered a virtual ground.

II.5 Output Impedance.

To calculate the output impedance as seen by the load Z_L, it is assumed that the operational amplifier is driven with a constant current, i_i. From equations (II.2), (II.3) and (II.4)

$$V_o = (Z_f + R_b)\, i_a - i_i Z_f \qquad \text{(II.20)}$$

From equations (II.4) and (II.5)

$$i_a = \frac{i_i - i_L}{A + 1} \qquad \text{(II.21)}$$

Hence (II.20) becomes

$$V_o = \frac{R_b - AZ_f}{A + 1}\, i_i - \frac{Z_f + R_b}{A + 1}\, i_L \qquad \text{(II.22)}$$

Now the output impedance is defined as

$$Z_o = -\frac{\partial V_o}{\partial i_L} \qquad \text{(II.23)}$$

so that equation (II.22) gives

$$Z_o = \frac{Z_f + R_b}{A + 1} \approx \frac{Z_f}{A} \qquad \text{(II.24)}$$

For the typical values $Z_f = 10K$ and $A = 10^4$, equation (II.24) yields

$$Z_o = 1\ \Omega$$

Clearly, the operational amplifier can handle resistive loads $\geq 100\ \Omega$, and the voltage gain will show very little dependence on the output load. It is interesting to note that the output impedance is independent of R_o.

APPENDIX III

TIME RESOLUTION

III.1 Data from Gatti and Svelto.

The time resolution theory of Gatti and Svelto was introduced in Chapter 9. Their curves are presented in this section.

Figure III.1 shows the contribution to the resolving time arising from $\epsilon^2_{t_1,A,em}$, the variance in the machine time due to the statistical fluctuation in photoelectron emission, spread in the photoelectric yield, and spread in the current gain. Its value is given by $\frac{\tau^2}{R}(1 + \epsilon_A^2 + \bar{F}\,\epsilon^2_{\gamma F})$ multiplied by a function of time. The coordinates have been chosen to represent the function with respect to the ratio C/R. τ, C and R have the same meaning as in section 9.4. ϵ_A^2 is the variance in the amplification A of individual photoelectrons. $\bar{F}$ is the mean yield of the photocathode, and $\epsilon^2_{\gamma F}$ is the relative variance of the photocathode yield. The curve for $\lambda/\tau = 0$ has been shown to be given by

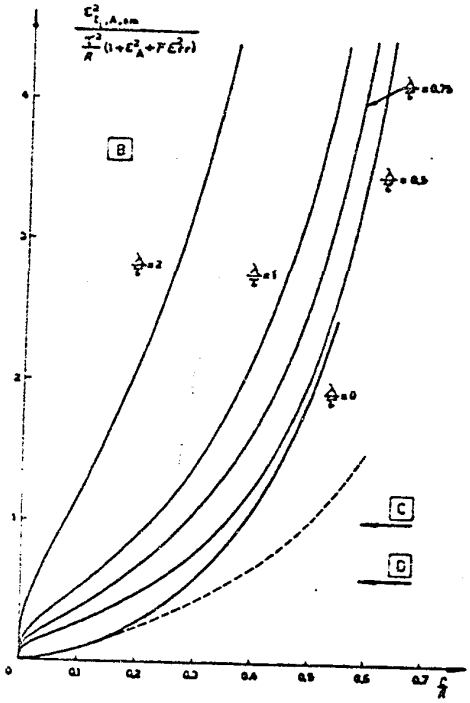

Fig. III.1. The machine time variance due to statistical fluctuations in photoelectron emission, spread in photoelectric yield, and spread in the current gain. From ref. 23.

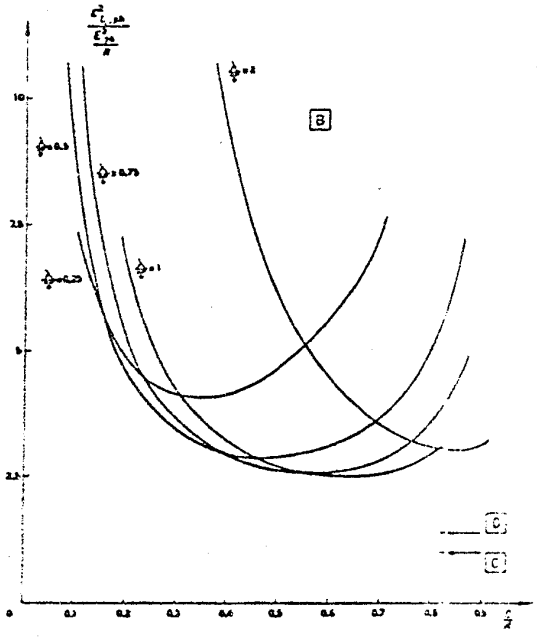

Fig. III.2. Machine time variance due to spread in the device delay time. From ref. 23.

$$\epsilon^2_{t_1,A,em} = (1 + \bar{r}\epsilon^2_{\gamma r} + \epsilon^2_A)\ \frac{\tau^2}{R}\ \frac{C/R}{(1 - C/R)^2}$$

$$\approx (1 + \bar{r}\epsilon^2_{\gamma r} + \epsilon^2_A)\ \frac{\tau^2 C}{R^2}\left[1 + \frac{2(C+1)}{R} + \ldots\right] \qquad \text{(III.1)}$$

This expression is close to the equation (9.2) given by Post and Schiff. By itself, it predicts that the best resolving time can be obtained for $C/R \to 0$.

Figure III.2 shows the machine time variance, $\epsilon^2_{t_1,ph}$, due to spread in the transit time of the electrons through the photomultiplier. Again convenient coordinates have been chosen to represent the function. ϵ^2_{ph} is given by

$$\epsilon^2_{ph} = \epsilon^2_{cd} + \frac{\epsilon^2_{dd}}{g - 1}\left(1 + \frac{2}{g}\right) \qquad \text{(III.2)}$$

where ϵ_{cd} is the standard deviation of the delay time for a photoelectron travelling from the cathode to the first dynode, ϵ_{dd} is the root-mean square deviation of the delay time between two successive dynodes, and g is the secondary emission factor. Note that this function increases again at low values of C/R.

Figure III.3 shows the variance in the machine time due to the spread in the S.E.R. width λ. $\epsilon^2_{\lambda,r}$ is the relative variance of the pulse width λ. This function

also increases for low C/R.

These three contributions are combined in the following way:

$$\varepsilon^2_{t_i} = \varepsilon^2_{t_i,A,em} + \varepsilon^2_{t_i,ph} + \varepsilon^2_{t_i,\lambda}$$

$$= \frac{r^2}{R}(1 + \varepsilon_A^2 + \bar{\varepsilon}^2_{yr}) \left[\frac{\varepsilon^2_{t_i,A,em}}{\frac{r^2}{R}(1 + \varepsilon_A^2 + \bar{\varepsilon}^2_{yr})}\right] + \frac{\varepsilon^2_{ph}}{R}\left[\frac{\varepsilon^2_{t_i,ph}}{\varepsilon^2_{ph}/R}\right]$$

$$+ \frac{r^2}{R} \cdot \varepsilon^2_{\lambda,r} \left[\frac{\varepsilon^2_{t_i,\lambda}}{\frac{r^2}{R} \cdot \varepsilon^2_{\lambda,r}}\right] \qquad \text{(III.3)}$$

For plotting on a graph this equation is divided by $\tau\varepsilon_{ph/R}$ to give

$$\frac{\varepsilon^2_{t_i}}{\tau\varepsilon_{ph/R}} = \left(\frac{r}{\varepsilon_{ph}}\right)(1 + \varepsilon_A^2 + \bar{\varepsilon}^2_{yr}) \left[\frac{\varepsilon^2_{t_i,A,em}}{\frac{r^2}{R}(1 + \varepsilon_A^2 + \bar{\varepsilon}^2_{yr})}\right]$$

$$+ \left(\frac{\varepsilon_{ph}}{\tau}\right)\left[\frac{\varepsilon^2_{t_i,ph}}{\varepsilon^2_{ph/R}}\right]$$

$$+ \left(\frac{r}{\varepsilon_{ph}}\right)\varepsilon^2_{\gamma,r} \left[\frac{\varepsilon^2_{t_i,\lambda}}{\frac{r^2}{R} \cdot \varepsilon^2_{\gamma,r}}\right] \qquad \text{(III.4)}$$

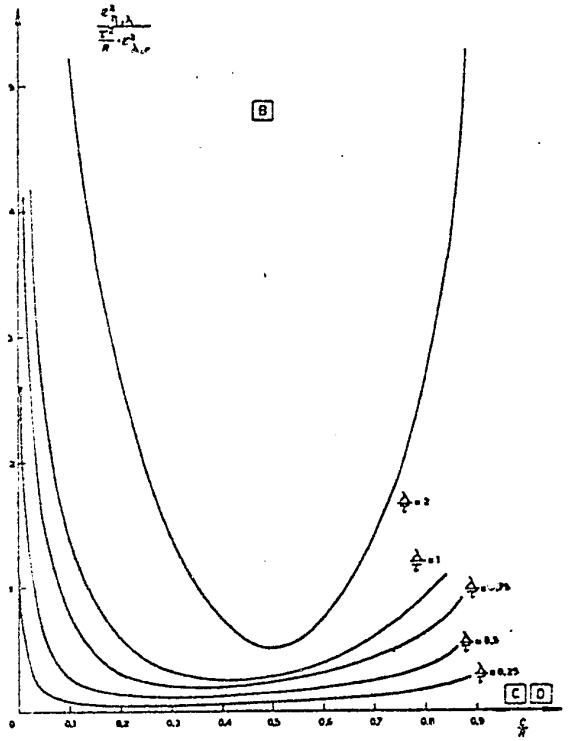

Fig. III.3. Machine time variance due to spread in the S.E.R. width λ. From ref. 23.

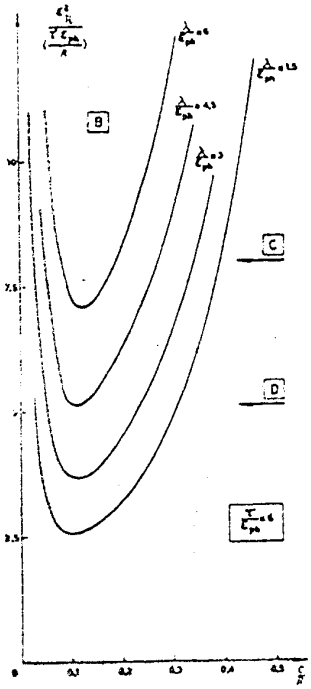

Fig. III.4. Total machine time variance for the fixed parameter $\sigma/\epsilon_{ph} = 6$. From ref. 23.

Figure III.4 shows a graph of equation (III.4) given by Gatti and Svelto for $\frac{\tau}{\epsilon_{ph}} = 6$. Figures III.5 and III.6 show rough sketches of the trend for $\frac{\tau}{\epsilon_{ph}} = 100$ and $\frac{\tau}{\epsilon_{ph}} = 10$.

It is obvious from these curves that, for a given R, the minimum resolving time is not achieved when $C/R \to 0$. Actually, the minimum machine time variance should be obtained for C/R somewhere in the range of 0.2 to 0.02.

III.2 A Schmitt Trigger with a Bias Control.

A Schmitt trigger circuit is proposed here for the fractional pulse height trigger suggested in section 9.7.

Figure III.7 shows the tentative trigger design. Omitting resistors R7, R8, R13, transistor Q3, and capacitors C4, C5 and C6, this circuit is a conventional, AC coupled, Schmitt trigger. Potentiometer R11 sets the DC bias, above which the input pulse must rise to trigger the circuit.

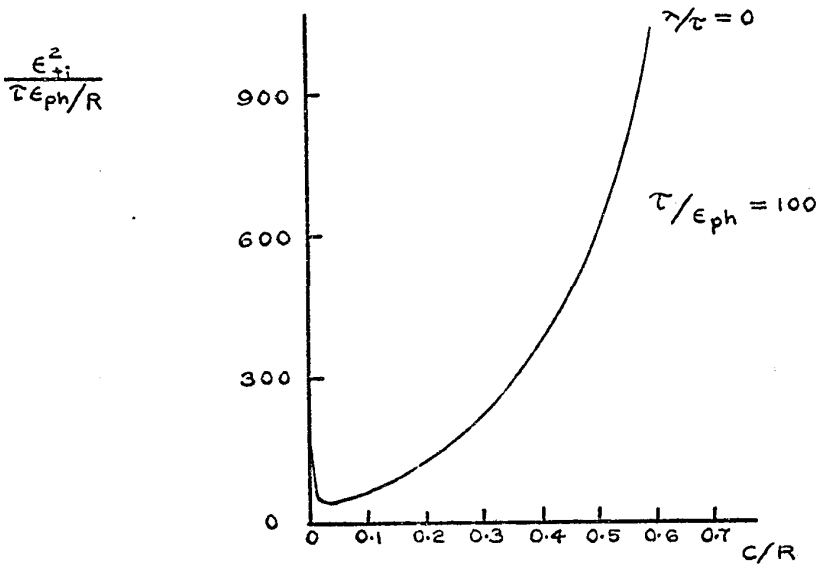

Fig. III.5. Sketch of total machine time variance for $\tau/\epsilon_{ph} = 100$.

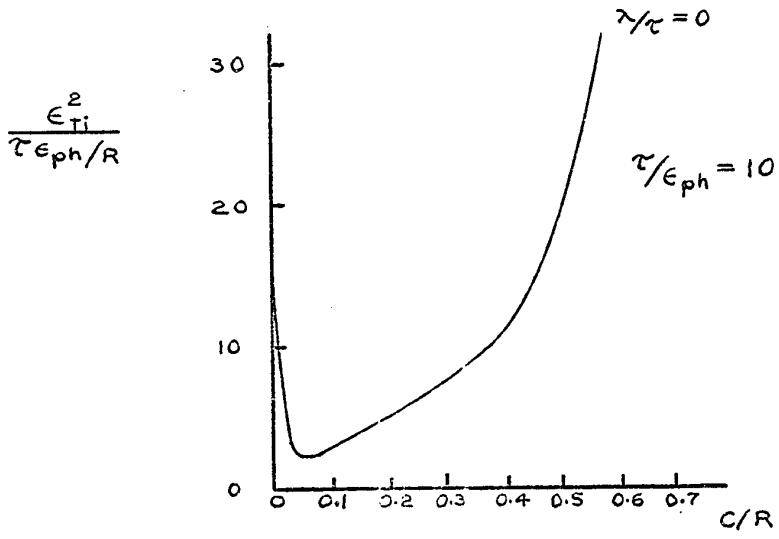

Fig. III.6. Sketch of total machine time variance for $\tau/\epsilon_{ph} = 10$.

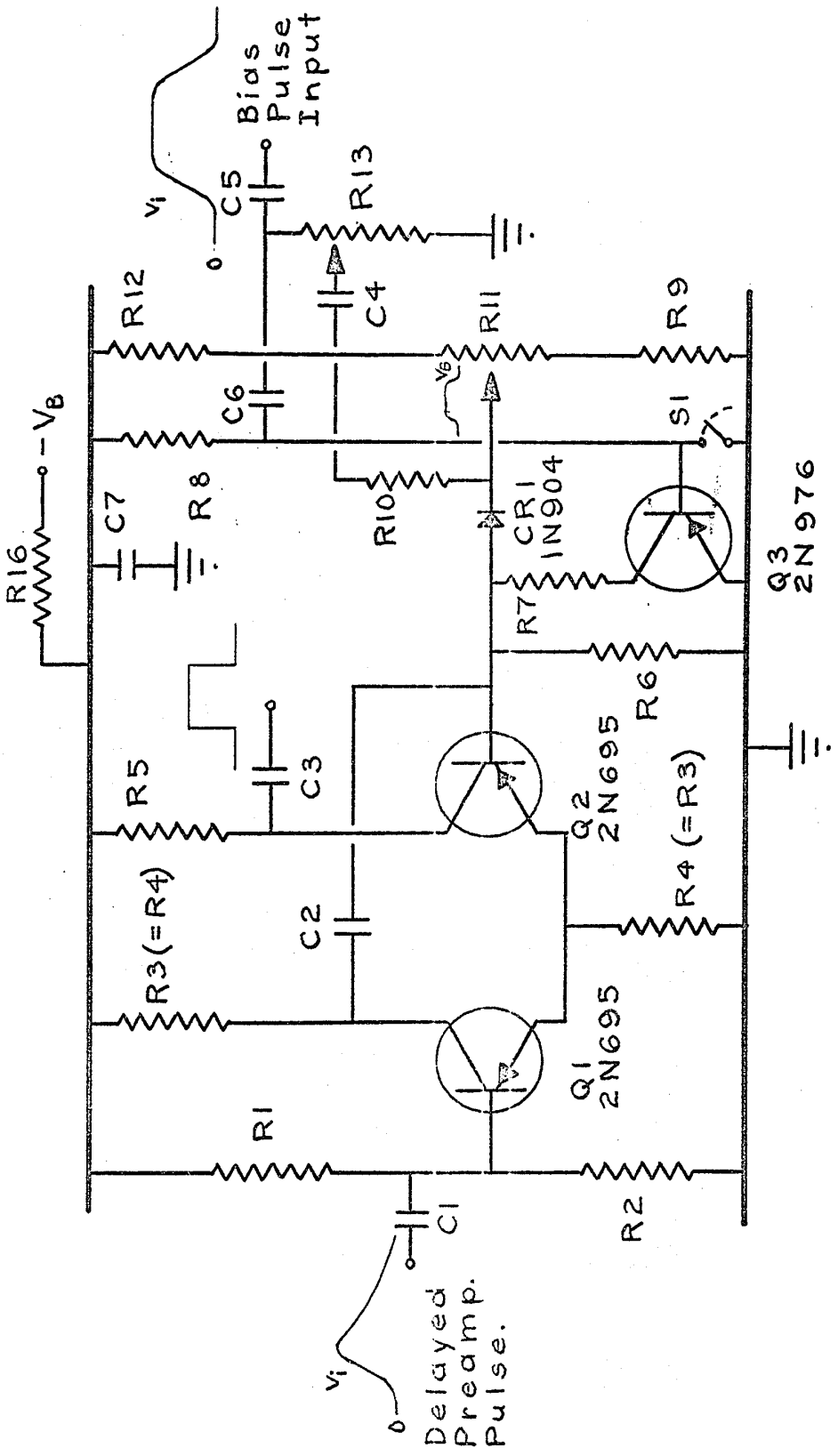

Fig. III.7. Fractional Pulse Height Trigger.

Transistor Q3 is normally held on by resistor R8. Consider the case where S1 is closed and Q3 is held off. Transistor Q1 is normally conducting so Q2 is held off by the reverse bias on its emitter-base junction. The back bias on Q2 is adjusted by the potentiometer R11. When the input pulse voltage is greater than this back bias transistor Q2 turns on and Q1 turns off. Due to the feedback capacitor C2, the switching is regenerative and occurs quickly. After a decay period, determined by R3 and C2, the circuit returns to its normal state. A positive output pulse is observed at the collector of Q2.

For adjusting the operation as a fractional pulse height trigger, switch S1 is closed and no input is supplied. Potentiometer R11 is tuned until the trigger just flips on its own. With this bias, the trigger is set to flip as soon as the input pulse starts to rise. Now the switch S1 is opened, and transistor Q3 turns on providing a temporary back bias on the base of Q2. This prevents the circuit from triggering of its own accord.

When the bias pulse is applied to C5, the attenuator R13 feeds a fraction of the pulse to the bias point at potentiometer R11. This introduces an additional bias proportional to the input pulse height. At the same time, the bias pulse turns transistor Q3 off, releasing the

temporary bias on the base of Q2. Now the bias the input pulse at Q1 must overcome to trigger the circuit is

$$V_B = kV_i$$

where k is the adjustable attenuation factor. Hence the input pulse triggers the Schmitt trigger at a fixed fraction k of its input pulse height. The fast rising output can be fed to a fast coincidence circuit or to a time-to-amplitude convertor.

The 2N695 transistor has been chosen because of its fast switching time (t_r = 1.6 nsec, t_f = 1.3 nsec). Of course, more detailed design is necessary to make this circuit function properly. Particular care must be taken in the design to achieve fast switching times.

APPENDIX IV

THE OSCILLATING TRITIUM TARGET.

The pictures in Figures IV.1, IV.2, and IV.3 show the construction of the oscillating tritium target. In Figure IV.2 the target block can be seen. A 3" x 1/2" copper-backed tritium target is clamped to the target block by the metal plate with the oblong hole in it. The tritium target forms a seal between the vacuum in the target chamber, and the cooling water in the target block. A rubber gasket behind the target ensures a good vacuum seal. Cooling water runs over the back of tritium target to dissipate the heat generated by the deuteron beam. The two copper pipes supporting the target block from the 7/8" shaft provide entrance and exit channels for the cooling water. A system of "O" rings seals the 7/8" shaft against the atmospheric pressure outside the target chamber. When the apparatus is assembled, as shown in Figure IV.1 and Figure IV.3, the tritium target is directly in line with the deuteron beam coming down the centre of the 2" tube on the front of the target chamber. A teflon gasket is placed between the flange on the 2" tube and the flange on the neutron generator, and the assembly is bolted to the

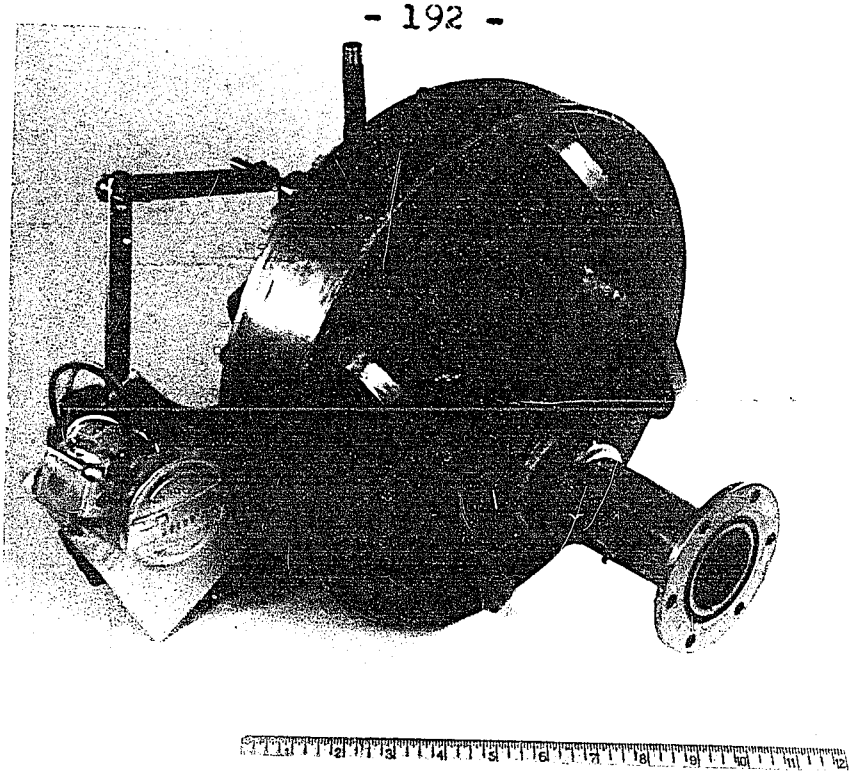

Figure IV.1 Front view of the target assembly.

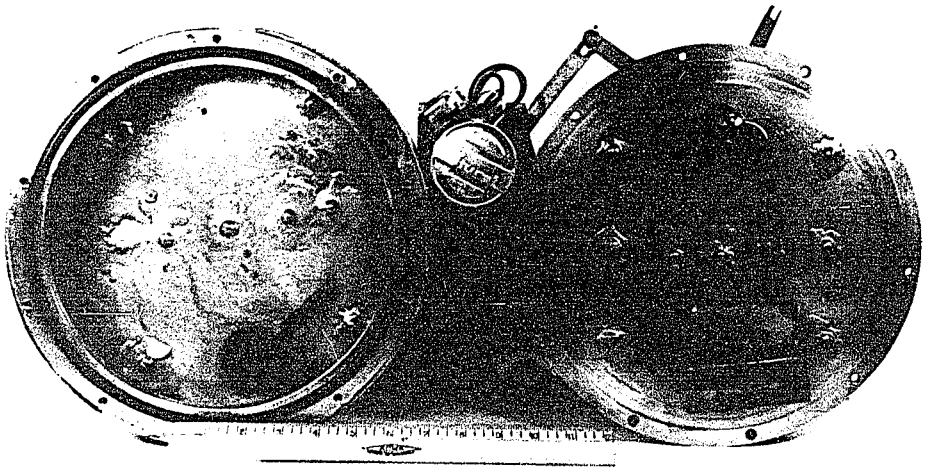

Figure IV.2a The inside of the assembly.

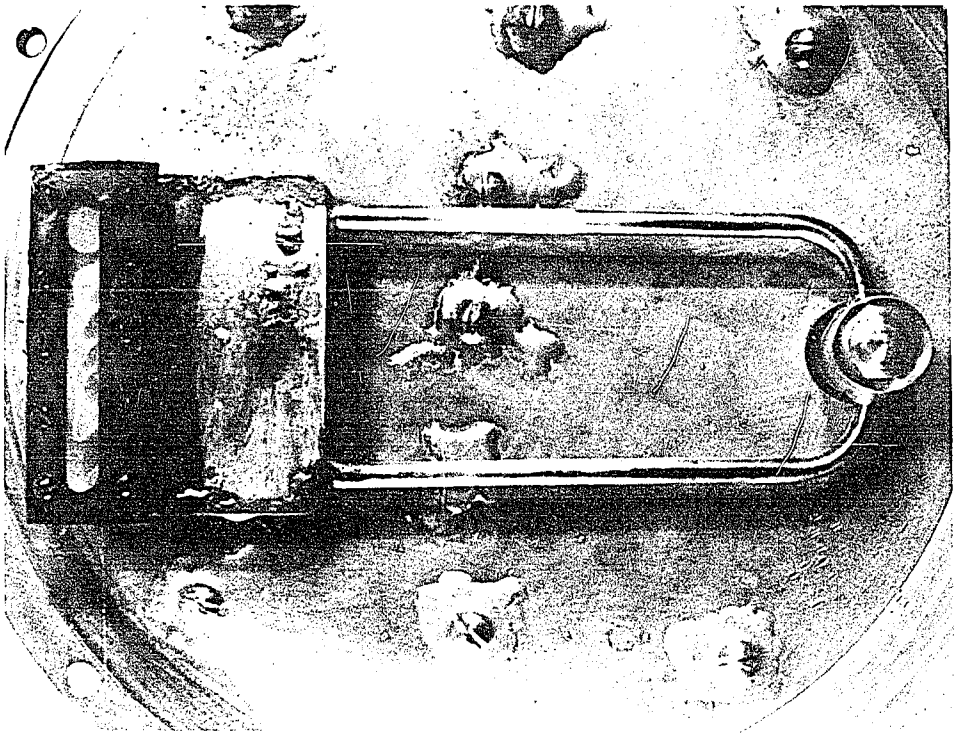

Figure IV.2b The target block.

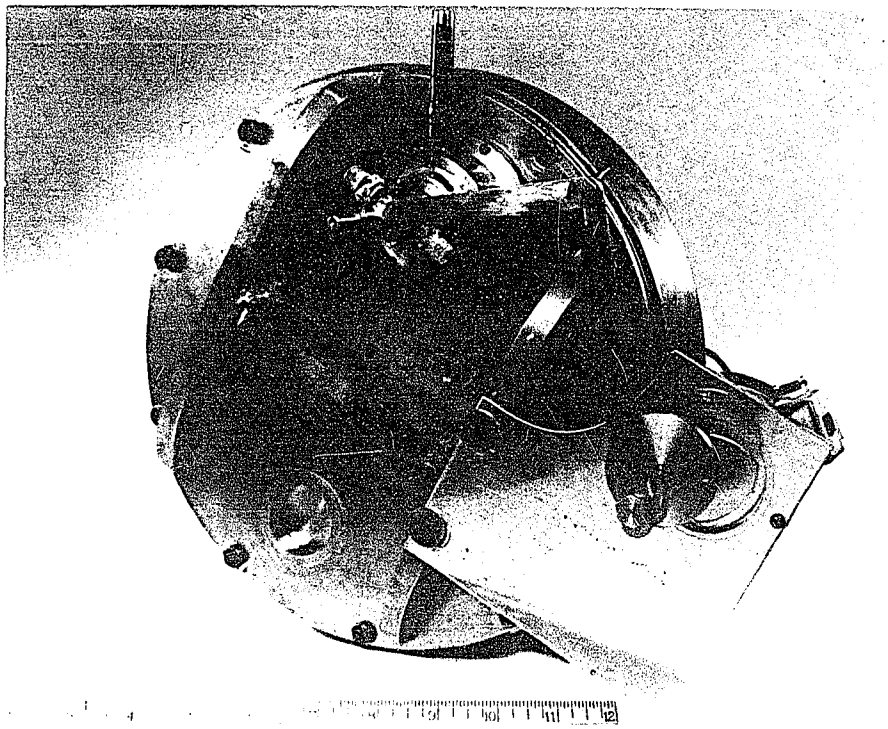

Figure IV.3 Back view of the assembly.

neutron generator drift tube. Insulating washers are used on the bolts, so that a wire from the target chamber allows reading the deuteron beam current. The small 1" tube projecting from the 2" tube is a port for viewing the tritium target, primarily for the purpose of lining up the deuteron beam.

The target is made to oscillate past the deuteron beam at the rate of 1 cycle per minute by the electric motor and 4-bar linkage on the back of the assembly (see Figure IV.3). In this way the deuteron beam scans the whole length of the tritium target. Two plastic couplings on the end of the 7/8" shaft permit hoses to be attached for the cooling water. An extra "backing-out chamber" is provided on the outside end of the shaft to lessen the pressure across the inner vacuum seal on the shaft. An oil type, vacuum pump is attached to the pipe on the backing-out chamber. The fittings on the 4-bar linkage permit adjustment of the centering and the throw of the target oscillations.

On the back plate of the target chamber, a 1 1/2" diameter indentation is found directly behind the target. Sources for activation are set in this hole. Using a

2 ucurie/cm^2 tritium target, it was possible to run at a flux of $\approx 10^7$ neutrons/cm^2/sec for 160 hours. The reaction is the well known

$$ {}_1D_1^2 + {}_1T_2^3 \rightarrow {}_2He_2^4 + {}_0n_1^1 \qquad \text{(IV.1)} $$

reaction which yields 14 MeV neutrons.

One imperfection encountered in the oscillating target arises from the 4-bar linkage drive. A simple analysis will show that the angular velocity of the oscillating target is not constant, but is considerably slower at the extreme ends of its swing. This characteristic causes the ends of the tritium target to be used up more quickly than the centre of the strip, making the neutron flux fluctuate as the target oscillates. The problem could be eliminated by driving the target shaft with a constant angular velocity cam. An increase in the oscillating frequency would also improve the control of the neutron flux.

REFERENCES

1. E. C. Stewart et al, "Harshaw Scintillation Phosphors (2nd edition)". The Harshaw Chemical Company, Cleveland, Ohio, 1962.

2. R. L. Chase, "Nuclear Pulse Spectrometry", McGraw-Hill Book Company Inc., New York, 1961, pp. 17 - 20.

3. J. Sharpe, "Nuclear Radiation Detectors", Methuen and Company Ltd., London, 1955, pp. 101 - 127.

4. R. C. Davis, P. R. Bell, C. G. Kelley, and M. H. Lazar; Response of 'Total Absorption' Spectrometer to Gamma Rays, I.R.E. Transactions, Vol. NS-3, Number 4.

5. Vis. Reference 2 - pages 193 to 203.

6. A. H. Hoogenboom, A New Method in Gamma-Ray Spectroscopy: A Two Crystal Scintillation Spectrometer with Improved Resolution, Nuclear Instruments and Methods, 3, 1958, pp. 57 - 68.

7. S. I. H. Naqvi, Operating Characteristics of a Sum-Coincidence Spectrometer, Nuclear Instruments and Methods 16 (1962), pp. 305 - 309.

8. G. Y. Mathé, D. Bérenyi and T. Scharber, Experiences on the Application of the Sum-coincidence Method, Nuclear Instruments and Methods 14, (1961), pp. 209 - 214.

9. R. D. Evans, "The Atomic Nucleus", McGraw-Hill Book Co., Inc., New York, 1955, pp. 234 - 244.

10. M. E. Rose, The Analysis of Angular Correlation and Angular Distribution Data, Physical Review, Vol. 91, No. 3, 1953, pp. 610 - 615.

11. S. C. Schriber and B. G. Hogg, Nuclear Instruments and Methods, 26 (1964), pp. 141 - 146.

12. L. Cathey, I.R.E. Trans. Nuc. Sci. NS5:3 (1958) 109.

13. D. F. Covell and B. A. Euler, Proceedings of the 1961 Conference on Modern Trends in Activation Analysis, p. 12.

14. B. R. Linden, F. N. Schenkel, P. A. Snell, I.R.E. Trans. Nuc. Sci., NS7:2-3 (1960) 61.

15. R. B. Murray and J. J. Manning, I.R.E. Trans. Nuc. Sci. NS7:2-3 (1960) 80-86.

16. J. D. Ryder, "Electronic Fundamentals and Applications", Prentice-Hall Inc., Englewood Cliffs, N.J., 1960, pp. 340 - 343.

17. J. Millman and H. Taub, "Pulse and Digital Circuits", McGraw-Hill Book Company Inc., New York, 1956, pp. 22 - 26.

18. F. Goulding, Transistorized Radiation Monitors, I.R.E. Trans. on Nuclear Science, vol. NS-5, p. 38, 1958.

19. J. S. Fraser and R.B. Tomlinson, Transistorized Circuits with Nanosecond Time Resolution, A.E.C.L. Reference numbers A-2811-D, A-2811-E, A-2812-A, A-2811-C.

20. pp. 45 - 46 of reference 2.

21. R. Bell, R. Graham, and H. Petch, Design and Use of a Coincidence Circuit or Short Resolving Time, Can. J. Phys., vol. 30, p. 35, 1952.

22. R. Post and L. J. Schiff, Phys. Rev. 80, (1950) p. 1113.

23. E. Gatti and V. Svelto, Nucl. Instr. and Meth., 4, (1959) 189 - 201.

24. A. Schwarzschild, Nucl. Instr. and Meth., 21, (1963) 1 - 16.

25. H. de Waard, Nucl. 13, Number 7, (1955) 36.

26. D. H. Wilkinson, J. Sci. Instr., 27, (1950) 36.

27. R. L. Chase, Suppl. to I.R.E. Trans. on Nucl. Sci. Vol. NS-9, No. 1, January 1962.

28. J. A. Ladd and J. M. Kennedy, A.E.C.L. Report, AECL-1417, CREL-1063, December 1961.

29. J. A. Ladd and J. M. Kennedy, Digital Stabilising Methods for Multi-Channel Analysing Systems, A.E.C.L. Report, Chalk River, April 1963.

30. J. A. Ladd and G. L. Harkley, A.E.C.L. Report, AECL-1751, CREL-1123, June 1963.

31. J. L. Demuynck and O. J. Seguert, Nucl. Instr. and Meth. 16 (1962) 358 - 359.

32. page 95 of reference 2.

33. R. H. Nussbaum and S. K. Suri, Phys. Rev., Vol. 105, No. 4, (1957) 1272 - 1277.

34. C. F. Schwerdtfeger, A. V. Ramayya, and A. C. G. Mitchell, Nucl. Phys. 49 (1963) 55 - 64.

35. H. G. Devare and P. N. Tandon, Nucl. Instr. and Methods, 22 (1963) 253 - 255.

36. I. S. Sokolnikoff and R. M. Redheffer, "Mathematics of Physics and Modern Engineering", McGraw-Hill Book Company, Inc., (1958) 776.

37. W. Magnus and F. Oberhettinger, "Formulas and Theorems for the Functions of Mathematical Physics", Chelsea Publishing Company, New York, (1954) 96.

38. E. A. Wolicki et al., Calculated Efficiencies of NaI Crystals, N.R.L. Report 4833.

39. R. L. Heath, "Scintillation Spectrometry Gamma-Ray Spectrum Catalog", Phillips Petroleum Company, Atomic Energy Division, Idaho Falls, Idaho.

VITA

NAME:	Dale A. Gedcke
BORN:	Kitchener, Ontario, Canada, 1939.
EDUCATED:	
Primary	Suddaby School, Kitchener, 1944-53.
Secondary	Kitchener-Waterloo Collegiate and Vocational School, 1953-56. Eastwood Collegiate, 1956-58.
University	McMaster University, 1958-62.
Course	Engineering Physics.
Degree	B. Eng. 1962.
APPOINTMENTS	Research Assistant U.O., 1962-64.
EXPERIENCE	Research and development at Atomic Energy of Canada Ltd., Chalk River, Ontario; May 1962 - September 1962.